NTNU

Norwegian University of
Science and Technology

Adequate linearization scheme for a jack-up in order to obtain sufficiently accurate fatigue assessments using a linear stochastic fatigue analyses

Marius Tveit Karlsson

Marine Technology
Submission date: June 2017
Supervisor: Sverre Kristian Haver, IMT
Co-supervisor: Jørgen Amdahl, IMT

Norwegian University of Science and Technology
Department of Marine Technology

Preface

This Master Thesis is the final project after 5 years at the Norwegian University of Technology and Science. This has been a 5 year journey with the best of what Norway has to offer when it comes to technology and science. Five years that has provided me with huge amounts of knowledge in highly specialized fields, but also in more wide senses. It has been a joy to absorb the greatness of academia in the professional, but also in the non professional way.

The journey has been long. A lot of people have contributed to make it exciting and interesting. First of all i would like to thank my supervisors Jørgen Amdahl and Sverre Haver. I have been extremely privileged to have two of you. The benefit of discussing with two such knowledgeable people is huge. It is vital for academic institution that such people with eager for their field and willingness to teach others are present. Their input has been crucial for the quality of the thesis. The meetings has been entertaining on all fronts, and I have always looked forward to these. I have always come out of these meetings with new motivation and new insight. I wish my supervisors all the best and hope to contact them with professional questions also in the future.

Antonio Goncalves and DNV GL has been contributing by pointing on relevant literature and providing me with models and drawings. The help is appreciated.

I would also like to thank my family, who have always been there for me. They have provided me with financial support such that I have been able to focus full time on my studies. They have also encouraged me in times when motivation has been on lower levels. They are inspirational people who i admire.

My colleagues and friends on office C1.084 also contribute to make every day at the office a joy. They all contributes in their own individual way to make the day interesting and entertaining. They also possess a lot of knowledge to supplement with my own in interesting discussions about marine structures as well as world economics.

To all the lads.

Abstract

Different techniques for linearizing the response of drag dominated structures is in this work inspected in terms of fatigue damage. To establish reference response characteristics, time domain simulations are carried out. Time domain simulations must be considered as state of the art methods for estimating fatigue damage., but do however demand huge computational capabilities.

Linear potential theory is used to calculate wave kinematics. To compensate for the deviation to higher order wave kinematics, adjusted drag coefficients are used. The JONSWAP spectrum is used to generate stochastic surface elevation and forces, which is realized using both randomness in phase and amplitude. This insures that a signal is never repeated within a short term sea state.

Stress concentration factors are used to generate stress processes from beam reactions. To calculate both cycle ranges, and amount of cycles, the rainflow algorithm is utilized, which result in stress range records that are used as input to SN curves and miner summation.

Ground conditions are selected to give a highest natural period of 7.67s, which is within energetic areas of the scatter diagram. Large dynamical amplifications contribute to move most important fatigue damage sea state down to a spectral peak period of 8.5s.

The linearization consists of evaluating the response of the structure to different harmonic input components with different frequencies in order to create transfer functions. In this regard, the question is how the wave heights used as input to these harmonic components is selected. Three schemes of selecting these are inspected. The two most promising are achieved by keeping the steepness or the ratio between height and period constant. They overestimate the total accumulated damage during 56 years by 20 % and 100% respectively. The steepness or the constant height-period ratio is calibrated by matching a spectrally calculated wave action with a deterministic calculated wave action. This calibration process is working well, and gives reasonable calibrated values. Both methods tend to be efficient and gives reasonable results. Whether the constant steepness approach is conservative might be questioned especially at higher frequencies. The constant height-period ratio however insures conservatism also at larger frequencies.

It might also be possible to switch the drag term to a linear term and replace the drag coefficient by a linear drag coefficient. This might open up for the use of simpler explicit methods to select appropriate calibrated values.

Sammendrag

Ulike teknikker for å linearisere responsen av dragdominerte strukturer er i dette arbeidet inspisert når det gjelder utmattingsskader. For å etablere referanse-responser utføres tidsplansimuleringer. Tids plan simuleringer regnes som den mest eksakte metoden for å estimere utmattingsskader, men krever imidlertid store beregningsmessige ressurser.

Lineær potensialteori brukes til å beregne bølgekinematikk. For å kompensere for avviket til høyere ordens bølgekinematikk, brukes justerte drakoeffisienter. JONSWAP-spekteret brukes til å generere stokastisk bølgeoverflate og krefter, som realiseres ved hjelp av både tilfeldighet i fase og amplitude. Dette sikrer at et signal aldri gjentas i en kort sjøtilstand.

Spenningskonsentrasjonsfaktorer brukes til å generere spenningsprosesser fra bjelke-ereaksjoner. For å beregne både syklusvidde og mengder sykluser, benyttes rain-flow algoritmen, noe som resulterer i sykel-vidde data som brukes som input til SN-kurver og Miner-summering.

Bunnforholdene er valgt for å gi en høyeste egenperiode på 7,67s, som ligger innen-for det energiske områder av scatterdiagrammet. Store dynamiske forsterkninger bidrar til å flytte viktigste tretthetskader sjøtilstand ned til en spektral peakperiode på 8,5 år.

Lineariseringen består av å evaluere strukturens respons til forskjellige harmoniske inputkomponenter med forskjellige frekvenser for å skape transferfunksjoner. I denne forbindelse er spørsmålet hvordan bølgehøyder som brukes som input til disse harmoniske komponentene, velges. Tre måter å bestemme disse på blir in-spisert. De to mest lovende oppnås ved å holde steilheten eller forholdet mellom høyde og periode konstant. Det gir et overestimat i skade på henholdsvis 20% og 100% gjennom 56 år akkumulert skade. Steilhet eller konstant høyde-periode forhold kalibreres ved å matche en spektralberegnet bølgekraft med en determinis-tisk beregnet bølgekraft. Denne kalibreringsprosessen fungerer godt, og gir rimelige kalibrerte verdier.

Begge metodene ser ut til å være effektive og gir rimelige resultater. Hvorvidt den konstante steilhet-tilnærmingen er konservativ, kan bli stilt spørsmålstegn ved spesielt ved høyere frekvenser. Den konstante høyde-periode tilnærmingen sikrer imidlertid konservatisme også ved større frekvenser.

Det kan også være mulig å bytte drag leddet til en lineær term og erstatte dragko-effisienten med en lineær dragkoeffisient. Dette kan åpne for bruk av enklere, eksplisitte uttrykk for å velge passende kalibrerte verdier.

Contents

List of Figures

List of Tables

List of symbols

H_S	Significant wave height
T_P	Spectral peak period
m_0	Variance of a spectrum
$S_{\zeta\zeta}$	Surface elevation spectrum function
f	Frequency
γ	Peakedness parameter
g	Gravity
u_w	wave particle velocity
u_c	Current velocity
V	wind velocity
τ	Constant
z_0	Constant
$\mathbf{F}$	Force vector
$\mathbf{M}$	Mass matrix
$\mathbf{m}$	Element mass matrix
$\mathbf{C}$	Damping matrix
$\mathbf{K}$	Stiffness matrix
$\mathbf{r}, \dot{\mathbf{r}}, \ddot{\mathbf{r}}$	Response vector, velocity and acceleration
ρ_w	Density sea water
D	Diameter
U	Internal strain energy
E	Modulus of elasticity
$u_{,x}, v_{,x}, w_{,x}$	Derivative of displacements
I_x, I_y	Second moment of area
H	Potential of external loads
δ	Notation for virtual of the following measure (e.g. work, displacement)
N	Normal force
A	Cross sectional area

ϕ^T	element shape functions
α_1, α_2	Damping coefficients
ξ	Damping ratio
ω	Circular frequency
C_D, C_M	Drag and inertia coefficients
u, w	Fluid velocity in x and z direction
a_x, a_z	Fluid acceleration in x and z direction
T	Period
ϕ	Velocity potential
ζ	Surface elevation
x,z	Horizontal and vertical coordinates
z'	Stretched z coordinate
d	Depth
C_{D0}	Inline drag coefficient for cylinder with rack mount
C_{D1}	Drag coefficient with rack perpendicular to flow
F_D	Drag force
F_M	Inertia force
$k_x, k_y, k_z, k_{\theta x}, k_{\theta y}, k_{\theta z}$	Spring coefficients for ground
ω_n	Natural frequency
$\mathbf{r}_n$Natural mode	
α, γ, β	Parameters of time integration algorithm
$\bar{xi}$	Algorithmic damping
$\bar{T}$	Algorithmic period
$S(\omega)$	Input surface elevation spectrum
$\Delta\omega$	Frequency increment
ϕ_i	Random phase
T_{rep}	Repetition period of signal
$R(\tau)$	Auto correlation
$F_H(h)$	Cumulative probability distribution of h
D	Damage
σ	Stress
σ_a	Stress amplitude
N	Allowable cycles
$\log(\bar{a})$	Constant in SN-curve
k	Thickness exponent
$\sigma_1 - \sigma_8$	Locations for stress measurement
SCF	Stress concentration factor
$\sigma_x, \sigma_{my}, \sigma_{mz}$	Axial and bending stress
T_n	Natural period
$\Delta\sigma$	Stress range
$f_{\Delta\sigma}$	Probability distribution of stress range

$\tilde{S}(\omega)$	Estimated spectrum from fatigue
s	Standard deviation
μ	Mean
η	Degree of freedom in χ dist.
χ^2	Chi distribution
$F_{\Delta\sigma}$	Cumulative distribution of stress range
β, λ, α	Distribution parameters in weibull 3 parameter dist.
$F_{D,a}, D_{M,a}$	Drag and inertia amplitude
s_σ	Standard deviation in stress
G	Parameter for scaling a JONSWAP like input wave-height
ΔF_{MPM}	Range in most probable maximum in wave actions (base shear)
H_{MPM}	Most probable maximum wave height
$C_{(C,L)}$	Equivalent linear drag coefficient
F_p	Force peak
$C^{(m)}$	Ratio to calculate equivalent drag coefficient
$\gamma(,), \Gamma(,)$	lower and upper incomplete gamma functions
$\Gamma()$	Gamma function
σ_u^2	Variance of velocity
K	Parameter to select equivalent drag coefficient

Abbreviations

CPU	Central processing unit
JONSWAP	Joint North Sea Wave Project
SCF	Stress concetration factor

Chapter 1

Introduction

.

1.1 Background

Fatigue is dependent on the stress range of the cyclic loading rather than the stress itself. This means that materials subject to cyclic stresses well bellow yield, may experience critical cracks after a certain amount of cycles. This becomes a vital phenomenon for offshore structures due to the cyclic nature of the wave loadings.

In stochastic fatigue analysis the relation between forces in each members and wave height is calculated with the assumption that there exist a linear relationship between the wave height and the resulting force. However, typically jacket and jack-up with lattice leg design are drag dominated. The drag forces are proportional to the square of the wave particle velocity. For such structures, the wave height to wave force relation is therefore not linear.

In offshore industry, linearization with respect to wave height is generally used. It is based on the selection of a characteristic wave height for each wave frequency of interest. Constant wave steepness is frequently used as such characteristics to select the linearized wave height. However, there are no proper guidelines or recommendations for selection the correct wave steepness for a specific sea state. Furthermore constant wave steepness usually results in over predicted drag at small wave frequencies and under predicted drag at large wave frequencies.

The fatigue damage at jack-ups are strongly dependent on the assumptions made in the linearization. Hence this might result in adding to much conservatism in order to rely on the analysis. An appropriate linearization scheme is needed in order to get more confidence in the results.

1.2 Scope

The scope of this thesis will be to investigate the linearization scheme with constant steepness, but also look into others. The goal is to come up with schemes that gives the correct amount of damage. To estimate the correct amount of damage, time domain simulations with stochastic input loads should be used. The computer program USFOS is used in order to perform these calculations. Such rime domain simulations require huge amounts of computational efforts and data handling. Hence they are not widely used in the offshore industry to estimate fatigue damage. In order to deal with these large computational demands, the need of multicore processing power is essential. Parallel processing will be carried out by running USFOS in parallel through MATLAB.

Detailed screening of critical heading and location of critical stress will not be conducted. The focus will be on the linearization for the particular selected joint. Furthermore there will be no effort given to use second order surface elevation.

The final goal for the work is to come up with linearization schemes designed for each block in the scatter diagram. These schemes should give a conservative amount of damage.

1.3 Deviation from problem description

Together with the supervisor it has been decided to exclude the following tasks from the problem description due to work load. See appendix C for the full problem description.

- Detailed analysis of current, and how current will invoke with linearizations, and the importance of current is not considered, however a brief discussion of the importance of current is included.

- Dividing the weather in different directional sectors will not be carried out.

1.4 Contributions

USFOS analysis has been implemented in MATLAB with the use of the parallel toolbox. This will enable future students to run USFOS through a familiar programing environment, and at the same time having access to the power of multi-core CPUs. The real benefit of this is when USFOS executions are part of perplexed algorithms.

More confidence on linearization techniques used in offshore industry, can from this work be taken. In addition a more conservative linearization scheme has been developed by using height-period ratio as tuning parameter instead of steepness.

Chapter 2

Jack-up rig CJ-62

In general a jack-up is a platform that has the ability elevate the topside relative to the legs. In addition to this it has the ability to float by itself when the legs are not in contact with the bottom. Different jack-up concepts exist where differences exist in both size and amount of legs, as well as in other parameters.

The jack-ups are usually seen as mobile drilling units, however they can also be used for installation of wind turbines and demolition of aging offshore installations. In operational phase the platforms are attached to the sea floor, making them stable compared to floating units of similar size, and suitable for delicate work. This combination of stability and mobility are what makes jack-ups attractive.
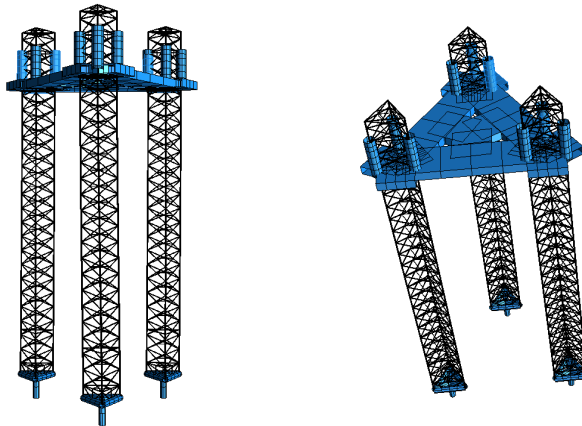
Figure 2.1: *Finite element model of the jack-up*

2.1   Design

The deck structure of the platform is formed as a equilateral triangle, and has three elevatable legs. This particular model is designed by the engineering company GustoMSC, and is classified by DNV GL.

The outer dimensions of the legs seen from above is equivalent to a equilateral triangle with 16 meter sides. Between the center of two of these legs, there are 62 meters. Furthermore the platform is designed to operate on depth as large as 130 meters, making this a large piece of construction.

A typical jack-up platform, including this, has legs made of trusses. These trusses has slender members compared to wavelength. They are also in fact slender compared to typical jacket structures. Leg design is based on triangular trusses with x-braces. In addition to braces, the trusses consist of chords. The difference between a brace and a chord is illustrated figure 2.2.
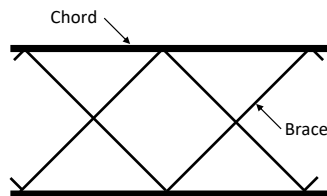
Figure 2.2: *Chords and braces on a truss*

The ability to elevate the deck structure comes with certain aspects. This includes a system to elevate the whole deck structure on three legs. Keeping in mind that the platform deck is a heavy structure this is a demanding task. This task is accomplished by attaching racks to the chords. The platform deck can then be elevated using gears. This means that in total nine racks are used to elevate the whole platform. These also introduces certain hydrodynamical properties. Non-circular geometry on the chords results in larger drag forces.

Depth ranges between 70m to 75m in the Ekofisk area where the platform location is assumed. However this particular jack-up model support water depth considerably deeper. At larger water depths the wave actions will inherit more overturning moment. Hence this analysis is investigating a larger water depth than what is present at the Ekofisk field.

In a design process wave heading direction must be accounted for. The directions might be splitted in sectors on 15 degrees. Due to symetry for this particular triangular platform, only inspection of a heading of 0 to 60° are needed. In this work only the wave heading of 0° is inspected.

Water depth	Air gap	Wave direction
110m	43m	0°

Table 2.1: *Operational properties*

2.2   Design challenges

The jack-up design comes with certain challenges. The relatively thin leg design with no stiffening in between legs makes the platform flexible compared to other fixed offshore installation. With low stiffness the natural period of the platform becomes significantly higher than jacket structures, and moves the period closer to high energy regions of the scatter diagram.

This induces large dynamic responses in translation of the deck as well as twisting. This demands a proper dynamical treatment of the motion of the platform in the analysis perspective.

Another aspect of the jack-up design is that it has slender members. Structural members becomes more and more drag dominated as they become thinner. Drag forces posses a nonlinear nature, and can not be treated in the frequency domain in the same manner as linear forces. This introduces assumptions and simplifications.

Another difficulty with the jack-up's is the fact that they are mobile. In the design phase it is not always known where the rig will operate during its life span. This also contributes to a complicated fatigue analysis, and in order to do proper fatigue analysis the load condition history is necessary since the loads will differ depending on location. In addition the transportation of the platform will add a share of fatigue damage.

Chapter 3

Metocean data

Environmental load data is established from meteorology and oceanography using sensor measurements and statistical models. Environmental loads includes loads from current, wind and waves. There is without doubt necessary to estimate these loads in a accurate way.

3.1 Location

Wind, waves and current will vary depending on location. For instance the weather in the North Sea is much harsher than in the Gulf of Mexico.

The wave record is used to describe the different wave statistics. The location for these measurements is the Ekofisk field, which is located at 56.549197N,3.209986E, south of the the Norwegian coast line, and can be seen in figure 3.1.

Figure 3.1: Ekofisk location

3.2   Short term wave statistics

In offshore industry a short term sea state is typically defined as a surface elevation process with a 3h duration. The two main parameters used to describe this surface is the significant wave height and spectral peak period. Significant wave height can be estimated by $H_S = 4m_0$, where m_0 is the variance of the surface elevation process [Myrhaug, 2007]. The spectral peak period can be considered as the average wave period during these 3h, or more precisely the period at which the peak of the wave specter occur.

A wave spectra is a mathematical description of the short term sea state behavior. These relations describes the energy present at every frequency present during these 3h. Wave spectra from measurements are not always on hand in a design phase. Standardized spectra is then frequently used to describe the surface. They depend upon what kind of sea conditions that is present. A typical breakdown is the following three wave conditions [Haver, 2017].

Wind sea

This is a condition generated from local winds.

Swell sea

This is a sea condition where the waves are not generated by local wind. It can typically be described as a rather narrow banded wave spectrum.

Combined sea

In practice almost every sea state will have one component generated from local wind and one from swell.

In the combined case, the waves generated form local wind will in general follow the direction of the wind. In addition the components from swell sea can typically propagate in another direction. For most applications conservatism is achieved by assuming that these will follow the same direction. For cases of combined sea, the Torsethaugen spectrum should be applied, which is a two peak spectrum. Depending on the how much the two peaks differ, this might induces problems with narrow banded assumptions.

In this project it is assumed that local wind is the only contributing condition, and that the sea is growing. This implies that the JONSWAP spectrum is suitable.

This is a spectrum is based on studies conducted in the seventies in the southern North Sea sin the area of the Ekofisk field. This spectrum is given by equation 3.1

$$S_{\zeta\zeta}(f) = 0.3125 H_S^2 T_P^{-4} f^{-5} \exp(-1.25 t_p^{-4} f^{-4})(1 - 0.287 \ln(\gamma)) \gamma^{\exp(-0.5(\frac{f - f_p}{\sigma f_p})^2)} \tag{3.1}$$

Where $f_p = 1/T_P$ and σ is 0.07 for $f \leq f_p$ and 0.09 otherwise. The peakedness parameter can be defined as in equation 3.2 [Haver, 2017]

$$\gamma = 42.2(\frac{2\pi H_S}{g T_P^2})^{6/7} \tag{3.2}$$

For simplicity the peakedness parameter will be taken as $\gamma = 3.3$ in this work.

3.3   Long term wave statistics: scatter diagram

Hindcast data is created for every 3h. Each of these short sea states comes with a significant wave height and a spectral peak period. These data can be grouped together for values of significant wave height and spectral peak period of similar magnitude in order to form a scatter diagram. A scatter diagram for the Ekofisk for 56 years is seen in figure 3.2.

2<TP<3

HS	2.5	3.5	4.5	5.5	6.5	7.5	8.5	9.5	10.5	11.5	12.5	13.5	14.5	15.5	16.5	17.5	18.5	19.5	20.5	Sum
0<HS<1 / 0.5	84	2440	9795	8508	4072	2487	1958	1335	846	473	302	159	75	66	43	18	13	5	2	32681
1.5	109	3925	14361	18546	11615	5862	4112	3278	1846	865	299	183	96	59	19	9	1			65185 Cutoff
2.5		7	641	7358	13621	7142	2828	1662	1439	993	412	155	83	18	7	4	0			36370
3.5			1	256	3121	8071	3685	1239	546	363	246	125	62	27	11	4	0			17757
4.5				1	55	2120	3936	1505	512	185	63	46	48	8	5	0	1			8485
5.5					1	172	1135	1455	582	189	29	24	11	8	1					3607
6.5							142	449	417	221	42	13	7	0	1					1292
7.5							7	70	143	112	44	19	6	0	1					402
8.5								8	29	61	31	12	8	3						152
9.5								1	6	17	25	14	13	1						77
10.5									1	7	9	7	7	1						32
11.5												3	5	4	0					12
12.5															1					1
	84	2549	13727	23511	30233	30900	25325	17180	10513	5994	3315	1362	678	411	169	63	30	7	2	166053

Figure 3.2: *Scatter diagram of the Ekofisk field during 56 years [Aarsnes, 2015]*

This data is essential for fatigue analysis. The values of T_P and H_S is distributed within each sea states, however the mean values is the only values considered in this work, i.e. for a sea state with a period in the range $T_P \in [2, 3]$ seconds will be treated as 2.5, even though the values will be spread throughout the whole 2 to 3 interval. Significant wave heights bellow 2m is considered to be uninteresting and are not included in the analysis.

3.4   Current

Current creates forces on the members introduced in the drag term as an additional velocity. Currents are slowly varying with time, and can be considered steady

compared to wave actions. The importance of current might be illustrated by equation 3.3. Wherein the drag term of Morison's equation is proportional to the square of velocity. In the most critical sea conditions regarding fatigue for this particular platform the wave induced water particle speed in the upper part of the water column is in the range of 1.3m/s to 2m/s.

$$(u_w + u_c)^2 = u_w^2 + 2u_w u_c + u_c^2 \tag{3.3}$$

u_w is wave induced water particle velocity and u_c is velocity from current. As the current is constant in nature it is possible to think that it will have low effect on the fatigue damage. However as illustrated in equation 3.3 there exist a cross term. This term will be oscillating due to the wave induced velocity, and be amplified by the current. For a case of a typical current of 0.3 m/s in combination with an important sea state of $H_S = 4.5$ and $T_P = 8.5$ gives a characteristic wave particle velocity amplitude in the upper part of the water column of $u_w =1.7$ m/s. This will give the following amplitudes on the oscillating part of the drag force.

$$u_w^2 + 2u_w u_c = 1.7^2 + 2(1.7)(0.3) = 2.9 + 0.9 \tag{3.4}$$

For this rare current condition, the current will contribute to increase the total oscillating wave particle amplitude by 30%. However the drag term also has a sign change which for low currents will reduce the importance of the cross term.

$$|u_w + u_c|(u_w + u_c) \tag{3.5}$$

Assuming that the current is lower than the wave particle amplitude the range between an amplitude and a valley in equation 3.5 will hence be

$$(u_w + u_c)^2 + (u_w - u_c)^2 = u_w^2 + u_c^2 \tag{3.6}$$

Which is still relying on the current. However if the current is small compared with the wave particle velocity it will no be as important. Figure 3.3 is included to illustrate this. Due to the sign change, the the amplitude of the valleys will increase and the range will hence not grow as fast as if the sign change did not take place.
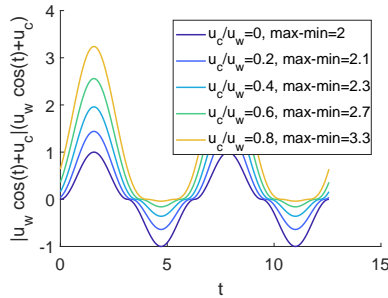
Figure 3.3: *Oscillating drag term for different currents*

Considering that the most important sea state has low to moderate wave particle velocity there is a possibility that current will contribute a lot to fatigue damage. In general, fatigue damage is proportional to the stress amplitude to the power of m. Where m is typically between 3 and 5. In practical terms this means that a stress increase of 15% will result in $1.15^5 = 2$ times the damage. In terms of load amplitude, 15% increase is present when the current is 40% of the wave particle amplitude.

Even though current is an important parameter for drag, it also introduces certain complexity to the process of linearizing the problem. Hence current is neglected in this work.

3.5 Wind

Wind has a much lower density than water, and gives in general lower magnitude of forces than wave actions. Wind do however add certain damage to a structure. What is interesting in this regard is the huge air gap of 43 meters. This might be even larger at certain locations. This is interesting because wind speed increases with the height above the sea. A logarithmic increase in wind speed are commonly used. Such a logarithmic relation can be seen in equation 3.7 [DNV GL, 2014a].

$$V(z) = \tau \ln \left(\frac{z}{z_0} \right) \tag{3.7}$$

Where U is wind speed, z distance from mean sea level, τ and z_0 are constants. Most of the wind forces will be induced on the deck hull due to its structural shape, and this is the highest part of the structure. This gives a higher wind force than a regular air gap of 20 meters. However the logarithmic function will not grow in huge scales by increasing z. The more important is the additional height added to the overturning moment arm. Large wind speeds tends to coincide with large sea states, and hence they should be included in an analysis. However wind is not considered in this work.

Chapter 4

Loads and responses

4.1 Equation of motion for dynamic and quasi static analysis

Newton's second law of motion form the basis of the dynamic equilibrium equation.

$$\mathbf{F} = m\mathbf{a} \tag{4.1}$$

$\mathbf{F}$ = Sum of forces
m = mass
$\mathbf{a}$ = acceleration

By moving damping forces and restoring forces to the same side as the mass and acceleration, the discrete dynamic equation for the finite element method becomes equation 4.2.

$$\mathbf{M\ddot{r}}(t) + \mathbf{C\dot{r}}(t) + \mathbf{Kr}(t) = \mathbf{f}(t) \tag{4.2}$$

$\mathbf{r}, \dot{\mathbf{r}}, \ddot{\mathbf{r}}$ = response, and time derivatives of response
$\mathbf{K}$ = Stiffness matrix
$\mathbf{M}$ = Mass matrix
$\mathbf{C}$ = Damping matrix
$\mathbf{f}(t)$ = Load vector
t = time

The quasi static equation is governed under the assumption of negligible accelerations and velocities. This results in equation 4.3. The matrices and force vector in these equations are discussed in the context of USFOS in the following sections.

$$\mathbf{Kr}(t) = \mathbf{f}(t) \tag{4.3}$$

4.1.1 Mass matrix

The mass matrix have two contributions, the mass of the structure itself, and the hydrodynamic added mass. The structural mass matrix can be set to either consistent or or lumped in USFOS [Søreide et al., 1993]. The consistent, which is used in this project, is based on interpolation functions for linear 3D beam. This implies that it is not a truly "consistent formulation" with the more complex shape functions used for the stiffness matrix. This is still accurate enough for most practical purposes [Marintek, 2001]. The consistent mass matrix for a 6 dof beam element is given by [Søreide et al., 1993]

$$
\mathbf{m} = \frac{\bar{m}l}{420}
\begin{bmatrix}
140 & 0 & 0 & 70 & 0 & 0 \\
0 & 156 & -22l & 0 & 54 & 13l \\
0 & -22l & 4l^2 & 0 & -13l & -3l^2 \\
70 & 0 & 0 & 140 & 0 & 0 \\
0 & 54 & -13l & 0 & 156 & 22l \\
0 & 13l & -3l^2 & 0 & 22l & 4l^2
\end{bmatrix}
\tag{4.4}
$$

$\mathbf{m}$ = element stiffness matrix
$\bar{m}$ = mass per unit length for beam
l = length of beam

The added mass forces have its origin in the radiation problem. The added mass forces are proportional to the accelerations of the members. Thus it behaves as a "added" mass in the dynamic equilibrium equation. The added mass is calculated by the following equation in USFOS [Marintek, 2010].

$$
dF_A = \underbrace{\frac{\rho_w \pi D^2}{4}(C_M - 1)dz}_{\text{Added mass}} \ddot{r}
\tag{4.5}
$$

dF_A = infinitesimal force on element
ρ_w = density of water
C_M = Innertia coefficient
D = Hydrodynamic diameter
dz = infinitesimal lenght
$\ddot{r}$ = acceleration of element

4.1.2 Stiffness

USFOS utilizes a finite element formulation that includes geometrical nonlinearity. For an elastic beam element the internal strain energy is written in equation 4.6 [Marintek, 2001].

$$
U = \underbrace{\frac{1}{2}\int_0^l EA(u_{,x} + \frac{1}{2}v_{,x}^2 + \frac{1}{2}w_{,x}^2)^2 dx}_{\text{Axial stiffness}} + \underbrace{\frac{1}{2}\int_0^l (EI_z v_{,xx}^2 + EI_y w_{,xx}^2) dx}_{\text{Bending stiffness}}
\tag{4.6}
$$

E = modulus of elesticity
A = cross sectional area of beam
l = length of beam element
v, w = lateral displacement
u = longitudinal displacement
I_z, I_y = Second moment of area

The potential of the external loads is written [Marintek, 2001].

$$H = -(F_i u_i + \int_0^l q_x u dx + \int_0^l q_y v dx + \int_0^l q_z w dx) \tag{4.7}$$

F_i = Point load in direction i
u_i = displacement direction i
q_x, q_y, q_z = Distributed loads

The variation of strain energy given in equation 4.8 is used to formulate the stiffness matrix.

$$\delta U = \int_0^l EA u_{,x} \delta u_{,x} dx + \int_0^l EI_z(v_{,xx}\delta v_{,xx} - \frac{N}{EI_z}v_{,x}\delta v_{,x})dx$$
$$+ \int_0^l EI_y(w_{,xx}\delta w_{,xx}\frac{N}{EI_y}w_{,x}\delta w_{,x})dx - \int_0^l (N + EA u_{,x})\delta u_{,x}dx \tag{4.8}$$

The element displacements are represented by shape functions ϕ^T. Test functions are also expressed in the same way.

$$u(x) = \phi^T q_u \tag{4.9}$$
$$v(x) = \phi^T q_v \tag{4.10}$$
$$w(x) = \phi^T q_w \tag{4.11}$$

For transverse displacement, the shape functions from the exact solution to the 4th order differential equation for beams is used. For compression this reads,

$$\phi^T = [\cosh(kx), \sinh(kx), x/L, 1] \tag{4.12}$$

And for tension;
$$\phi^T = [\cos(kx), \sin(kx), x/L, 1] \tag{4.13}$$

k^2 $= \frac{|N|}{EI_z}$

Similar expressions are used for the displacement fields w(x) and u(x). A great benefit for this type of element is that it allows simple modeling e.g. one element per member [Marintek, 2001].

4.1.3   Damping

Both structural damping and hydrodynamic damping is present. The hydrodynamic damping is included in the force vector due to the relative velocity in Morrison's equation. Rayleigh damping is used for structural damping. Raleigh damping holds important orthogonality properties.

$$\mathbf{C} = \alpha_1 \mathbf{M} + \alpha_2 \mathbf{K} \tag{4.14}$$

α_2 = coefficient
α_1 = coefficient
$\mathbf{M}$ = Mass matrix
$\mathbf{C}$ = Damping matrix
$\mathbf{K}$ = Stiffness matrix

The Rayleigh damping has one term that is proportional to the mass matrix and one that is proportional to the stiffness matrix as seen in equation 4.14. Mass and stiffness are orthogonal, thus the damping matrix formed by Raleigh damping must be orthogonal. This enables the writing of equation 4.15.

$$\xi = \frac{1}{2}\left(\frac{\alpha_1}{\omega} + \omega\alpha_2\right) \tag{4.15}$$

ξ = Damping ratio
ω = Frequency

The two coefficients can be used to specify the damping ratio at two frequencies. The structural damping ratio should be 2-3% and soil damping 0-2% according to [DNV GL, 2015]. Soil damping is neglected in this work. By specifying the damping ratio at two frequencies, two equations can be established, and used to find α_1 and α_2.

ξ	f
0.3	0.05
0.3	1

Table 4.1: *Damping ratio*

The damping ratio curve generated by Table 4.1 is depicted in figure 4.1, where the red points are the ones given in Table 4.1. It is important to have structural damping also for the larger sea states, thus the frequency of 0.05 is selected as the lower limit, corresponding to a period of 20 s. Waves of significance are not asociated with frequencies above 1 Hz (period of 1 s), thus this is selected as the upper limit. The damping is at least 1.5% in the most important interval between 0.05 and 1 Hz, and not above 3 which is the upper limit in [DNV GL, 2015].
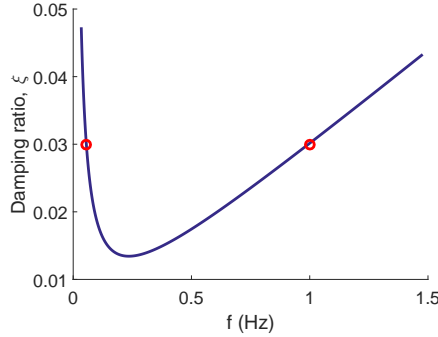
Figure 4.1: Damping ratio as a function of frequency

4.1.4 Forces

Strip theory is assumed sufficient to describe the forces acting on the cylindrical members. Strip theory is used together with Morisons's equation to describe the forces acting on the structure. Morison's equation is given in equation 7.1 [Marintek, 2010].

$$dF = \underbrace{\frac{1}{4}\rho\pi D^2 C_M a}_{\text{Inertia}} + \underbrace{\frac{1}{2}C_D\rho D u_{rel}|u_{rel}|}_{\text{Drag}} \qquad (4.16)$$

ρ = Density of fluid
D = Diameter of pipe
C_M = Inertia coefficient
C_D = Drag coefficient
a = Fluid acceleration perpendicular to cylinder
u_{rel} = $u_x - \dot{r}$ Relative fluid speed perpendicular to cylinder

In order for the Morison's equation to be valid, long waves are required [Faltinsen, 1993]. In practical application the validity limit $\frac{\lambda}{D} > 5$ is often used. The largest structural members of the jack-up have a diameter of 0.75m. For linear potential theory with deep water assumptions this implies that the lowest valid wave period is according to equation 4.17. Wave periods bellow this limit is associated with small amounts of energy and are not critical.

$$T > \sqrt{\frac{10\pi D}{g}} = 1.5s \qquad (4.17)$$

T = Wave period
D = Diameter of pipe
g = gravity acceleration

31

What should be noted is that the drag term has a nonlinear dependency on fluid speed. It also results in force components oscillating with different frequencies. A decomposition of the drag term results in the followingg different frequencies.

$$\sin(x)|\sin(x)| = \frac{8}{3\pi}\sin(x) - \frac{8}{15\pi}\sin(3x) + \frac{8}{105\pi}\sin(5x)... \qquad (4.18)$$

Equation 4.18 and figure 4.18 illustrates how the drag term contains several frequency components. This induces responses in several frequencies for a structure subject to a regular wave with one frequency component. Hence in general, care should be taken at waves that oscillates at three times the eigenperiod of the structure. However for this structure the period of the waves at three times the egienperiod of the structure will be 23s, which is both a period that is rare, and that are seen in combinations with small wave heights.
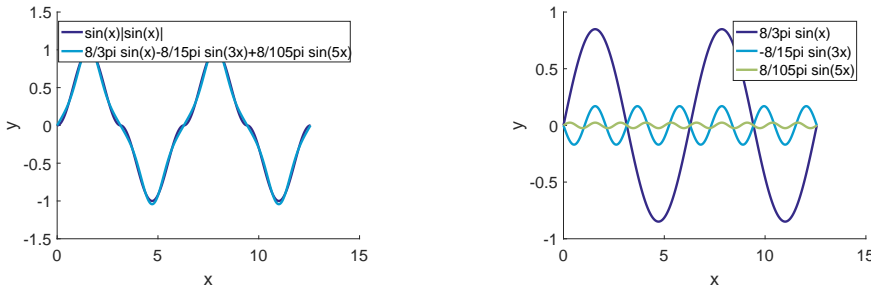
Figure 4.2: Decomposition of the drag term

4.1.5 Linear wave kinematics

Linear theory is used in order to describe wave kinematics. Linear theory is not considered to give a sufficient representation of the kinematics in the surface area, and at least second order wave kinematics should be used in a design process. In this work the drag coefficients are tweaked in order to compensate for the difference between linear and higher order theory. Linear theory is based on certain basic assumptions.

- Incompressible fluid
- Inviscid fluid
- Irrotational fluid motion
- A velocity potential can be used to describe the fluid field

In addition to this kinematic boundary conditions and dynamic free-surface condition are applied. For a regular wave component this results in the velocity potential,

wave elevation, fluid particle speed, and acceleration found in equation 4.19 to 4.24 [Faltinsen, 1993]. This are kinematics acting in the xz plane.

$$\phi = \frac{g\zeta_a}{\omega} e^{kz} \cos(\omega t - kx) \tag{4.19}$$

$$\zeta(t) = \zeta_a \sin(\omega t - kx) \tag{4.20}$$

$$u = \omega \zeta_a e^{kz} \sin(\omega t - kx) \tag{4.21}$$

$$w = \omega \zeta_a e^{kz} \cos(\omega t - kx) \tag{4.22}$$

$$a_x = \omega^2 \zeta_a e^{kz} \cos(\omega t - kx) \tag{4.23}$$

$$a_z = -\omega^2 \zeta_a e^{kz} \sin(\omega t - kx) \tag{4.24}$$

Due to linear theory several frequency components can be achieved by simply superposition of waves with different frequencies.

4.1.6 Drag coefficient for linear wave theory and higher order wave theory

The general consensus is that higher order wave theories is necessary to insure a correct representation of the wave kinematics. However this is a procedure that increase the computational demand significantly. If linear potential theory is used, a simplification that can be used to compensate for nonlinear effects is to increase the drag coefficients in a way that gives similar forces [NORSOK, 2007]. In linear potential theory the wave kinematics are just defined up to the mean surface elevation meaning that values above this needs to be extapolated somehow. The method used in this work, and that NORSOK has defined in combination with increased drag coefficient is by wheeler stretching. This both stretches the kinematics up to wave crest level, but also down to wave through. The stretching is carried out according to equation 4.25.

$$z' = (z - \zeta)\frac{d}{d + \zeta} \tag{4.25}$$

z' = new depth variable
z = old depth variable
ζ = surface elevation
d = depth

The drag coefficients recommended in NORSOK for both the stretched first order, and higher order theory is given in table [NORSOK, 2007].

	C_D	z values
1st order stretched	1.15	$z > 2(m)$
1st order stretched	1.15	$z \leq 2(m)$
Higher order wave theory	0.65	$z > 2(m)$
Higher order wave theory	1.05	$z \leq 2(m)$

Table 4.2: Coefficients in Morison's equation for perfectly cylindrical members

4.1.6.1 Braces

The braces have regular circular cross section, which makes it possible to select drag coefficients according to Table 4.3. The coefficients used for the braces in this work, is given in Table 4.3, this is based upon what is recommended in [NORSOK, 2007], and [Goncalves, 2017].

C_D	C_M	z values
1.15	2.0	$z > 2(m)$
1.15	1.8	$z \leq 2(m)$

Table 4.3: Coefficients in Morison's equation for braces

4.1.6.2 Chords

The chords are not perfectly tubular, due to the rack that are mounted on the chords. These racks are used to elevated the legs. However these racks induces irregularities in the legs geometry and hydrodynamic properties. The legs will have a different hydrodynamic profile depending on direction. This cross sectional area can be seen in figure 4.3.
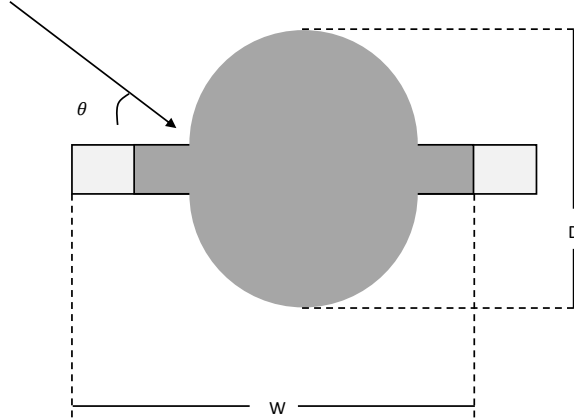
Figure 4.3: *Chord cross sectional area. The different color at the tips indicates that these are the areas which the gears are*

The drag coefficient is adjusted to compensate for these irregularities in geometry. For such cross sectional areas as the on above the relation in equation 4.26 [DNV GL, 2014a]

$$C_D = C_{D0} + (C_{D1}\frac{W}{D} - C_{D0})\sin^2(\frac{9}{7}(\theta - 20°))$$

(4.26)

For cases where $20° \leq \theta \leq 90°$, W and D is defined as in figure 4.3, and for this structure the ratio between them is $\frac{W}{D} = 1.05$. The C_{D0} is the the regular coefficient used for cirvular cylinders, and the C_{D1} is the drag coefficient for flow normal to the rack ($\theta = 90°$). For a wave heading in the x-direction, the chords in this structure will either have θ equal 90° or 60°. For the structure this results in the drag coefficients given in Table 4.4.

C_{D1}	C_{D0}	z values	C_M	C_D for $\theta = 90°$	C_D for $\theta = 60°$
2.04	0.65	$z > 2(m)$	2.0	2.14	1.56
2.04	1.05	$z \leq 2(m)$	1.8	2.14	1.71

Table 4.4: *Drag coefficients for chords, z is the distance from the mean surface level, positive upwards.*

Linear irregular Gaussian sea surface is to be used in the analysis. In order to

compensate for this, an increased drag coefficient can be used [NORSOK, 2007]. This is achieved by letting the drag coefficient be 1.15 over the whole depth for regular cylinders. However in this case the drag depend on the angle and geometry. Thus the same scaling is used for the drag coefficient for the chords as for regular cylinders. This involves a scaling of $\frac{1.15}{1.05}$ for the original coefficients valid for depths above +2m, and let this drag coefficient be valid for the whole depth.

z values	C_M	C_D for $\theta = 90°$	C_D for $\theta = 60°$
$z > 2(m)$	2.0	2.34	1.87
$z \leq 2(m)$	1.8	2.34	1.87

Table 4.5: *Drag coefficients for chords, with the use of NORSOK scaling to compensate for Gaussian sea surface.*

4.1.6.3 Comparison of higher order kinematics and adjusted stretched kinematics

In order to tell weather or not the adjusted drag coefficients are conservative or not, the wave kinematics and drag forces for one case is investigated. 5th order stoke waves are used as reference, and a regular wave component is stepped through the structure, and investigated under the crest and through. This results in the velocity to depth relations given in figure 4.4.
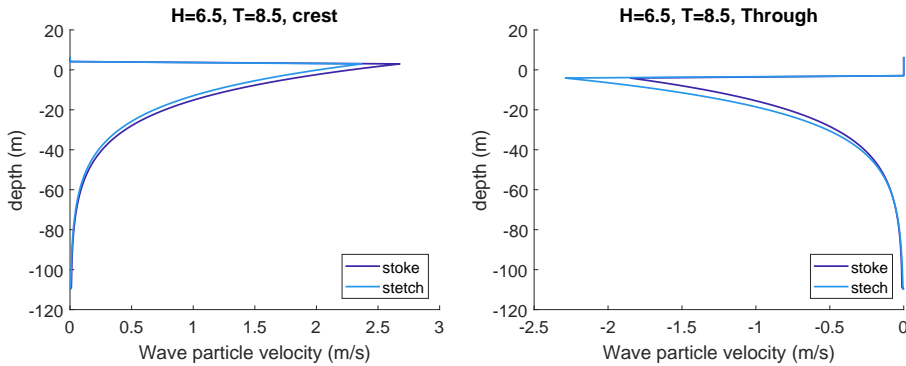
Figure 4.4: *Wave particle velocity under crest and through for 5th order stoke waves, and stretched airy waves*

The nonlinear wave has a larger maximum wave particle speed achieved under the crest. Under the through however the stretching is the conservative. The resulting forces are also of interest to compare. By dividing the drag forces by the terms not of interest, a comparison can easily be carried out. This is the parameters except drag coefficient and velocity, and is given in equation 4.27.

$$\frac{F_D}{0.5D\rho} = C_D|u|u \tag{4.27}$$

The results for drag forces acting on the chords that has a 60 degree angle on the flow, the chords with 90 degrees angle on the flow and the braces are all included under the though and crest in figure 4.5. The maximum forces are experienced under the wave crest, and under the wave crest, the adjusted coefficient for linear theory closes the gap in force between linear and stokes 5th order wave kinematics. It is still not conservative when the largest force is considered. However under the through, the adjusted coefficient with stretching gives much larger forces than the higher order wave kinematics with regular drag coefficient. Considering the high degree of dynamics that this structure inherit, it is not unlikely that this is actually conservative due to the larger change in force between through and crest. In addition to this, fatigue is sensitive to stress range, and not peak. If the range in force is larger, the range in stress is also probably larger. Hence it is assumed that the adjusted drag coefficient is a conservative approach for fatigue analysis. Considering the scope of this work, it will neither be constructive usage of time to work with higher order irregular wave kinematics.
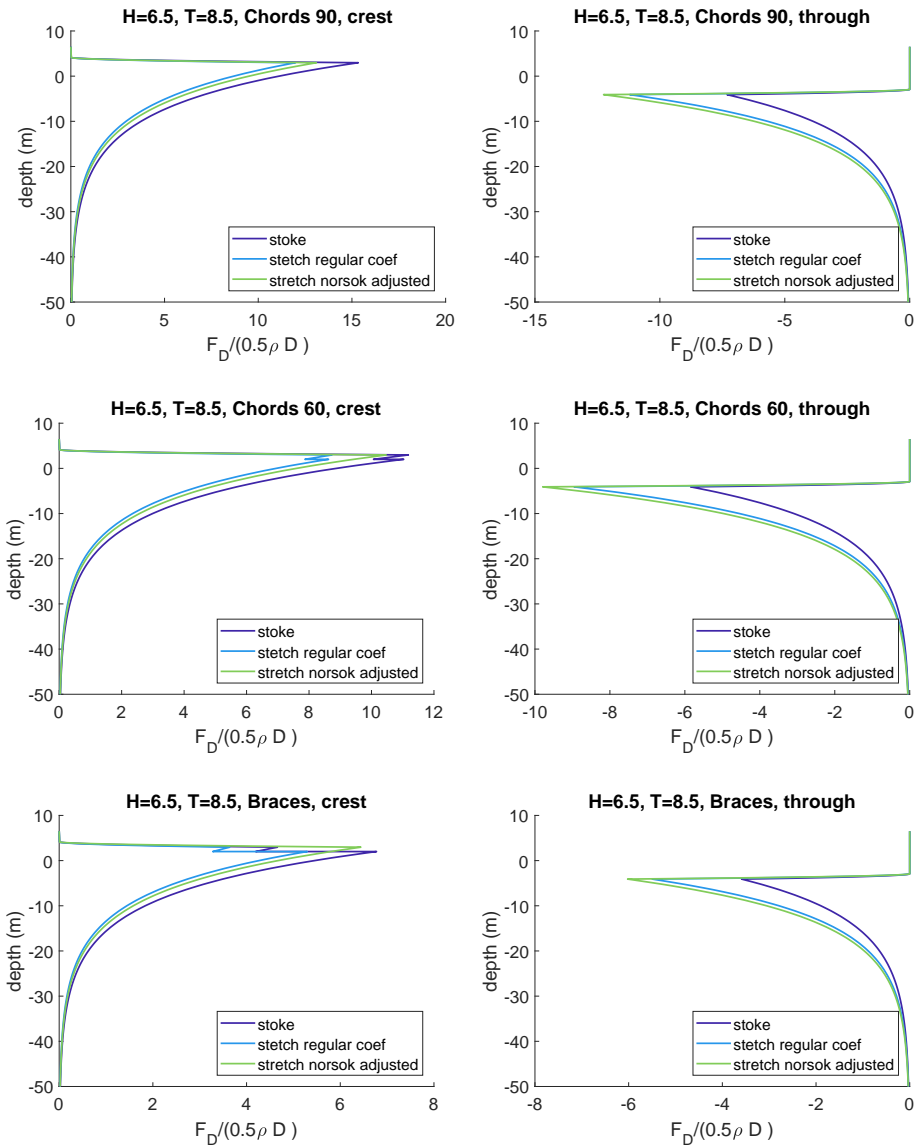
Figure 4.5: *Difference in forces for linear theory and higher order wave theory, for one wave component. Discontinuities are due to change in components at +2m*

4.2   Spring connections to ground

Different types of ground fixation exist for jackups. Two such types are exemplified in figure 4.6. These systems utilizes the platform weight to be pushed down into the ground, which fixates the legs in terms of bending and translation.
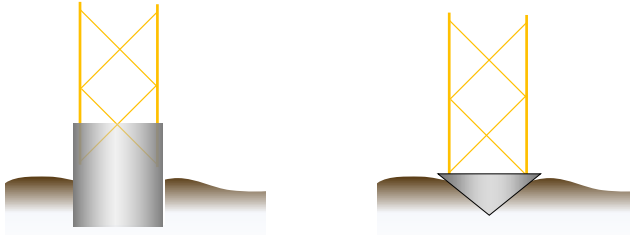
Figure 4.6: Different types of ground fixation

Structural integrity relies on bottom conditions. Overturning stability, stiffness, responce at resconance etc. are all influenced by the bottom conditions [DNV GL, 2015]. Bottom conditions vary from location to location, and should be modeled accordingly [DNV GL, 2015]. With no specific location for this report, the values in Table 4.6 are used. These values gives quite a dynamic structure with a resonance period of above 7 seconds.

Figure 4.7: Bottom model of one of the legs. Left: rotation springs, Right: Translation springs

The bottom conditions are modeled as in figure 4.7. The bottom end of the leg are modeled with larger pipe sections. In addition rotational and translational springs are attached to the bottom node.

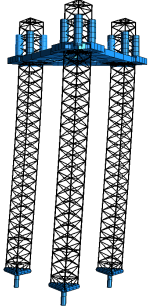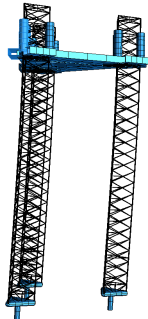| Spring coefficient	Assigned value
k_x	4.000E+10 (N/m)
k_y	4.000E+10 (N/m)
k_z	5.000E+10 (N/m)
$k_{\theta x}$	5.157E+10 (Nm)
$k_{\theta y}$	5.157E+10 (Nm)
$k_{\theta z}$	1.500E+10 (Nm)

Table 4.6: *Spring coefficients*
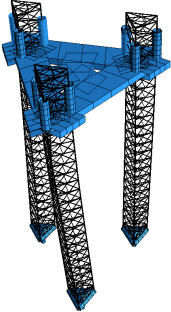
4.3 Eigenvalue analysis

Eigenfrequency or natural frequency are the oscillating periods the structure experiences in the absence of damping and external forces. These periods are important structural properties, and force excitation oscillating at these periods will result in large responses. Equation 4.28 defines the eigenfrequencies [Langen and Sigbjornsson, 1986], and these can be solved in USFOS.

$$(\mathbf{K} - \omega_n^2\mathbf{M})\mathbf{r}_n = 0 \tag{4.28}$$

The amount of wetted surface and hence the water depth has a large influence on the eigenfrequency due to the change in the added mass, which is also included in the mass term, $\mathbf{M}$. The eigenfrequency is also heavily reliant on the ground conditions, due to the boundary conditions huge influence on the stiffness matrix $\mathbf{K}$. The 3 largest eigenperiods are presented in Table 4.7 alongside with the mode shape.

A lot of smaller eigenperiods also exist for the structure. These are presented in the bottom of Table 4.7 and have different modes. As described in Section 4.1.4, excitations with smaller periods than the wave period are present in the drag term in Morison's equation. This might result in smaller amplitude oscillations that might hit the smaller eigenperiods. However these oscillations are so small in size, that it is probably not of any concern.

Eigenmode	Eigenperiod
Translation in yz plane	7.67s
Translation in xz plane	7.67s
Twisting about z axis	6.75s
Smaller eigenperiods	0.609s 0.607s 0.590s 0.588s 0.587s 0.565s 0.536s 0.534s 0.534s 0.533s

Table 4.7: Eigenperiods and eigenmodes

4.4 Solving the dynamic and quasi static equation of motion

The solving of quasi static equilibrium is rather easy, and is in principle the same as solving a static problem at every time step. For linear analysis this consist of inverting the stiffness matrix and multiply the inverted matrix with the force vector. This is done at every time step, and the stiffness matrix does not change with time as long as buckling and yielding does not occur.

$$\mathbf{r}(t_n) = \mathbf{K}^{-1}\mathbf{f}(t_n) \tag{4.29}$$

The solution of the dynamic equation 4.2 is much more complex. In order to solve the dynamic equation, time integration schemes are utilized. A lot of different time integration schemes exists, with different properties regarding accuracy and speed. The newmark beta method is often used in this context, however it has several drawbacks, and can't have both sufficient numerical damping, second order accuracy and be unconditionally stable [Hughes, 2000].

Second order accuracy is beneficial, and considered a necessity if an algorithm should even be considered. Second order accuracy will in practice translate to reducing the error to a $\frac{1}{4}$ by halving the time increment. This allows larger time step to be used compared with first order accurate algorithms, which in turn lead to faster analysis.

Numerical damping is also a vital concept, and necessary to exclude high-frequency oscillations and vibrations not of interest or introduced by finite element discretization.

USFOS uses the Hilber-Hughes-Taylor method, or often refereed to as α-Method. This scheme inherit the advantages from the trapezoidal method of a second order accuracy, while overcoming the problems related to the lack of numerical damping [Hughes, 2000]. The numerical scheme is given by equation 4.30 to 4.32 [Hughes, 2000].

$$\mathbf{M}\ddot{\mathbf{r}}_{n+1} + (1+\alpha)\mathbf{C}\dot{\mathbf{r}}_{n+1} - \alpha\mathbf{C}\dot{\mathbf{r}}_n + (1+\alpha)\mathbf{K}\mathbf{r}_{n+1} - \alpha\mathbf{K}\mathbf{r}_n = (1+\alpha)\mathbf{F}_{n+1} - \alpha\mathbf{F}_i \tag{4.30}$$

$$\mathbf{r}_{n+1} = \mathbf{r}_n + \Delta t \dot{\mathbf{r}}_n + \frac{\Delta t^2}{2}(1 - 2\beta)\ddot{\mathbf{r}}_n + \Delta t^2 \beta \ddot{\mathbf{r}}_{n+1} \tag{4.31}$$

$$\dot{\mathbf{r}}_{n+1} = \dot{\mathbf{r}}_n + \Delta t(1 - \gamma)\ddot{\mathbf{r}}_n + \Delta t \gamma \ddot{\mathbf{r}}_{n+1} \tag{4.32}$$

This integration scheme will be unconditionally stable if α is between 0 and $-\frac{1}{3}$ and the other Newmark parameters are determined by equation 4.33 and 4.34.

$$\gamma = \frac{1}{2}(1 - 2\alpha) \tag{4.33}$$

$$\beta = \frac{1}{4}(1 - \alpha)^2 \tag{4.34}$$

In this work α is set to -0.1, resulting in the parameters in Table 4.8.

α	β	γ
-0.1	0.3	0.6

Table 4.8: *Coefficients for numerical integration*

The selection of time step is important in order to insure good accuracy, but it also has impact of the analysis time. The ideal time step is the largest time step that gives an acceptable accuracy. It is necessary to have a decent accuracy both in amplitude decay and relative period error. These are indicated in figure 4.8 as, amplitude decay: AD, and relative periodical error: $\frac{\bar{T}-T}{T}$. Under the assumption that the system is undamped and freely oscilating, the amplitude decay during one cycle is proportional to the algorithmic damping by a constant 2π.
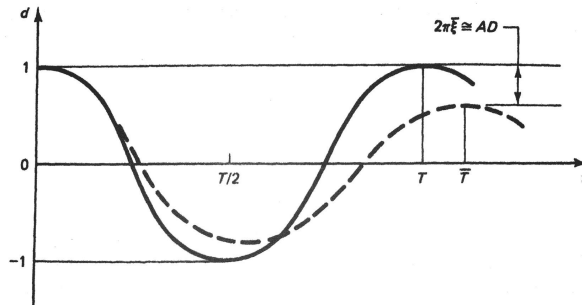
Figure 4.8: *Error in amplitude and period from [Hughes, 2000]*

It is questionable how much these errors can be in order to be acceptable. Time domain simulations is in this work going to be used as a reference. Hence a quite good accuracy is needed. Engineering insight reveals that the response will be primarily in the first 3 modes, where the first three modes is defined as $0 < \omega_1 < \omega_2 < \omega_3$, and can be found in Section 4.3 as $\omega_n = \frac{2\pi}{T_n}$. Enforcing a maximum of 1% relative period error and amplitude decay per cycle is considered to give a good and sufficient accuracy. This results in the criteria given in equation 4.35 and 4.36.

$$AD = 2\pi\bar{\xi} < 0.01 \Rightarrow \bar{\xi} < 0.0016 \tag{4.35}$$

$$\frac{\bar{T} - T}{T} < 0.01 \tag{4.36}$$

The algorithmic damping and periodical error per cycle is given in Figure 4.10 and 4.9, for the alpha method of $\alpha = -0.05$ and $\alpha = -0.3$. By using the graph of $\alpha = -0.3$ the limit of Δt will be conservative. The requirement on amplitude decay from equation 4.35 result in equation 4.37 by using Figure 4.9
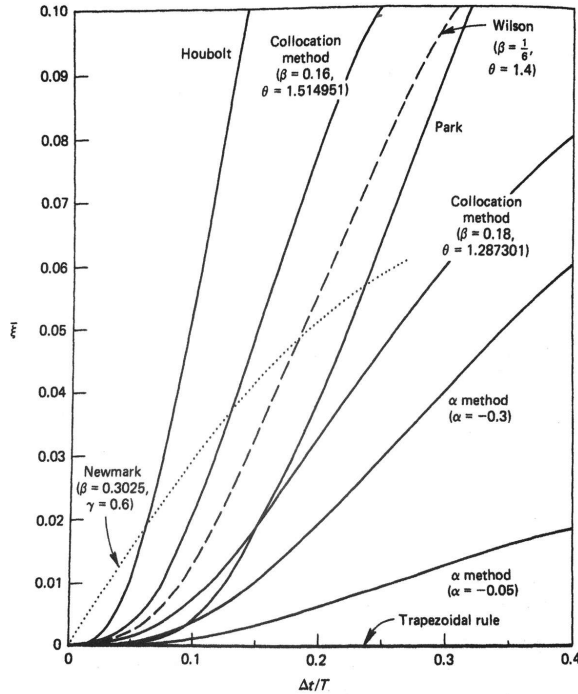
$$\bar{\xi} < 0.0016 \Rightarrow \frac{\Delta t}{T} < 0.08 \tag{4.37}$$

For the relative periodical error, similar result is present in equation 4.38. Here Figure 4.10 is utilized.

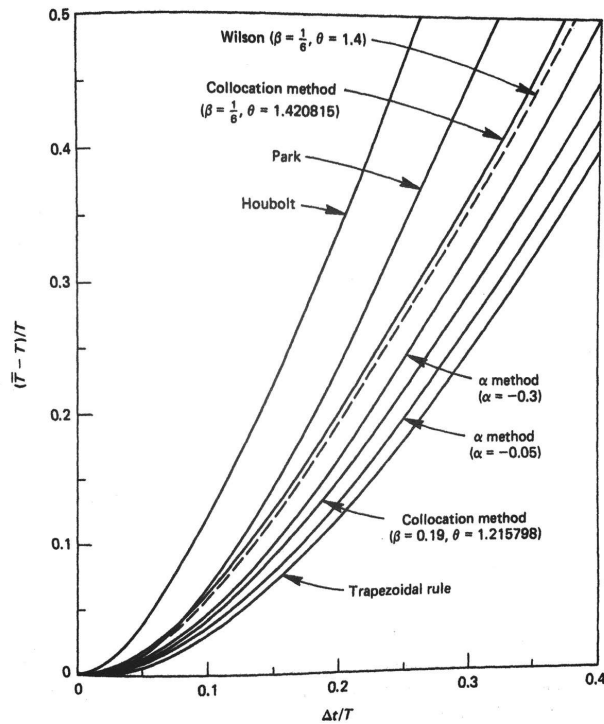$$\frac{\bar{T} - T}{T} < 0.01 \Rightarrow \frac{\Delta t}{T} < 0.03 \tag{4.38}$$

Meaning that relative periodical error will be limiting the time increment. The lowest of the relevant eigenperiod is $T_3 = 6.75$, and hence the time increment is set to

$$\Delta t = 0.03T_3 = \underline{0.2s} \tag{4.39}$$

Figure 4.9: *Algorithmic damping. From: [Hughes, 2000]*

Figure 4.10: *Relative periodical error. From: [Hughes, 2000]*

## 4.5   Overshoot and errors in initial responses

In the initial phase of the analysis the structure has no response displacement or velocities. This in term contributes to a different ratio between loads and responses compared to later in an analysis where the structure is moving along with the waves. There exists different methods to apply the loads in USFOS, they can be gradually applied by an S-curve with a given duration. However this will still not give a true signal since the loads are just partly applied at the initial first seconds. Another aspect that is present is the HHT-α method tendency to overshoot the velocities in the initial first analysis steps. It does not overshoot displacement by nature [Hilber and Hughes, 1978]. However the velocities is used in the forcing term and the damping of the structure. This will in turn will overshoot damping in the initial phase. The overshoot by the HHT-α will eventually die after certain analysis steps as illustrated in figure 4.11. Keep in mind that the scale on the y-axis is logarithmic.
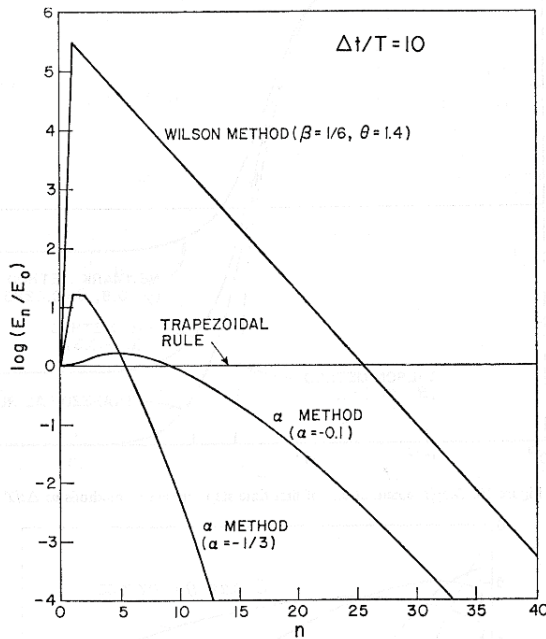
Figure 4.11: *Comparison of energy overshoot for n time steps, from [Hilber and Hughes, 1978]*

These two factors will influence the stress in the initial phase of the simulation. An example case is illustrated in figure 4.12. This is solved by letting the structure stabilize a certain period of time before the time signal is counted. For a 3h stochastic simulation the first 2min is not counted.

When harmonic inputs are used to find dynamic transfer functions, the amplitudes are of interest. In this case the sensitivity is even greater. Hence 4 minutes of stabilization is used in order to capture the response amplitudes.
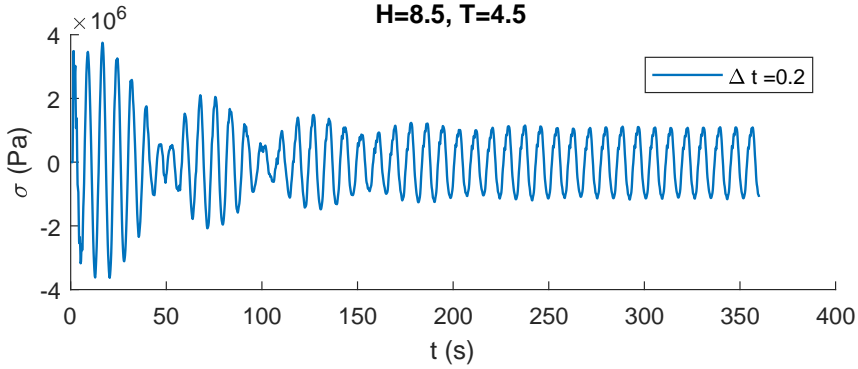
Figure 4.12: *Initial stress with one harmonic input component*

4.6   Irregular sea surface

In offshore environments the sea surface does not behave as an regular sine wave. Waves with such sine surface elevation is referred to as regular waves. Regular waves have simple kinematic relations. A common approach to obtain a surface close to reality, is by summation of several regular wave components.

Sensors have been monitoring the surface elevation in the north sea for decades. This enables the establishment of statistical descriptions of the sea surface. This statistic is utilized in the summation of regular wave components, such that they they as a sum, reflects reality. Equation 4.40 states how such a summation is carried out.

$$\zeta(t) = \sum_{i}^{N} \zeta_{a,i} \cos(\omega_i t + \phi_i) \qquad (4.40)$$

$$\zeta_{a,i} = \sqrt{2S(\omega_i)\Delta\omega_i} \qquad (4.41)$$

ζ = Wave elevation
$\zeta_{a,i}$ = Amplitude of component i
ω_i = Frequency of component i
$\Delta\omega_i$ = Frequency increment i
ϕ_i = Random phase angle between 0 and 2π
N   = Number of components
S(ω)   = Wave spectrum function

Amplitude and frequency of each wave component are determined by the use of short term statistics. 3h is the most used duration of a short term sea state. The description of these short term sea states is in offshore industry introduced as spectrum functions. The spectrum used in this work is the JONSWAP spectrum. This spectrum applies when the growth of the waves is limited bythe size of generation sea Almar-Næss [1985]. The JONSWAP spectrum is given in equation 4.42, and for different values of period and wave height can be seen in figure 4.13.

$$S(\omega) = \alpha g^2 \omega^{-5} \exp\left\{-1.25\left(\frac{\omega}{\omega_p}\right)^{-4}\right\} \gamma^{\exp(-(\omega/\omega_p - 1)^2/2\sigma^2)} \tag{4.42}$$

α = $5.061(1 - 0.287\log\gamma)\frac{H_S^2}{T_P^4}$
γ = 3.3 (a commonly used value, however not always the case)
σ = $\begin{cases} \sigma = 0.07, & \omega \leq \omega_P \\ \sigma = 0.09, & \omega > \omega_P \end{cases}$
ω = angular frequency of wave
ω_P = $\frac{2\pi}{T_P}$
g = Gravitational acceleration

The representation of the sea surface is carried out by dividing the spectrum in several parts and create one wave component for each part. The amplitude of these components is given in equation 4.41. This splitting is illustrated in figure 4.13.
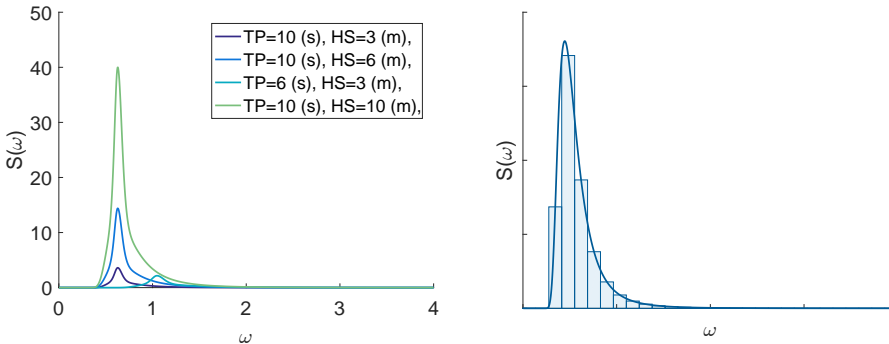
Figure 4.13: *PM spectrum for different sea states and summation technique*

The phase angle gives randomness to the sea surface. This makes sure that each surface realization is different from each other, even though they represents the same sea state.

4.6.1 Alternative integration technique

One issue that arises in the context of spectrum integration is repetition within one signal. The amount of frequencies that is used to represent the sea surface is directly linked to the period when the signal repeat itself.

$$T_{rep} = \frac{1}{\Delta f} = \frac{2\pi}{\Delta \omega} \tag{4.43}$$

When the left integration technique illustrated in figure 4.14 is use, i.e. the simplest, equation 4.43 describes the period at when the signal is repeated. This gives a certain requirement on how many wave components necessary to create a true 3h sea surface, which is not repeated. For 500 wave components, with frequency range at about 1Hz, the repetition period is about 500s, which is far bellow 3h. Increasing the amount of wave components is one solution, but this will increase the computation time by a large amount, and are not feasible. In order to deal with this issue in another way, the integrating technique can be modified as indicated in the left of figure 4.14. By introducing some randomness within each interval, the surface should not repeat itself in such a manner.
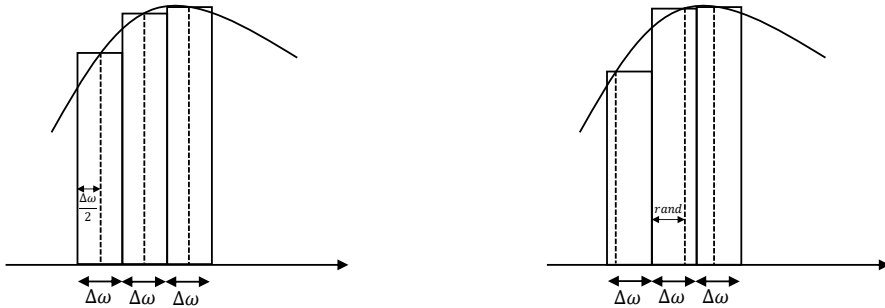
Figure 4.14: *Integration techniques. Without randomness in amplitude (left) with some randomness in amplitude (right)*

In the standard procedure, ω_i is picked as the middle value within one interval. Here, ω_i can be written as in 4.44, where ω_0 is the smallest frequency in the domain.

$$\omega_i = \omega_0 + (i + 0.5)\Delta\omega \tag{4.44}$$

The method illustrated in the right of figure 4.14, introduces a random location of ω_i within one interval. This can in turn be written as equation 4.45.

$$\omega_i = \omega_0 + (i + rnd)\Delta\omega \tag{4.45}$$

The only difference between these two is the rnd, which is a random number between 0 and 1. The one with randomness is supposed not to give the same kind of repeating elevation after T_{rep}. The usual way to give a measurement of repetitiveness is by use of the auto correlation function. For a stationary process it can be written as in equation 4.46, where τ is the lag, and X_t is the signal at time t.

$$R(\tau) = \frac{E[(X_t - \mu)(X_{t+\tau} - \mu)]}{\sigma^2} \tag{4.46}$$

For values of τ which gives $R(\tau) = 1$, a perfect reproduction of the signal is present, with a time lag of τ. In a discrete sense, this can be calculated by equation 4.47 and 4.48 [Box et al., 1994].

$$R_k = \frac{c_k}{c_0} \tag{4.47}$$

$$c_k = \frac{1}{T-1} \sum_{t=1}^{T-k} (X_t - \mu)(X_{t+k} - \mu) \tag{4.48}$$

c_0 is the variance of the time signal and T is the discrete size of the whole signal. The discrete autocorrelation is used to verify that the method with randomness does not reproduce signal in the same sense as the standard procedure.
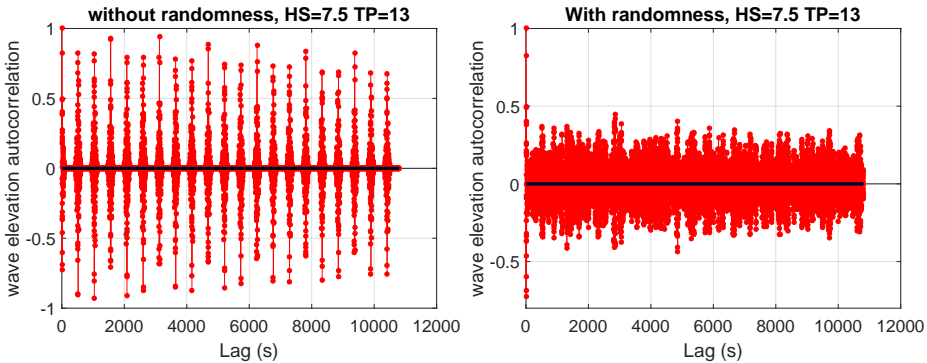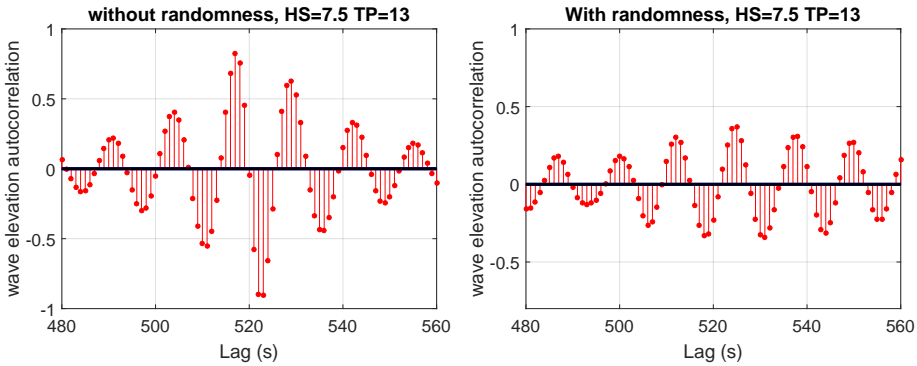

Figure 4.15: *Autocorrelation of surface elevation With and without randomness in amplitude*

In figure 4.15 the autocorrelation for both cases are plotted. In this example, 500 wave components are used and the frequency bonds are set to $f \in [0.04, 1]Hz$. This gives a period of repetition of $T_{rep} = 520s$. In the approach without the amplitude randomness there are large peaks in the autocorrelations at approximately every 520(s) of lag. This indicates that a huge degree of repetition are present at periods equal this lag, and agrees well with previously stated.

The attempt to improve the drawback by adding randomness to the amplitude is clearly working. A true reproduction of the surface is never present within the 3h. The autocorrelation is never above 0.5, which is far from perfectly correlation at 1. Hence this approach is beneficial. Zoomed in version of figure 4.15 is found in figure 4.16. Each of the peaks visible in figure 4.15 has an similar build up as in figure 4.16.

*Figure 4.16:* *Autocorrelation of surface elevation*

The distribution of wave heights should follow a Rayleigh distribution, given that the process is narrow banded [Myrhaug, 2016]. The JONSWAP spectrum can be classified, or at least close to considered narrow banded. It is important that the alternative integration technique tends to follow the Rayleigh distribution. The best graphical way to illustrate how the elevation follow a distribution is by linearizing the distribution, and plot the cumulative distribution in a linearized probability paper.

$$F_H(h) = 1 - \exp\left(-\frac{h^2}{8m_0}\right) \tag{4.49}$$

The Rayleigh cumulative distribution given in equation 4.49 can be linearized by letting the y axis in the plots bee as illustrated in equation 4.50. Then straight lines will be Rayleigh distributed. In these equations, m_0 is a distribution parameter, and h individual wave heights.

$$y = \sqrt{-\ln(1 - F_H(h))} = \frac{h}{\sqrt{8m_0}} \qquad (4.50)$$

In figure 4.17 this is done for one sea state for both methods of integration. It turns out that the alternative method with amplitude randomness outperforms the standard method when it comes to follow the Rayleigh distribution i.e. be a straight line. By increasing the number of components, the distributions tends to be more straight for both integration techniques. However, at only 500 components, the alternative method is already very close to straight, which the standard method is far from. The reason for the vertical behavior of the case without amplitude randomness is linked to the repeated surface elevation. The largest value in every repeated signal will be the same, and hence the resulting vertical lines.
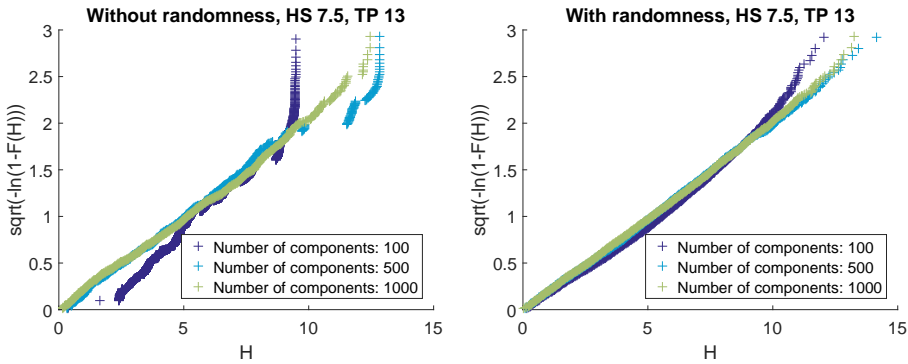
Figure 4.17: *Linearized Rayleigh distributions*

Based on the above argumentation, 500 components in combination with the alternative integration technique are considered to give sufficient results for the rest of the work. The arguments can be summarized as follows:

- The sea surface is not repeated

- It follows the Rayleigh distribution impressively well

- It is enough components to capture the spectrum function well

Chapter 5

Fatigue analysis of tubular joints

Fatigue is a failure mode of materials. It is related to the material stamina rather than material strength. Fatigue damage is present when the material is subject to cyclic loading. Fatigue damages are a result of a three stage process consisting of the following three stages Almar-Næss [1985].

1. Initiation or crack nucleation

2. Crack growth

3. Final failure

Fatigue is dependent on the stress range of the cyclic loading rather than the stress itself. This means that materials subject to cyclic stresses well bellow yield, may experience critical cracks after a certain amount of cycles. This becomes a vital phenomenon for offshore structures due to the cyclic nature of the wave loadings.

5.1 Fatigue damage in this work

This work concerns jack-ups which are mobile units. Their mobility involves several phases of loadings. A few are listed bellow.

- Transit i.e. floating, traveling to new site

- Lifting and lowering legs

- Operation at site, attached to the seafloor

These phases will have different influence on the fatigue life of the structure. The most critical fatigue spots in the process of elevating the legs might be the gears that are used for lifting, while the transit phase might have a part of the hull as

critical spot. The scope of this work however, will be the fatigue damage in leg joints during operational phase.

The fatigue assessments in this work is carried out by the use of Miner summation and SN-curves. The logic of this process can be split in four steps, which are further discussed in details.

1. Beam reactions are achieved by finite element analysis

2. Stress concentration factors (SCF) are used to generate stress processes

3. The amount of cycles at different stress ranges are calculated by the use of rainflow counting

4. Cumulative damage is estimated by the use of Miner summation together with SN-curves

5.2 Joint selection

In order to select critical joints with respect to fatigue damage, a quite detailed screening is necessary in a design process. Considering the scope of the work in this thesis, only a simple screening is carried out. This screening consist of comparing the stresses at the bottom of the legs, and the top of the legs (right under the deck) for a few waves. The joint that turns out to be critical is at the top of the legs.

This might be changed if the springs that models the attachment to sea floor is stiffer than the ones used in this work. Then it is believable that the bottom joints also be significantly subject to fatigue damage.

For simplicity only one of the joints in the top area of the legs is investigated further. The joint selected is indicated with red color in Figure 5.1. The braces used to estimate stresses is indicated with red color.
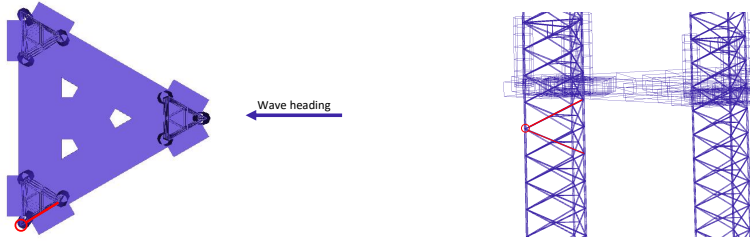
Figure 5.1: *Location of critical joint*

5.3 Miner summation

The load history acting on marine structures has a stochastic nature. They vary in both amplitude and frequency over time. This establishes the need of rules on how to count the cumulative fatigue damage due to the load history. Numerous such rules or theories may be found in the literature Almar-Næss [1985], but Miner summation stand out as a simple and good approach.

The basic assumption for the Miner summation is that the damage contribution for a load cycle is constant at a given stress amplitude. The damage from one such load cycle is given in equation 5.1.

$$D = \frac{1}{N} \tag{5.1}$$

Where D is Damage, and N Endurance of the material at the given amplitude. The cumulative damage from a load history of several different stress ranges can then be written as a sum as given in equation 5.2. Failure will occur when this exceeds 1. The endurance of the material at a given stress amplitude is often described by what is called SN-curves. The SN-curves are described in the next section.

$$D = \sum_i \frac{n_i}{N_i} \tag{5.2}$$

Where D is Damage, N_i Endurance of the material at stress amplitude i and n_i number of cycles at stress amplitude i

5.4 SN curves

In order to obtain material characteristics of fatigue SN, testing is performed. SN testing deals with machined specimens which are exposed to cyclic stress usually at constant amplitudes. However, to a certain level, the mean stress in the material also to some extend contribute to the fatigue life. Several models have been proposed to deal with this Almar-Næss [1985]. The simple idea is displayed in Figure 5.2 where the the allowable ratio between amplitude and mean stress are displayed for different models.
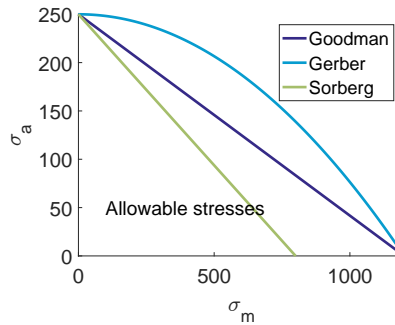
Figure 5.2: *Example on allowable combinations of mean stress and stress amplitude*

These three models are given in equation 5.3 Almar-Næss [1985], where $\sigma_{a,N}$ are the limiting stress amplitude, σ_u ultimate stress and σ_y yield stress. None of these models are valid in general, and are obtained under different test conditions Almar-Næss [1985]. In a jack-up rig there will be mean stresses different from zero in the legs. This is due to constant reactions, including gravity buoyancy etc. However due to the scope of this work, these aspects are not covered, and the problem will be treated as it has zero mean stresses.

$$\text{Modified Goodman: } \sigma_a = \sigma_{a,N}(1 - \frac{\sigma_m}{\sigma_u})$$

$$\text{Gerber relation: } \sigma_a = \sigma_{a,N}(1 - \frac{\sigma_m}{\sigma_u}^2) \qquad (5.3)$$

$$\text{Soderberg relation: } \sigma_a = \sigma_{a,N}(1 - \frac{\sigma_m}{\sigma_y})$$

Design code SN-curves describes the allowable amount of cycles at a given stress range. They are material and detail specific, and obtained by tests. The standard version of a SN-curve is given in equation 5.4 Almar-Næss [1985]. Modifications to this is made in DNV GL design rules with respect to plate thickness effects DNV GL [2015] as seen in eqution 5.5. Furthermore the different parameters depend on

the classification society. The values recommended by DNV GL, will be used in this work.

$$\log(N) = \log(\bar{a}) - m\log(\Delta\sigma) \tag{5.4}$$

$$\log(N) = \log(\bar{a}) - m\log\left[\Delta\sigma\left(\frac{t}{t_{ref}}\right)^k\right] \tag{5.5}$$

N = Allowable cycles
$\log(\bar{a})$ = Interception of the $\log(N)$ axis
m = The inverse negative slope of the SN-curve, can be two slopes, m_1 and m_2
$\Delta\sigma$ = Stress range
t_{ref} = For tubular joints the reference thickness is 32 mm
t = Thickness through which a crack will most likely grow.
    $t = t_{ref}$ is used for thickness less than tref
k = Thickness exponent.

The SN-curves that DNV GL recommends are highly dependent on the local geometry of the particular structural detail. The scope of this work is not related to the actual design of the structure, but rather the investigation of linearizations and how these influence the fatigue life. The choice of SN-curve will not be as important in this context as long as the same SN-curve are used for all the different comparisons. The S-N curve for the detail category T in DNV GL [2014*b*] is selected for analysis by request from DNV GL.

$$m = \begin{cases} 3.0 & , N \le 10^6 \\ 5.0 & , N > 10^6 \end{cases} \tag{5.6}$$

$$\log(\bar{a}) = \begin{cases} 11.764 & , N \le 10^6 \\ 15.606 & , N > 10^6 \end{cases} \tag{5.7}$$

$$k = 0.25 \tag{5.8}$$

The equivalent to equation 5.6 with stress as limit instead of N is given in equation 5.9

$$m = \begin{cases} 3.0 & , \Delta\sigma > 86.26 \text{ MPa} \\ 5.0 & , \Delta\sigma \le 86.26 \text{ MPa} \end{cases} \tag{5.9}$$

5.5 Stresses in joints

Joints and welds are critical locations for development of fatigue cracks. At these locations the concentration of stress are typically a lot larger than locations with a certain distance to the weld. This leads to the need of a careful consideration of the particular joint. As this is not a design paper, large focus will not be given to to describe these stresses in details. Local finite element models with a very fine mesh is typically used to capture detailed stresses in joints. However this introduces a lot of modeling work, as well as increased analysis time. Known relations for tubular joints is here used as an alternative as described in the next section.

5.5.1 Stress concentration factors and super positioning of stresses

Experimental data, analyzes and tests forms the basis of the DNV GL fatigue recommendations. Within this work, known relations for different tubular joints are utilized. Empirical models and relations are made for standard, widely used joints. By the use of these models, no local detailed finite element model is needed. The joint problem is broken down by super positioning the different bending- and axial contributions. As seen in Figure 5.3 the total load is a sum of axial, in plane and out of plane bending moments.
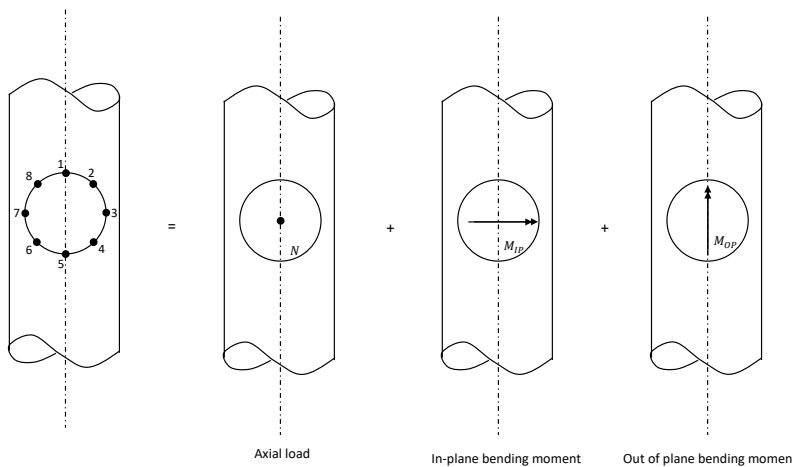
Figure 5.3: *Superposition of joint contributions and the eight locations of stress evaluation*

The stress level is most intensive along the weld of the joint. In order to obtain a good description of these stresses, they are not only evaluated at the saddle and the crown, but also an intermediate value between the saddle and the crown. The

value at these points are derived by a linear interpolation for axial stress, and harmonic interpolation for the bending stress between the saddle and crown. This leads to 8 locations as indicated in Figure 5.3. Here 1 and 5 are the crown, and 3 and 7 the saddle. The rest of the locations are intermediate locations. The stresses at these locations are given by equations containing nominal stresses and stress concentration factors. In equation 5.10 these relations are given.

$$
\begin{aligned}
\sigma_1 &= \text{SCF}_{\text{AC}}\sigma_x + \text{SCF}_{\text{MIP}}\sigma_{my} \\
\sigma_2 &= \frac{1}{2}(\text{SCF}_{\text{AC}} + \text{SCF}_{\text{AS}})\sigma_x + \frac{1}{2}\sqrt{2}\text{SCF}_{\text{MIP}}\sigma_{my} - \frac{1}{2}\sqrt{2}\text{SCF}_{\text{MOP}}\sigma_{mz} \\
\sigma_3 &= \text{SCF}_{\text{AS}}\sigma_x - \text{SCF}_{\text{MOP}}\sigma_{mz} \\
\sigma_4 &= \frac{1}{2}(\text{SCF}_{\text{AC}} + \text{SCF}_{\text{AS}})\sigma_x - \frac{1}{2}\sqrt{2}\text{SCF}_{\text{MIP}}\sigma_{my} - \frac{1}{2}\text{SCF}_{\text{MOP}}\sigma_{mz} \\
\sigma_5 &= \text{SCF}_{\text{AC}}\sigma_x - \text{SCF}_{\text{MIP}}\sigma_{my} \\
\sigma_6 &= \frac{1}{2}(\text{SCF}_{\text{AC}} + \text{SCF}_{\text{AS}}\sigma_x - \frac{1}{2}\sqrt{2}\text{SCF}_{\text{MOP}}\sigma_{mz} \\
\sigma_7 &= \text{SCF}_{\text{AS}}\sigma_x + \text{SCF}_{\text{MOP}}\sigma_{mz} \\
\sigma_8 &= \frac{1}{2}(\text{SCF}_{\text{AC}} + \text{SCF}_{\text{AS}})\sigma_x + \frac{1}{2}\sqrt{2}\text{SCF}_{\text{MIP}}\sigma_{my} + \frac{1}{2}\sqrt{2}\text{SCF}_{\text{MOP}}\sigma_{mz}
\end{aligned}
\tag{5.10}
$$

In the above relations, SCF are stress concentration factors, and σ nominal stresses. AC, AS, MIP and MOP stands for axial crown, axial saddle, Moment in plane, moment out of plane respectively.

These SCF's can be picked from tables for known joint sections. However the geometry for the cross sectional area in the chords is not perfectly circular which illustrated in Figure 5.4. This cross section has a flat bar welded in between the two half parts of the pipe. This flat bar is due to the gearing system used to lift and lower the legs, which introduces more stiffness to the chord. Due to this complex geometry, the stress concentration in the braces are selected for further analysis, and the chord is treated as a circular pipe. The stress concentration in the braces also rely on the stiffness in the chord, but it is assumed that this is not to important. If this was a design paper, this method is not recommended, but for research on linearization it should be sufficient.
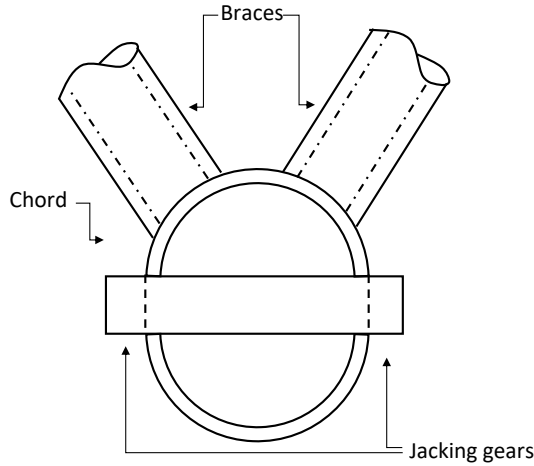
Figure 5.4: *Chord cross sectional geometry*

The SCF's are picked from tables in [DNV GL, 2014*b*]. These are long equations, and reference is here made to appendix B, tubular K-joints, in DNVGL RP-C203 DNV GL [2014*b*]. For the braces this result in the SCF given in Table 5.1.

SCF	Value
SCF_{AC}	3.2155
SCF_{AS}	3.2283
SCF_{MIP}	1.9032
SCF_{MOP}	1.8839

Table 5.1: *Stress concentration factors for braces*

As seen in Table 5.1, the SCF for axial stresses are close to equal in size. This makes the first axial terms in equation 5.10 close to similar. The difference in the 8 spots is thus more influenced by the bending stresses. In Figure 5.5 σ_1 to σ_8 is plotted for a time snip. Bending stress is clearly present, due to the different mean values for all 8 different stresses. What is also possible to see, is that the variation behaves quite similarly.
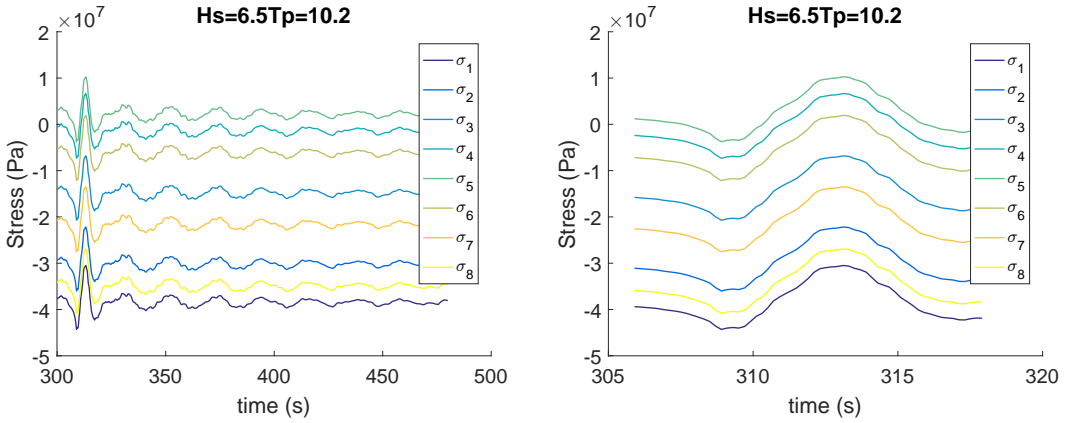
Figure 5.5: Stress process over a short, and shorter time interval

This is investigated further by subtracting the signal mean. Evident in Figure 5.6 where the same stresses are plotted, but with the mean subtracted, is that the signals are very close to equal. This indicates that bending stresses are mainly due to constant loads, such as gravity. This is very beneficial, because then their variation will behave similarly, and variation is the important in context of fatigue. Thus only one of them needs to be concerned. For further analysis only σ_1 will be used.
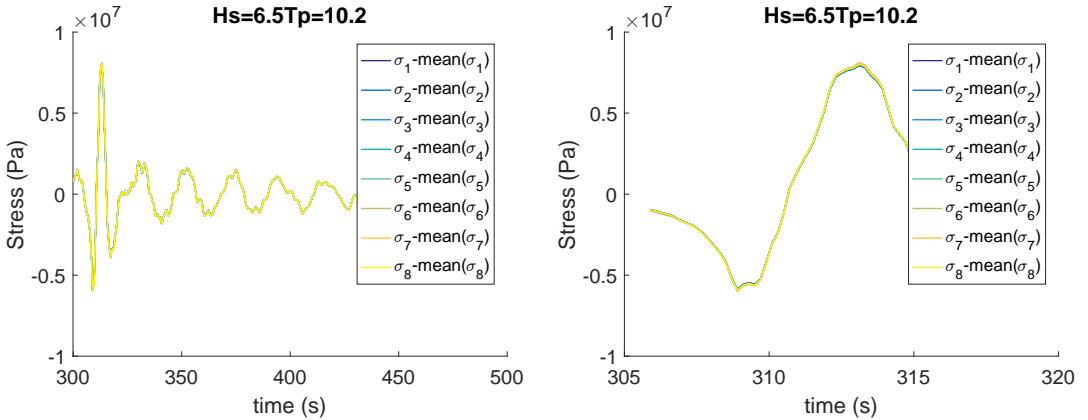
Figure 5.6: Stress process over a short, and shorter time interval

It should be noted that the estimated damage is extremely sensitive to the stress amplitudes. The stress concentration factors needs to be carefully considered, and

in design processes local modeling of this non standard cross section should be considered.

5.6 Cycle counting using rainflow and the WAFO toolbox

For fatigue, the stress range within a cycle, and amounts of cycles are essential. There exist different ways to count cycles for a stochastic process. What is challenging with a stochastic signal compared with regular sine waves are their local peaks and slowly varying cycles. General consensus is that the rainflow counting method is superior to other methods for welded joints in high cycle fatigue Almar-Næss [1985]. The rules of rainflow counting are the following Almar-Næss [1985]:

1. Rain flow down the roof, starting in either the peak or the valley. It drips down when it reaches an edge

2. The rain stops, and the cycle is completed, when the flow reaches another flow falling from above.

3. It also stops when a peak/valley of larger amplitude than where the it started from is encountered.
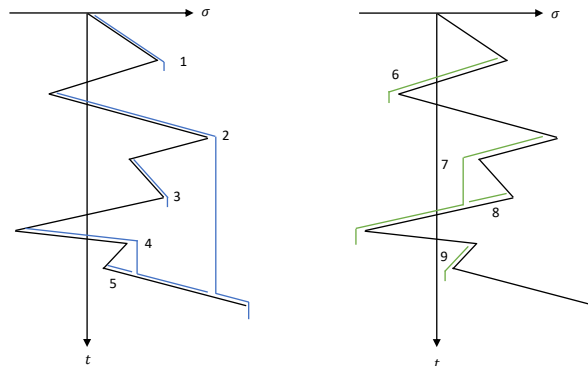
Figure 5.7: *Rainflow counting scheme*

Figure 5.7 illustrates how this algorithm works. In blue, the water is flowing from valleys, and green from peaks. Each of the colored flows represent a half cycle. Cycle 1, 3, 6, 9 are examples on when rule 3 is present. In 4, 5, 8 rule 2 stops the cycle. The WAFO toolbox for MATLAB is used for cycle counting [WAFO-group, 2011]. This toolbox uses the rainflow counting algorithm. One of the difficulties

with the rainflow algorithm might be unpaired half cycles Almar-Næss [1985]. The WAFO toolbox gives an output consisting of cycles. In some cases this means that different half cycles must be paired. The stress ranges have to be sorted in groups, i.e. discretized. For this work 200 levels of stress range will be used. This means that between the largest and the smallest stress range within the time signal, 200 levels are present. A simple signal, consisting of two regular sine waves are used in order to give a certain idea on how this algorithm detects cycles.
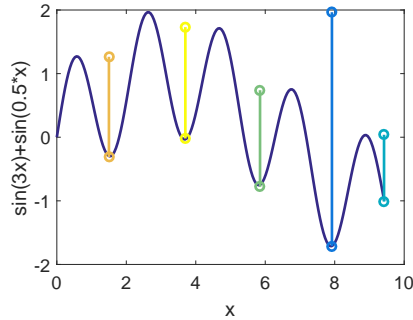
Figure 5.8: WAFO cycles

In Figure 5.8 the different cycles, detected by the WAFO toolbox, are included with colors. The associated signal range are also indicated. If water flows from the peaks, this is exactly the peaks generated by the use of the 3 rules of rainflow algorithm.

It is interesting to compare the rainflow counting with a simple zero up crossing counting. Zero up crossing counting takes the stress range as the maximum minus the minimum value of the signal between two zero up crossings. This is illustrated in Figure 5.9.
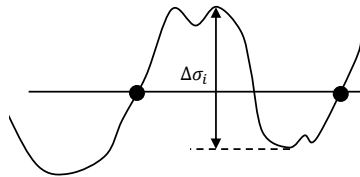
Figure 5.9: Zero up crossing counting. Zero up crossings marked as black dots

The two methods gives very close to the same distributions evident in Figure 5.10. The stress range distributions are plotted in a linearized Weibull probability paper, a plot technique described further in Section 6.2. As expected the largest stress range from the rainflow method is larger than the largest from the zero up crossing

method, however the difference is small. The largest stress range may significantly contribute to the fatigue damage and might be important to capture. The total damage is calculated using miner summation and the SN-curve. The rainflow counting gives a larger damage than the zero up crossing method. However this mighe be considered negligible in this case. Rainflow counting gives 5% more damage.
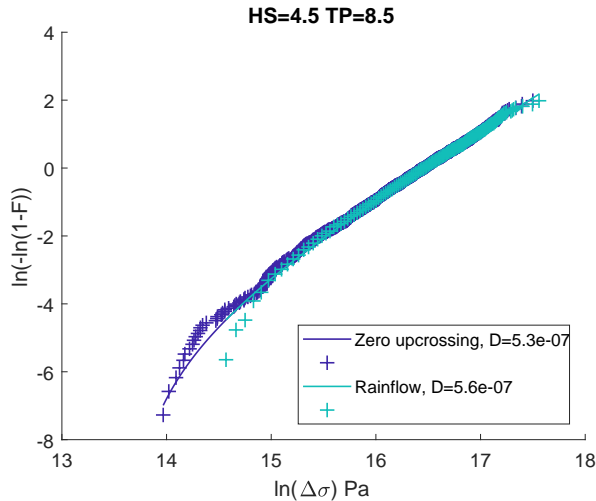
Figure 5.10: *Cumulative distribution in Weibull paper of zero up crossing counting vs rainflow counting. D is the total accumulated damage during 3h*

5.7 Stochastic fatigue analysis in thr frequency domain

A frequency domain analysis is often preferable. For linear problems this will be the most efficient way to carry out a fatigue analysis. In order for a frequency analysis to be conducted the response spectrum has to be known.

5.7.1 Stress response spectrum

A response spectrum is a relation similar to wave elevation spectrum. It states how much energy the system is subject to under different frequency influences. In linear systems the relation between any input spectrum and thr response spectrum can be described by a single transfer function. If the response spectrum is known, two ways can be used to calculate fatigue damage described in Section 5.7.1.2 and 5.7.1.1.

5.7.1.1 Probability distribution

For a narrow band process, which is the result of a resonant system subject to a certain excitation. In such systems there will be $\frac{10800}{T_n}$ cycles during a 3h short term sea state on average. The encountered fatigue damage can then be calculated using equation 5.11 [Newland, 2005].

$$\frac{10800}{T_n} \int_0^\infty \frac{1}{N(\Delta\sigma)} f_{\Delta\sigma}(\Delta\sigma) d\Delta\sigma \qquad (5.11)$$

Where $N(\Delta\sigma)$ is the SN-curve given in equation 5.5. For a kinked SN-curve this involves splitting the integral in two. The probability distribution will for a Gaussian narrow banded process be Rayleigh distributed, and the parameter can be calculated from the response spectrum.

5.7.1.2 Realization of stress process

Even dough Section 5.7.1.1 might be the easiest and most convenient way to estimate the damage, it involves assumptions of Gaussian narrow banded process. This will not always be the case when the system is subject to a sharply peaked input spectrum, which might result in a double peaked response spectrum.

Instead, the stress process can be realized in similar manner as the surface proses is realized described in Section 4.6. Without inverting any stiffness matrices or doing any kind of time integration, a realization of the stress process can be created given that the response spectrum is known. This is obviously a much faster approach than doing time domain analysis. The difficulties however lies within how these response spectra are generated, which will be discussed throughout this thesis. For the cases where they are known, and a realization is generated, the same technique of calculating fatigue as for time domain simulations can be used. This is by using rainflow counting and miner summation.

5.7.2 Discrete Fourier transform of signal

The spectra covered in Section 4.6, creates the foundation of generating time signals. However it is sometimes convenient to go the other way around, to generate spectra from time signals. This includes creating response spectra from response signals.

All signals processed in this work is discrete, hence the Discrete Fourier transforms are used to generate spectra from time signals. When Discrete Fourier transforms are used to create spectra, the estimated spectra becomes very noisy, and are not usable to any practical purposes. This noise however hold certain statistical properties. The distribution of the signals in the estimated spectrum from Fourier

transform, $\tilde{S}(\omega_i)$, can bee approximated by a chi-square distribution with 2 degrees of freedom Newland [2005].

One of the easiest ways to accommodate the noise is by averaging adjacent estimated spectrum values. This is in fact the only possible thing to do in order to improve statistical accuracy [Newland, 2005]. As an example to underline that this will provide a better estimate, the following averaging can be used as an example.

$$S(\omega_i) = \frac{1}{3}\tilde{S}(\omega_{i-1}) + \frac{1}{3}\tilde{S}(\omega_i) + \frac{1}{3}\tilde{S}(\omega_{i+1}) \qquad (5.12)$$

The distribution of the error of this linear combination will be a chi-square distribution χ^2_η with $\eta = 6$ degrees of freedom. For the general case, when $2n+1$ adjacent values are averaged their distribution will have a chi-square distribution with $\eta = 4n+2$ degrees of freedom making it a much more statistical reliable value for increased values n. This is clearly evident in the ratio between standard deviation, s and mean, μ in equation 5.13, which is true for a chi square distribution. By increasing η there is more confidence that the sample measurement lies close to the true mean.

$$\frac{s}{\mu} = \sqrt{\frac{2}{\eta}} \qquad (5.13)$$

However this can only be achieved at the expense of frequency resolution [Newland, 2005]. In order to get insight in how many adjacent points used in averaging that are beneficial, the JONSWAP spectrum is realized with 5000 wave components. The raw one sided spectrum from Fourier transform can be seen in Figure 5.11 as the spectrum with no smoothing.
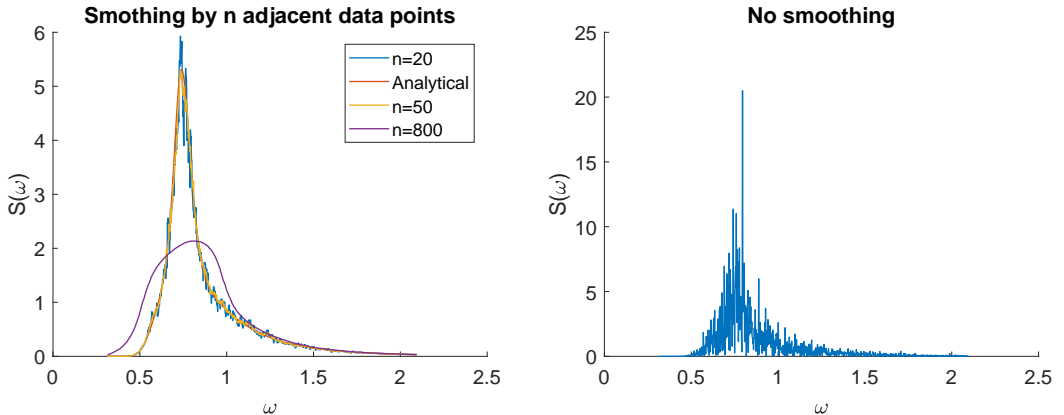
Figure 5.11: *Example of spectrum with and without averaging. JONSWAP with $H_S = 4.5$, $T_P = 8.5$*

When 5000 components are included, n=50 seem like a good value to use in averaging . The higher values of n, gives bad results due to insufficient frequency resolution.

Chapter 6

Time domain simulation

In this chapter, the results from time domain simulations are presented. Time domain simulations are considered the state of the art method to estimate the fatigue damage, and this will be used as reference when linearizations are considered.

The importance of different phenomenons are also investigated such as hydrodynamic damping and dynamic amplification. In addition different realizations of the same sea state are compared.

6.1 Hydrodynamic damping, and dynamic influence

The hydrodynamic damping is included as relative velocity in the drag forces. This damping may significantly contribute to reduce the fatigue damage by damping out the response. Hydrodynamic damping is without doubt present, but whether or not this hydrodynamic model is conservative or not may be questioned. In order to establish a certain understanding on how much damage that is added by removing this damping, a few cases are compared. The stress response from two sea states are included in figure 6.1, and it might be hard to see the difference between damped and undamped response, but the undamped response is slightly larger than the damped. However this small difference might be significant to the fatigue damage.
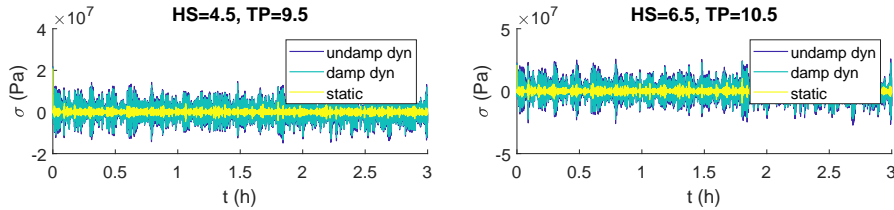
Figure 6.1: *Short term stress repsonse with and without hydrodynamic damping and static analysis*

In table 7.6 some of the most critical sea states when fatigue is considered are included. The damping clearly removes a lot of damage, and about 40-50% of the damage is avoided when the damping is included.

The fact that these particular sea states are the most important with their associated low periods gives rise to another aspect. The largest eigenperiod of the structure is within this region. The largest eigenperiods are 7.67s and 6.75s. Due to this, it is expected that the dynamic effects in the motion will be significant. In figure 6.1 the difference between dynamic and static is huge. It is also interesting to see how these dynamical effects influence the experienced damage. The same sea states are also included by the use of static analysis in table 7.6. It turns out that the dynamical effects are very important in terms of fatigue damage.

H_S (m)	T_P (s)	Damage with hyd. damping	w/o hyd. damping	Static
4.5	9.5	1.4e-07	2.4e-07	2.4e-09
3.5	7.5	3.6e-07	5.6e-07	1.4e-09
3.5	8.5	1e-07	1.6e-07	1.7e-09
5.5	9.5	6.2e-07	1.2e-06	3.9e-09
6.5	11.5	1.4e-06	3e-06	8.3e-09

Table 6.1: *Short term sea states (3h) with and without hydrodynamic damping in addition to a pure static simulation*

Even dough it might be more conservative to exclude hydrodynamic damping, the rest of the work is based on simulations with hydrodynamic damping included.

6.2 Fitting the short term stress range with Weibull probability distribution

The two parameter weibull distribution has shown to represent the stress range in jackets in a fairly sufficient manner [Tahery, 2015], however certain mismatch between statistical and true distribution showed to be present. Jackets do have

more stiffness than jack-up's, but share a lot of structural properties with jack-ups. They both have thin structural members. A 3-parameter weibull distribution will improve the lower tail behavior. Much of the mismatch in the two-parameter distribution also might be corrected by the third parameter. The use of the Weibull model reduces the complexity of the stress range to three parameters. The cumulative distribution function is given in equation 6.1.

$$F_{\Delta\sigma}(\Delta\sigma) = 1 - \exp\left\{ \left(\frac{\Delta\sigma - \lambda}{\alpha} \right)^{\beta} \right\} \tag{6.1}$$

The might most practical way to estimate these parameter is by the use of method of moments. The idea is to let the mean, variance and the coefficient of skewness be the same in the data and the fitted distribution. The skewness is for a data set is given by equation 6.2, where g_1 is the skewness of the data , $\Delta\sigma_k$ is a member of the sample of stress ranges, and $\mu_{\Delta\sigma}$ and $s_{\Delta\sigma}$ the sample mean and standard deviation.

$$g_1 = \frac{\frac{1}{N}\sum_{k=1}^{N}(\Delta\sigma_k - m_{\Delta\sigma})^3}{(s_{\Delta\sigma}^2)^{3/2}} \tag{6.2}$$

For a 3 parameter Weibull distribution the mean, variance and skewness is given by equation 6.3 to 6.5. By equating g_1 and γ_1, β can be found by numerical equation solvers, and then α and λ can be found explicit.

$$\mu_{\Delta\sigma} = \lambda + \alpha\Gamma(1 + 1/\beta) \tag{6.3}$$

$$\sigma_{\Delta\sigma}^2 = \alpha^2 \left[\Gamma(1 + 2/\beta) - \Gamma^2(1 + 1/\beta) \right] \tag{6.4}$$

$$\gamma_1 = \frac{\Gamma(1 + 3/\beta) - 3\Gamma(1 + 1/\beta)\Gamma(1 + 2/\beta) + 2\Gamma^3(1 + 1/\beta)}{[\Gamma(1 + 2/\beta) - \Gamma^2(1 + 1/\beta)]^{3/2}} \tag{6.5}$$

These three parameters are found for 93 different sea states. Dynamic simulations with 3h duration are used to generate the stress history, and rainflow is used for cycle counting. Stresses bellow 1 Mpa is left out because they give minimal damage, and are associated with noise. To get an idea on how well these samples are fitted with a 3-parameter Weibull distribution, a linearized Weibull plot is used.

By doing some algebraic manipulation, equation 6.1 can be changed such that the right hand side behaves linearly. By letting the y axis be the same as the left hand side of equation 6.6 and the x axis be $\ln(\Delta\sigma - \lambda)$, a cumulative Weibull distribution will behave linearly.

$$\ln(-\ln(1 - F_{\Delta\sigma}(\Delta\sigma))) = \beta\ln(\Delta\sigma - \lambda) - \beta\ln(\alpha) \tag{6.6}$$

The cumulative distribution of a sample is given by equation 6.7, where $\Delta\sigma_k$ is the k'th member of the sample, and n is the size of the sample.

$$F_{\Delta\sigma}(\Delta\sigma) = \begin{cases} 0 & \text{when } \Delta\sigma < \Delta\sigma_1 \\ \frac{k}{n} & \text{when } \Delta\sigma_k \geq \Delta\sigma < \Delta\sigma_{k+1} \\ 1 & \text{when } \Delta\sigma > \Delta\sigma_n \end{cases} \qquad (6.7)$$

If the distributions show to be Weibull distributed, the cumulative distribution of the sample will behave as a straight line. It is also of interest to see how the fitted distributions compares to the histograms of the actual cycle history. If the probability distribution is multiplied with the width of a bars in the histogram in addition with the total number of cycles as in equation 6.8, the expected number of cycles can be plotted.

$$E[dn] = f_{\Delta\sigma}(\Delta\sigma)d\Delta\sigma \cdot N_{tot} \qquad (6.8)$$

Two such distributions with linearized Weibull distribution in addition to the histogram of the data is given in figure 6.2 and 6.3. The other of the 93 sea states can be seen in appendix B. The lower tail has a low degree of importance for the fatigue damage. In the lower tail a certain degree of missmatch is present, but this area is not of importance. In the upper tail, the Weibull distribution seem to give good results. It is concluded that 3 parameter Weibull distribution is adequate to represent the stress range process.
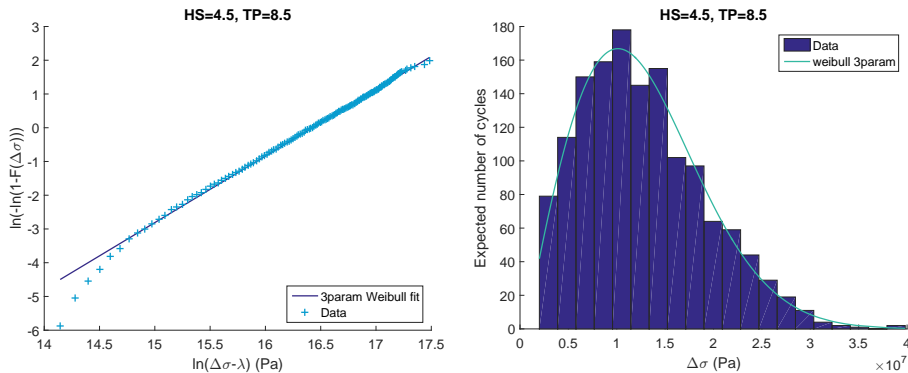
Figure 6.2: *Linearized 3 parameter weibull plot of stress range during a 3h realization*
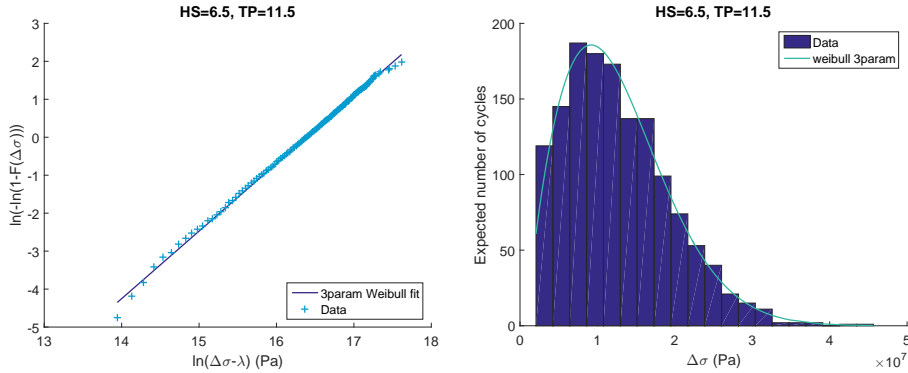
Figure 6.3: *Linearized 3 parameter weibull plot of stress range during a 3h realization*

6.3 Damage of same sea state with different realizations

Different realizations of the same sea state give different elevation at a given point in time. Different surface realizations can be generated by re-generate the random phase angles and the random amplitudes in the sea surface generation. It is known that different realizations will give different maximum surface elevation even dough the sea state is the same.

However it is unclear weather or not this also has an influence on the fatigue damage. It is possible to think that the influence of these random selected phases will not be of importance for fatigue damage since fatigue is related to the stress range over time, and that these will be equal when the duration of the simulation is as long as 3h. It is however important to keep in mind that large waves will give much larger damage than small ones due to the exponent in the SN-curve. In order to draw any conclusions, the effect of different realizations on fatigue damage is investigated further. Figure 6.4 clearly illustrates how much the particular realization might influence the total damage.
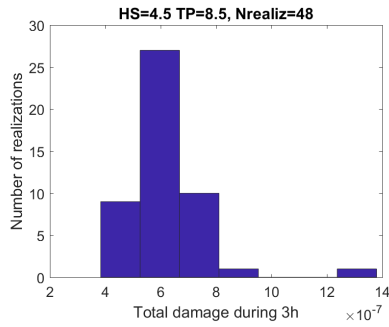
Figure 6.4: *Distribution of total damage for different realizations of the same sea state*

The variation of damage is large, and the most damage encountered during a realization is more than twice the smallest value. However most of the realizations gives damage that is within a reasonable deviation of the mean. Due to the time consumption of running several realizations of each sea state this will not be preferred for other sea states, but is included for this sea state to underline the importance of different realizations. If the time consumption of time domain simulation had been smaller, at least three surface realizations of the same sea state should be averaged in order to obtain more statistical accuracy.

The standard deviation of the stress processes along with the standard deviation in the surface elevation process is included in Table 6.2. The deviation between maximum and minimum standard deviation in stress is not large. However keep in mind that the slope of the SN-curve is 5 for the most stress ranges. This means that the damage is proportional to the the stress to the power of 5. The largest standard deviation is 21% larger then the smallest. With $1.21^5 = 2.7$ the the huge variation in damage in Figure 6.4 seem reasonable

Realization	$s_{\Delta\sigma}$	s_ζ	Realization	s_σ	s_ζ
1	5.19e+06	1.13	2	5.14e+06	1.12
3	4.83e+06	1.12	4	5.11e+06	1.13
5	5.05e+06	1.13	6	5.14e+06	1.12
7	4.96e+06	1.12	8	**5.79e+06**	1.14
9	4.97e+06	1.13	10	5.05e+06	1.13
11	4.87e+06	1.13	12	5.27e+06	1.12
13	5.29e+06	1.11	14	**4.75e+06**	1.12
15	4.94e+06	1.13	16	5.19e+06	1.12
17	5.10e+06	1.12	18	5.11e+06	1.12
19	4.96e+06	1.12	20	5.09e+06	1.13
21	5.32e+06	1.13	22	5.08e+06	1.12
23	4.97e+06	1.12	24	5.16e+06	1.13
25	4.98e+06	1.13	26	5.02e+06	1.12
27	5.05e+06	1.13	28	5.02e+06	1.13
29	5.06e+06	1.13	30	5.11e+06	1.13
31	4.79e+06	1.12	32	4.82e+06	1.12
33	5.42e+06	1.12	34	5.01e+06	1.13
35	5.07e+06	1.13	36	4.86e+06	1.12
37	5.15e+06	1.13	38	5.14e+06	1.12
39	5.29e+06	1.13	40	4.96e+06	1.13
41	5.13e+06	1.13	42	4.80e+06	1.12
43	5.03e+06	1.12	44	5.10e+06	1.12
45	5.10e+06	1.13	46	5.09e+06	1.13
47	5.03e+06	1.12	48	5.02e+06	1.12

Table 6.2: *Standrad deviations for stress process and surface elevation process* $H_S = 4.5$, $T_P = 8.5$. $s_\sigma = \sqrt{\frac{1}{N}\sum_{i=1}^{N}\sigma_i^2}$, $s_\zeta = \sqrt{\frac{1}{N}\sum_{i=1}^{N}\zeta_i^2}$

The distribution of stress range in these 48 realizations of the same sea state will differ slightly. It is interesting to compare these in order to get a picture on where the different damage contributions are located. The stress range of the realization that gives the most, and the one that gives the least damage is depicted in figure 6.5. In this figure, linearized probability plot of the cumulative Weibull is used.
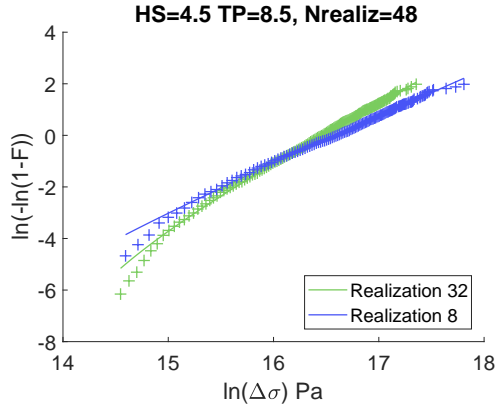
Figure 6.5: *Weibull plot of the two realizations that gives most and least damage during a 3h simulation, fitted with 3 parameter Weibull distribution. Keep in mind that $\ln(\Delta\sigma)$ is on the axis, not the $\ln(\Delta\sigma - \lambda)$*

Even dough the two realizations might seem to give quite similar distributions, the accumulated damage from these realizations differs by a factor of more than two. A 3 parameter Weibull distribution is used to fit the different realizations, and explains the curved fitting tails. The fit results in three parameters, α, β and λ. The cumulative Weibull distribution is given in equation 6.9

$$F_{\Delta\sigma}(\Delta\sigma) = 1 - \exp\left\{\left(\frac{\Delta\sigma - \lambda}{\alpha}\right)^{\beta}\right\} \tag{6.9}$$

Each realization can be described by these three parameters. This means that also the parameters will differ for the different realizations. In figure 6.6 the parameters for all the 48 different realization are included in histograms.
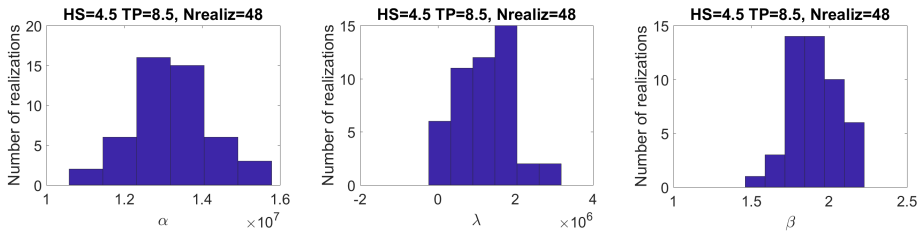
Figure 6.6: *Distribution of the three parameters in the Weibull fit for different realizations. A total of 48 realizations of the same sea state are included*

6.4 Weibull parameters for several short term sea states

The stress range history has been generated for numerous short term sea states. The corresponding three parameters for the Weibull distribution has been calculated according to Section 6.2. It is possible to believe that the nature will behave smooth to some extend, and that these parameters can be described by a quite smooth surface. Piecewise linear interpolation polynomials are used to represent this surface. The three parameters are visualized in Figure 6.7. Both the β and the α parameters behaves very well, and gives a smooth surface. The λ surface tends to be less smooth. However since the resolution of data points is so good, the model is assumed to give a good representation of the stress range process.
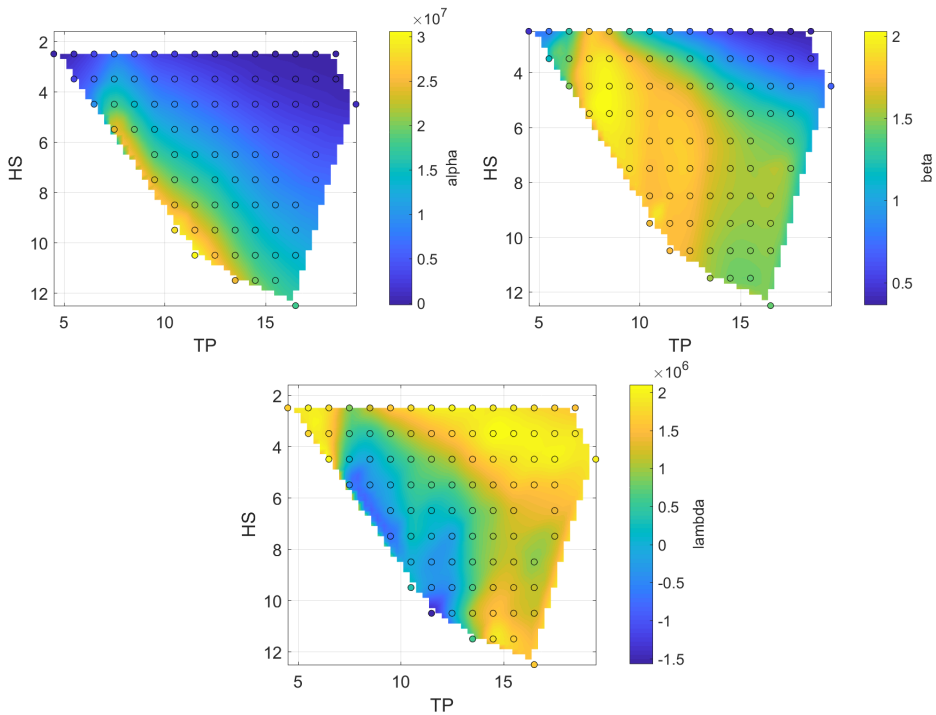
Figure 6.7: *Weibull parameter values for different sea states. Data points are indicated with circular dots*

6.5 Fatigue damage from short term sea states

The total fatigue damage is next to be calculated for every sea state described in previous section. This can be carried out in two ways, where one consist of a

explicit expression of the the Weibull parameters and SN-curve and the other of miner summation of the cycles. The expression for the explicit case can be seen in equation 6.10 [Larsen, 2014].

$$E_{3h}[D] = N_{3h} \int_0^\infty \frac{f_{\Delta\sigma}(\Delta\sigma)d\Delta\sigma}{N(\Delta\sigma)} \tag{6.10}$$

Where N_{3h} is the total amount of cycles within a 3h sea state, $N(\Delta\sigma)$ the SN curve as a function of stress range and $f_{\Delta\sigma}(\Delta\sigma)$ the probability distribution of the stress range, which in this case is the 3 parameter Weibull probability density function. This integral has a simple explicit expression as long as simple SN-curves are used. However a kinked SN-curve is used in this work, and hence the simpler implementation is numerical integration of the integral. The total number of cycles are gathered from the rainflow counting, and will vary with sea state. However the dominant resonance period will have the largest influence on this. This number is $\frac{10800}{T_n} = 1408$. By evaluating the rainflow counting record, it turns out to be correct that these variations are quite small for most of the sea states. This can be seen in figure 6.8. The majority of the sea states has a N_{3h} of about 1500.
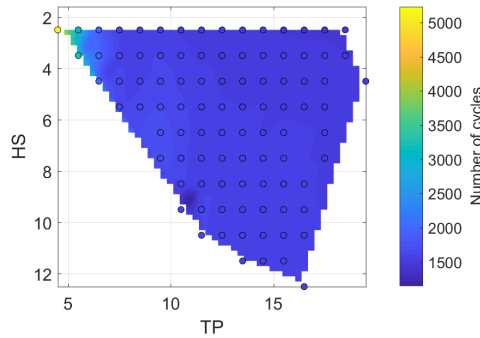
Figure 6.8: *Number of cycles for different short term 3h sea states, Data points are indicated with circular dots*

The other method consist of using miner summation to count the cycles as outlined in chapter 5. Both these methods should give close to the same damage. The results are illustrated in figure 6.9.
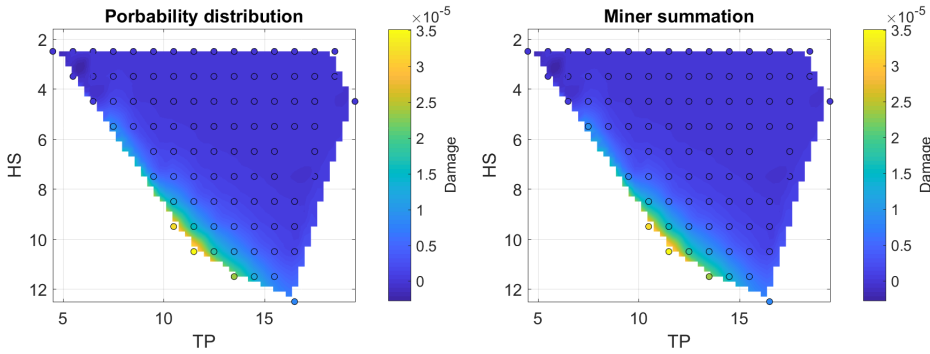
Figure 6.9: *Short term damage calculated by both the probability distribution and by counting, Data points are indicated with circular dots*

More specific the error between these methods is of order 10^{-6}. As expected sea states with high H_S/T_P ratio will generate the most damage.

6.6 Damage in the scatter format

The short term damage resulting from time domain simulations is presented in the scatter format in Table 6.3

2<TP<3	2.5	3.5	4.5	5.5	6.5	7.5	8.5	9.5	10.5	11.5	12.5	13.5	14.5	15.5	16.5	17.5	18.5	19.5	20.5	Cutoff
0<HS<1 0.5																				
1.5																				Cutoff
2.5			2.22E-09	3.96E-09	1.18E-08	4.54E-08	1.56E-08	5.56E-09	4.30E-09	3.47E-09	2.85E-09	2.56E-09	2.28E-09	2.00E-09	1.81E-09	1.68E-09	1.62E-09			1.07E-07
3.5				1.36E-08	7.68E-08	3.59E-07	1.02E-07	2.70E-08	1.74E-08	1.10E-08	7.28E-09	5.51E-09	4.28E-09	3.30E-09	2.77E-09	2.42E-09	2.26E-09			6.35E-07
4.5					4.83E-07	2.05E-06	5.59E-07	1.41E-07	8.55E-08	4.58E-08	2.56E-08	1.68E-08	1.10E-08	7.14E-09	5.04E-09	4.03E-09	0.00E+00	3.38E-09		3.44E-06
5.5						9.19E-06	2.42E-06	6.18E-07	3.72E-07	1.84E-07	9.50E-08	5.72E-08	3.32E-08	1.88E-08	1.17E-08	8.54E-09				1.30E-05
6.5								2.28E-06	1.37E-06	6.72E-07	3.31E-07	1.94E-07	1.06E-07	5.70E-08	0.00E+00	2.21E-08				5.03E-06
7.5								7.35E-06	4.44E-06	2.12E-06	1.04E-06	5.96E-07	3.18E-07	1.65E-07	0.00E+00	6.14E-08				1.61E-05
8.5									1.27E-05	6.00E-06	2.99E-06	1.72E-06	9.03E-07	4.54E-07	2.53E-07					2.50E-05
9.5									3.18E-05	1.54E-05	7.68E-06	4.57E-06	2.36E-06	1.20E-06	6.63E-07					6.37E-05
10.5										3.51E-05	1.80E-05	1.09E-05	5.91E-06	3.00E-06	1.62E-06					7.45E-05
11.5												2.37E-05	1.33E-05	6.96E-06	0.00E+00					4.40E-05
12.5															8.47E-06					8.47E-06
0	0	2.22E-09	1.75E-08	5.72E-07	1.16E-05	3.1E-06	1.04E-06	5.08E-05	5.95E-05	3.02E-05	4.18E-05	2.29E-05	1.19E-05	1.1E-05	1E-07	3.88E-09	3.38E-09	0		0.000254

Table 6.3: *Short term damage of structure (3h)*

The long term damage takes into account how many of each sea states that occurs over a period of time. The scatter diagram describes how many of each sea state that is present for a period of time. The history is usually generated by physically measure the surface elevation at the site. The scatter used in this work is the scatter for the Ekofisk field, generated by measurements over 56 years.

It is possible to estimate the damage encountered during these 56 years in each block by multiplying the number of short term sea states encountered during 56 years with the damage from each short term sea state. The damage from each short term sea state is given in figure 6.3. As expected wave with a high height to amplitude ratio gives the largest damage.

This results in the the total accumulated damage given in figure 6.4. The total damage encountered from all block is quite low, and indicate low degree of damage, maybe lower than one could expect. However simplifications are made throughout the work.

2<TP<3	2.5	3.5	4.5	5.5	6.5	7.5	8.5	9.5	10.5	11.5	12.5	13.5	14.5	15.5	16.5	17.5	18.5	19.5	20.5	Cutoff
0<HS<1 0.5																				
1.5																				Cutoff
2.5		1.32E-08	1.23E-06	6.34E-05	0.000583	9.19E-05	1.03E-05	4.05E-06	2.42E-06	1.31E-06	5.35E-07	2.36E-07	1.72E-07	4.73E-08	2.28E-08	1.55E-08	0			7.59E-04
3.5			1.00E-08	1.80E-05	0.001118	0.000801	9.21E-05	1.85E-05	4.43E-06	1.67E-06	7.38E-07	2.64E-07	9.76E-08	3.78E-08	1.51E-08	6.55E-09	0			2.06E-03
4.5				4.56E-07	0.000113	0.001187	0.000555	0.000125	2.13E-05	3.98E-06	8.00E-07	3.34E-07	2.02E-07	2.19E-08	1.04E-08	0	1.76E-09			2.01E-03
5.5					9.16E-06	0.00042	0.000716	0.000544	0.000104	1.70E-05	1.49E-06	6.58E-07	1.60E-07	6.81E-08	5.83E-09					1.81E-03
6.5						0.000332	0.000621	0.000278	7.21E-05	7.79E-06	1.26E-06	3.50E-07	0	1.86E-08						1.31E-03
7.5						5.28E-05	0.000312	0.000302	0.000116	2.57E-05	5.74E-06	9.21E-07	0	5.67E-08						8.15E-04
8.5							0.000101	0.000172	0.000181	5.20E-05	1.04E-05	3.47E-06	7.30E-07							5.22E-04
9.5								3.17E-05	9.15E-05	0.000129	0.000111	3.16E-05	1.49E-05	6.42E-07						4.10E-04
10.5									3.52E-05	0.000126	9.48E-05	3.92E-05	1.99E-05	1.57E-06						3.16E-04
11.5										7.01E-05	6.31E-05	2.62E-05	0							1.59E-04
12.5															8.06E-06					8.06E-06
	0	0	1.32E-08	1.24E-06	8.19E-05	0.001823	0.0025	0.001758	0.001757	0.001011	0.000648	0.000365	0.000153	6.63E-05	1.12E-05	1.3E-07	2.21E-08	1.76E-09	0	0.010176

Table 6.4: *Long term damage of structure during 56 years*

6.7   Conclusive remarks for time domain results

The damage encountered during 56 years at Ekofisk is lower than one would expect. However no detailed screening is present. The sea state that turns out to be most critical, might have a lower significant wave height than one could expect. The natural period of the structure is accountable for this. It induces an increased damage in a region of the scatter that has a high occurrence frequency. It must also be stated that more statistical reliable results can be obtained by at least average three realizations of the same sea state.

Chapter 7

Linearization

Linearization is a commonly used feature to avoid the time consuming time domain simulation. In short it involves the establishment of a linear relationship between response and wave elevation. It is commonly used in fatigue life estimation. In fatigue damage, moderate sea states are the most critical, thus making it easier to linearize waves about these most critical values. Linearization might even give very accurate response estimate for certain structures. However for jack-ups, which are heavily drag dominated due to the small dimensions of the members, it is not possible to describe the response perfectly by a linear relationship. This is due to the fact that drag forces are nonlinear. These nonlinear forces can be seen in the drag term of Morison's equation 7.1.

$$dF = \underbrace{\frac{1}{4}\rho\pi D^2 C_M a}_{\text{Inertia term}} + \underbrace{\frac{1}{2}C_D\rho D u_{rel}|u_{rel}|}_{\text{Drag term}} \tag{7.1}$$

ρ = Density of fluid
D = Diameter of pipe
C_M = Inertia coefficient
C_D = Drag coefficient
a = Fluid acceleration perpendicular to cylinder
u_{rel} = Relative fluid speed perpendicular to cylinder

7.1 Motivation for proper drag force treatment

In order to make proper assumptions in the linearization process it is important to understand how important the drag term is. The ratio between drag force amplitude and inertia force amplitude is an parameter that is easy to calculate,

and gives a good first impression of the importance of drag. In general the ratio between drag force amplitude and inertia force amplitude can be written as in equation 7.2 if the structure self velocity is neglected in the relative velocity.

$$\frac{F_{D,a}}{F_{M,a}} = \frac{\frac{1}{2}C_D D \zeta_a^2 \omega^2}{\frac{1}{4}C_M \pi D^2 \zeta_a \omega^2} = \frac{C_D}{C_M \pi D}H \tag{7.2}$$

Drag coefficient vary with the members. The chords that is 90° aligned with the flow has a larger drag coefficient than the ones that are 60°. The braces on the other hand has a lower drag coefficient, but also a smaller diameter. In Figure 7.1 the ratios for the different types of members are plotted as a function of wave height. The dashed lines indicates where the drag forces becomes larger than the inertia forces. For this particular jackup this is experienced at quite low wave heights. In comparison a typical jacket member with a diameter of 2m and a drag coefficient of 1.15, will give a limit wave height of about 10m for where drag becomes more important than inertia.
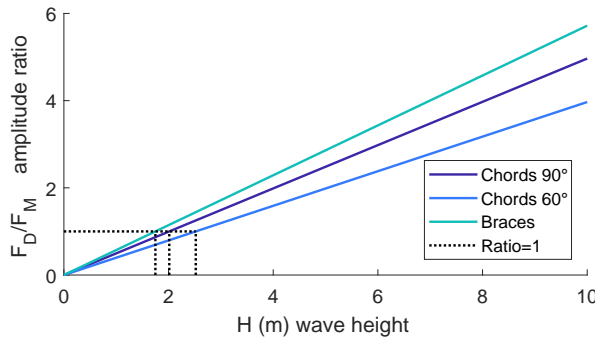
Figure 7.1: *Ratio between amplitudes of drag force and inertia force as a function of wave height*

A significant wave height of 4.5m is the height of one of the most critical sea states for fatigue damage. At these wave heights the drag force amplitude is about twice the amplitude of the inertia force for all the members. The braces a bit more. This underlines the importance of the drag forces, and that they are included in a sufficient manner.

The importance of drag is investigated further by a case. The jack-up response from the same stochastic surface elevation with and without drag forces are compared.
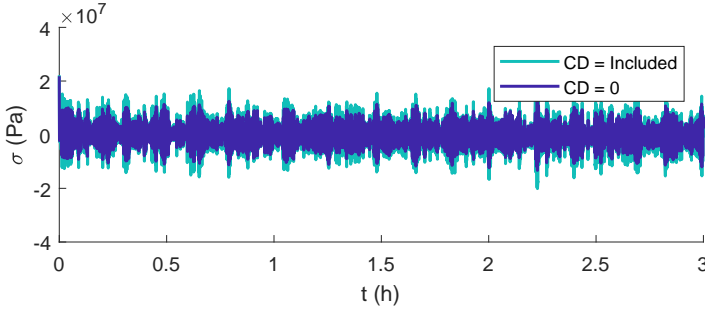
Figure 7.2: *Short term stress response fro comparison of drag vs no drag.* H_S=4.5, T_P=8.5

In Figure 7.2 the stress response for a short term sea state is included. The case with drag forces clearly gives larger stress than for the case without drag. However the difference might not be as large as one could believe from Figure 7.1. It should also be kept in mind that turning on drag also turns on hydrodynamic damping in this regard.

$$s_\sigma = \sqrt{\frac{1}{N} \sum_{i=1}^{N} \sigma_i^2} \tag{7.3}$$

The standard deviation of the signal is an important parameter to characterize the signal and is given in equation 7.3. Both the standard deviation of his process and the damage calculated using rainflow counting can be seen in Table 7.1.

	C_D =Included	$C_D = 0$
s_σ	4.9e06	3.7e06
Damage	0.55e-06	0.13e-06

Table 7.1: *Damage and standard deviation during 3h for different values of C_D.* $T_P = 8.5$, $H_S = 4.5$.

Even dough the ratio between the standard deviation for the case with and without drag is only 1.3, it increases the damage by a significant amount. Keep in mind that the kink of the SN-curve is located at 86 MPa, which means that all the stress cycles for this short term sea state will be in the area where the slope of

the SN-curve is m=5. This suggests that the ratio between damage from the case with and without drag should be $1.32^5 = 4.1$. This corresponds well with what is conducted with the rainflow counting. Increasing the damage by a factor of 4 must be considered significant.

The stress range distribution for the two cases seen in Figure 7.3. Keeping in mind the logarithmic scale, the difference is actually quite large. It also underlines how important the slope in the weibull distribution is in the context of fatigue.
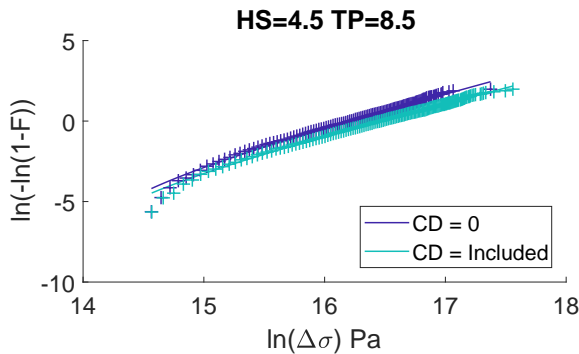
Figure 7.3: *Short term stress distribution (3h) for drag vs no drag*

7.2 Harmonic inputs used to create transfer functions

In offshore industry it is common practice to linearize for wave height. This is done by calculating the response amplitude for regular harmonic inputs with different frequencies and use this to estimate a transfer function. A major question in this context is how to select the wave heights for the harmonic inputs in order to capture the nonlinearities due to drag forces in a good way. Different methods can be used to select proper values of wave height for the harmonic input wave. Constant wave steepness is frequently used to select these wave heights. However there are no proper guidelines on how to select the wave steepness.

7.2.1 Linearization schemes included in analysis

Three different schemes are investigated. These schemes describes what wave heights to be used as inputs when transfer functions are established.

7.2.1.1 Using constant wave steepness for selecting wave heights

Usually the ratio between wave height and wave length is defined as steepness. However for deep water this value is proportional to the wave height divided by the period squared, which is more convenient in this work, and are hence used as a measurement of wave steepness as given in equation 7.4.

$$\frac{H}{\lambda} \propto \kappa = \frac{H}{T^2} \tag{7.4}$$

Constant wave steepness is frequently used to select wave heights. Much of the reasoning behind this might be explained by the ratio between drag force amplitude and wave height.

$$\frac{F_{D,a}}{H} \propto H\omega^2 \tag{7.5}$$

By inserting wave heights determined by a constant wave steepness given in equation 7.6 in equation 7.5,

$$H = \kappa T^2 = \frac{\kappa}{4\pi^2\omega^2} \tag{7.6}$$

the drag force divided by wave height will behave as a constant independent of ω.

$$\frac{F_{D,a}}{H} \propto \kappa \tag{7.7}$$

When transfer functions are established the response amplitude is divided by the wave height. Hence by selecting input wave heights from constant steepness a constant transfer function of drag is achieved. This might be an adequate property for use in linearization.

Keeping the steepness constant will give unrealistically large responses at low frequencies. Hence a cutoff might be necessary. The low frequencies should be capped at wave height equal the one year return period [ISO, 2007]. For the Ekofisk field, this can be calculated from the Weibull distribution as in equation 7.8 with $\rho = 1.99$ and $\beta = 1.35$ [Aarsnes, 2015].

$$H_{S,1year} = \rho \left(\ln \left(\frac{1}{2920} \right)^{\frac{1}{\beta}} \right) \tag{7.8}$$

β	ρ	$H_{S,1year}$
1.35	1.99	9.26m

Table 7.2: *Significant wave height with one year return period for the Ekofisk field*

However as it will turn out, this cutoff limit is not suitable for all sea states. It is for instance to low for a sea state with a significant wave height of 7m. When

the cutoff is applied, the wave heights used in the harmonic inputs will look like the lines in Figure 7.4. It is worth noting that the waves will be breaking with a steepness value of $\kappa = 0.23$ (this corresponds to $\frac{H}{\lambda} = \frac{1}{7}$). The goal is to calibrate κ in such a way that is will produce similar responses as reality.
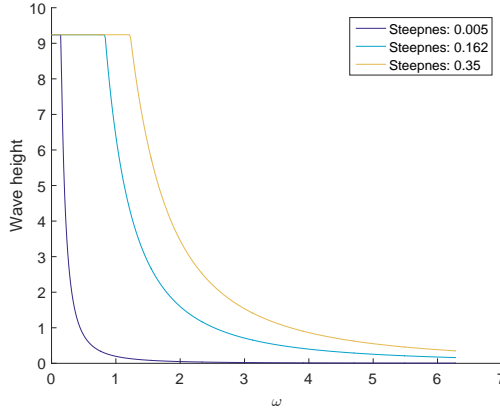
Figure 7.4: *Constant wave steepness curves with cutoff at one year return period*

7.2.1.2 Using constant wave height-period ratio for selecting wave heights

Instead of tuning the model for wave steepness, the ratio between wave amplitude and period might be an option, considering that drag is the most important parameter. By letting the wave height be determined by having a constant ratio between wave height and period certain properties are achieved. This ratio is described as c in equation 7.9.

$$c = \frac{H}{T} \Rightarrow H = cT \tag{7.9}$$

For each value of c the drag force amplitude will behave constant at all values of ω. The amplitude of the drag force will then be constant for the wave heights used as input.

$$F_{D,a} \propto (\zeta\omega)^2 \propto c^2 \tag{7.10}$$

In Figure 7.5 some of these constant height-period curves are included. Also in this case a cutoff height might be necessary. The goal is to calibrate c in such a way that is will produce similar responses as reality.
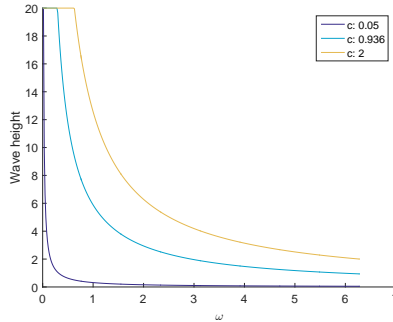
Figure 7.5: *Wave heighs used as input given constant ratio between wave height and period*

7.2.1.3 Using the input spectrum

Instead of letting the wave height used in input be equal to constant wave steepness other possibilities may be considered. An approach that seem reasonable is to letting the wave heights be somewhat equal to the different sectors in the wave spectrum. This will result in the wave heights used in the input having similar characteristics as the stochastic signal. This means that the high energetic sectors of the spectrum will have a higher input wave height. A good first starting point in order to do this is by considering the relation 7.11.

$$H(\omega_k) = 2\sqrt{2S(\omega_k)\Delta\omega} \tag{7.11}$$

However the $\Delta\omega$ complicates this. By increasing the resolution of the frequencies used to estimate the transfer functions, the wave height will decrease ($\Delta\omega$ decrease). The wave heights used as inputs should not decrease by counting more frequencies. By tweaking the relation with a constant G to form equation 7.12 the representation of the wave heights will still be similarly distributed as the stochastic process. The constant G can then be determined by using the calibration technique given in Section 7.2.2

$$H(\omega_k) = G\sqrt{S(\omega_k)} \tag{7.12}$$

7.2.2 Calibration

The value of the wave parameters (κ, c and G) can be calibrated by the two main steps in Section 7.2.2.1 and 7.2.2.2. In Section 7.2.2.1 spectral methods are used to calculate the most probable maximum wave action (base shear) for several vales of the parameter. Then a deterministic most probable maximum wave action is calculated in Section 7.2.2.2. The deterministic value is then matched with the spectral calculated value in order to find a calibrated parameter. The parameter will in turn be used to generate stress transfer functions. Here steepness is used

to explain the calibration process, but is works in the same manner for the other schemes.

7.2.2.1 Spectral calculation of most probable maximum wave action

The total applied wave actions are used for this calibration i.e. quasi-static base shear. The goal is to calculate the most probable maximum (MPM) value of the wave actions for different steepness values. This is done by establishment of the transfer function of the wave actions with a constant wave steepness. These transfer functions are established by looking at one frequency at the time. The wave height for these harmonic inputs are determined by the constant steepness. The output base shear amplitude is then used to calculate the transfer function value for a given frequency. The response amplitude divided by the input wave amplitude in order to get the value of the transfer function at the particular frequency and steepness.

$$h_{\zeta F}(\omega_k) = \frac{2F_{amplitude}}{H_{input}} \tag{7.13}$$

Where F is the base shear, and H_{input} is the input wave height which will depend on what steepness value that is selected. This results in several transfer functions for different values of steepness. Three of them are included in Figure 7.6. Note that these are quasi static transfer functions, thus no resonant areas are present. However cancellation and amplification is still present, which is the reason for the peaks that is present.
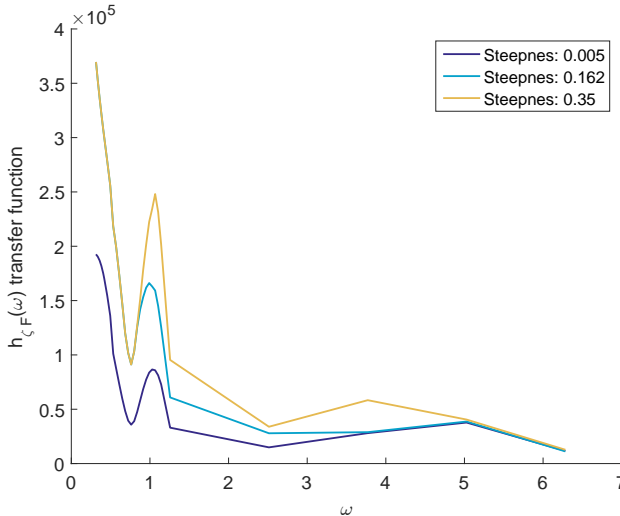
Figure 7.6: *Transfer functions from wave elevation to wave action with different constant steepness*

The next step is to use these transfer functions to calculate the value of the most probable maximum of wave actions depending on steepness. This is carried out by standard spectral methods. First by calculating the variance of the process, which is the integral of the response spectrum, in this case the spectrum of applied total wave action.

$$m_0 = \int_0^\infty S_{FF}(\omega)d\omega \tag{7.14}$$

The response spectrum can be found using the transfer function according to equation 7.15. The square of the absolute value multiplied with the input spectrum will give the spectrum of the output.

$$S_{FF}(\omega) = |h_{\zeta F}(\omega)|^2 S_{\zeta\zeta}(\omega) \tag{7.15}$$

The input spectrum will be the particular sea state of interest. The most probable maximum range in wave action can then be calculated from equation 7.16 for large values of N [Myrhaug, 2007], where N is the number of waves, which can be taken as $N = \frac{10800}{T_P}$. It is important to point out that this is the range in wave action.

$$\Delta F_{MPM} \approx 2\sqrt{2m_0 \ln N} \tag{7.16}$$

Two resulting curves for most probable maximum wave action range as a function of steepness is given in Figure 7.7. The reason for these to be different is that different input spectra are used to calculate the wave action.
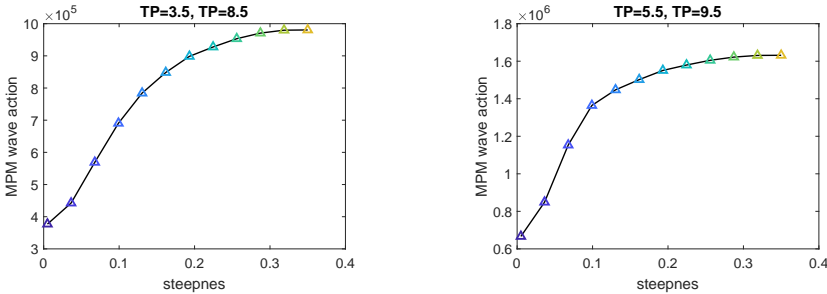
Figure 7.7: *Most probable maximum of total applied wave action (quasi-static base shear).*

These curves are the relevant results of this first step of calibration. It might seem strange that these curves do flat out for larger values of steepness, since the forces will be higher with larger values of steepness. However the reason for the flat out is the cut off height from Table 7.2 and Figure 7.4. At a certain steepness almost all harmonic components will be limited by the cutoff frequency, and hence an

increasing steepness will not result in an increasing height used in the harmonic input components.

7.2.2.2 Deterministic calculation of most probable maximum wave action

A deterministically most probable maximum is next to be calculated using a harmonic input, and stepping one wave through the structure. The period of the input should be the same as the zero mean up crossing period as the sea state of interest, and the wave height should be the wave height that corresponds to the most probable maximum wave height for that particular sea state. The most probable maximum wave height is calculated using equation 7.17 where N is the number of zero up crossings [Myrhaug, 2007].

$$H_{MPM} = H_S \sqrt{\frac{\ln N}{2}} \qquad (7.17)$$

The deterministic range of most probable maximum wave action is the maximum minus the minimum of the resulting wave action. For certain sea states this results is given in Table 7.3.

Sea state		Harmonic input and output		
H_S (m)	T_P (s)	T (s)	H_{MPM} (m)	ΔF_{MPM} (N)
3.5	8.5	8.5	6.6	4.9e+05
4.5	9.5	9.5	8.4	1.1e+06
5.5	9.5	9.5	10.3	1.6e+06

Table 7.3: Deterministic most probable wave action, $H_{cutoff} = 9.26m$

7.2.3 Calibration at the center of fatigue

A simplified analysis is here conducted as an initial study of the calibration of steepness. It is an very fast way to estimate the fatigue damage. However it turns out to be extremely sensitive to initial assumptions.

This method is described in [ISO, 2007]. The overall idea is to create one transfer function that has a good accuracy for the most important sea states when fatigue is considered. The most important sea state is not known in an initial phase. However by assuming a straight SN-curve, and a linear relationship between stress range and wave height, there is possible describe a ratio that is proportional to the damage [ISO, 2007]. There will then be proportionality between damage and wave height by the power of m (The slope of the SN curve). There will also be an inverse proportionality to the mean zero crossing period (T_P) due to the number of cycles during 3h. This relation does not support kinked SN-curves with several values of

m. The SN curve used in this work has a slope of 3 or 5 depending on the stress range.

$$D \propto \frac{N(H_S)^m}{T_P} \tag{7.18}$$

The total accumulated damage for a certain sea state is then given by the proportionality in equation 7.18 [ISO, 2007], where N is the number of occurrences in the scatter diagram. The sea state considered the most important, and where the transfer function is calculated, is for the H_S value where there are equal amount of damage for larger H_S values as for smaller H_S values. The same thing goes for T_P. This most important region is called the center of fatigue.
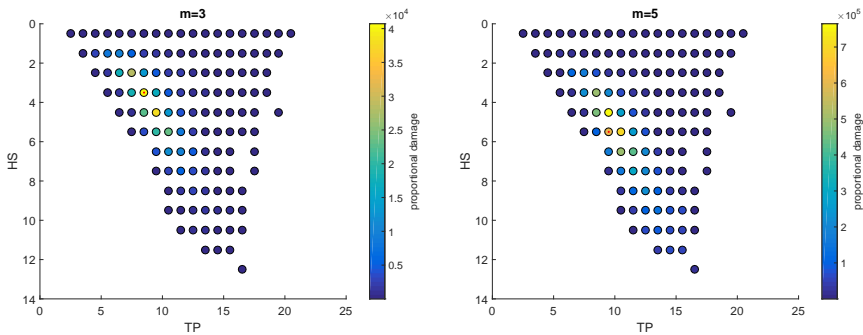
Figure 7.8: *Proportional accumulated damage for different sea states. The centre of fatigue contains a red dot. Ekofisk scatter diagram is used*

The proportional damage for different sea states is plotted in Figure 7.8. The center of fatigue turns out to be in the same area as the sea state that contributes with the most proportional damage for both values of m. The center of fatigue for both cases is given in Table 7.4 along with the intermediate value m=4, and the result from time domain simulation. It is hard to tell up front which of the slopes that will be contributing the most to the damage of a structure. However in this case, time domain simulations are in hand, and in most sea states all the stress cycles are bellow the limit of the kink in the SN-curve. This is evident in appendix B, where stresses bellow 86.2 MPa will have m=5 as slope. This indicates that m=5 might give the best approximation.

m	H_S	T_P
3	3.5	8.5
4	4.5	9.5
5	5.5	9.5
time domain	4.5	8.5

Table 7.4: *Centre of fatigue*

However as seen in Table 7.4 the cases for m=3 and m=4 are closest to the true center of fatigue (the one from time domain simulations). m=5 however gives to large values of both period and wave height and is expected to overestimate the stresses.

7.2.3.1   Results for center of fatigue assumtions

For these cases the cutoff height of 9.26m is used. This results in the steepness values given in Table 7.5. These vales are used when the stress transfer function is calculated. The stress transfer function is calculated with the same method as for the total wave force, but using the calibrated value of steepness. Dynamic effects are also included in the calculation of the stress transfer function.

m	H_S	T_P	Calibrated steepness, κ
3	3.5	8.5	0.05
4	4.5	9.5	0.10
5	5.5	9.5	0.29

Table 7.5: *Calibrated steepness*

The steepness value of the case with m=5 is beyond the breaking limit. This indicates that the cutoff height might be to low for this particular sea state. With the steepness given in Table 7.5, the stress transfer functions are calculated. Evident in Figure 7.9 is that the larger values of steepness results in larger values in the stress transfer function.
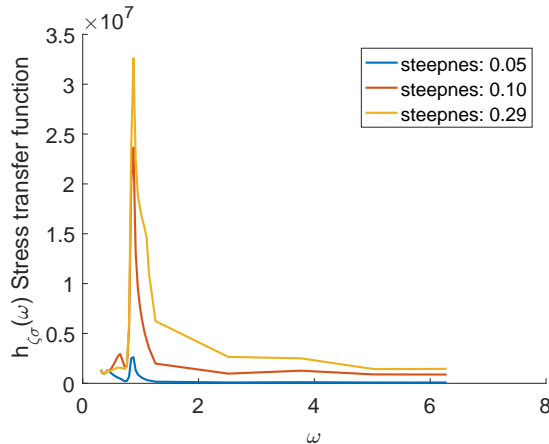
Figure 7.9: *Dynamic stress transfer functions, for the calibrated steepness*

When the stress transfer function is known, the stress response spectrum can be calculated in a similar way as in equation 7.15. This spectrum can then be used to directly create a realization of the stress process as described in Section 5.7.1.2. On these time series the same procedure as for time domain time series is used to calculate damage, i.e. rainflow counting and mine summation with kinked SN-curve.

The resulting short term damage depicted in Figure 7.10. The damage resulting from time domain simulations is also included as reference. These are only short term sea states, and the goal for the linearization technique is not that the estimates shall bee accurate for all sea states. More important is that the regions of importance, i.e. the regions around the centre of fatigue is about right. The case when center of fatigue is estimated with m=4 gives the best results in this area. This is also the case which has the same significant wave height at the center of fatigue in time domain simulation (Table 7.4).
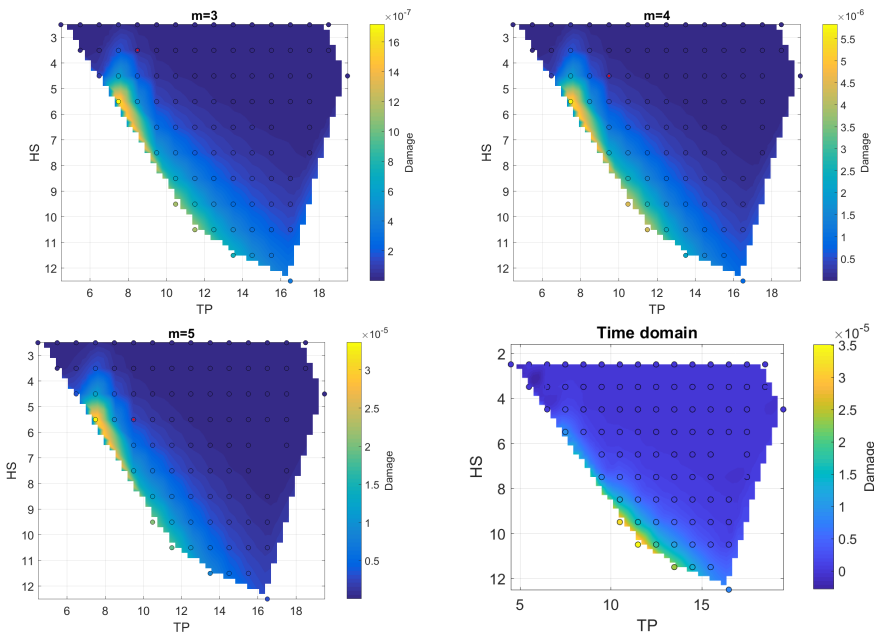
Figure 7.10: *Damage during short term sea states (3h) using transfer functions at the center of fatigue and constant wave steepness. Be aware of the different values on the color axis. Keep in mind that the values of m is only used to estimate the center of fatigue, and are not involved in the damage calculation.*

In order to get the long term damage, it is necessary to multiply the damage from each sea state by the number of occurrences over a period of time. In this case the scatter diagram for Ekofisk is used for the purpose. It is given for 56 years. The total damage experienced from one sea state over these 56 years are calculated

by the multiplying number occurrences of short term sea states with the damage achieved by one short term sea state. The total damage is depicted in Figure 7.11.
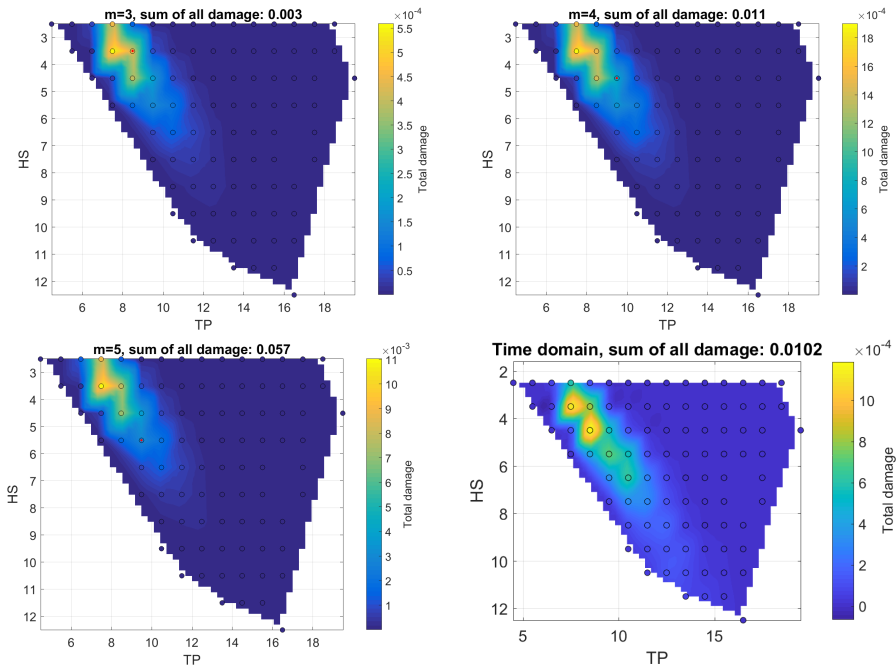
Figure 7.11: *Total damage during 56 years, linearized method. Keep in mind that the values of m is only used to estimate the center of fatigue, and are not involved in the damage calculation.*

On the top of the plots in Figure 7.11 the total damage from all sea states is indicated. This is calculated simply by adding the contribution from all sea states.

As mentioned, the case of m=4 and m=3 gives a center of fatigue that is closer to the true center of fatigue. Thus it is reasonable to believe that these will give better results than for the case of m=5, which in fact is the case. However m=5 is the only case which actually over predicts the fatigue damage.

It turns out that the total damage collected from all sea states is about right in the case when m=4 decides the center of fatigue. It coincides with the total damage resulting from the time domain simulation. Even though the total damage is correct in this case, the technique gives a wrong impression on how much each sea state contributes to the total damage. That being said, the technique gives a good overall indication on the fatigue damage.

What turns out to be a very important parameter for this technique is the location of the center of fatigue. The simplicity of the technique is its huge advantage. However it might be a bit optimistic to let only one transfer function estimate the

response for all sea states. It might be possible to extend this to several transfer functions, and split up the domain in this manner. This is investigated in Section 7.2.6

7.2.4 Static transfer functions comparison

The calibration is going to be carried out for every sea state in Section 7.2.6. In this regard it is of interest to investigate the static transfer functions of stress. However to generate transfer functions from time domain simulations, for comparison, requires huge computational effort. The reason for this is that the frequency resolution need to be considerably higher in order to generate a transfer function. Thus this is only carried out for a few cases in this section.

If the response spectrum is known together with the input spectrum, and the response is stationary, then there exist a relationship between them. Equation 7.19 describes the relation between stress response- and input spectrum [Conte, 2016]. It is possible to establish a response spectrum according to Section 5.7.2. This demands a time signal of stress response, which can be achieved by time domain simulation.

$$S_{\sigma\sigma}(\omega) = |h_{\zeta\omega}(\omega)|^2 S_{\zeta\zeta}(\omega) \tag{7.19}$$

The transfer function can then be calculated by equation 7.20. However in order to achieve a decent response spectrum, the frequency resolution needs to be well above the 500 components used in previous sections. In this section 5000 wave components are used which seem to produce a response spectrum of good quality. Averaging by the 50 adjacent points is utilized, as it worked well in Section 5.7.2 for a signal of 5000 components.

$$|h_{\zeta\omega}(\omega)| = \sqrt{\frac{S_{\sigma\sigma}(\omega)}{S_{\zeta\zeta}(\omega)}} \tag{7.20}$$

Constant steepness

Here the same technique with constant steepness is here inspected, however with larger cutoff heights. Both of these cutoffs allows quite high sea states to be calibrated. The results obtained from linearization are compared with the one from time domain simulations.

In Figure 7.12 a comparison between the two cutoff frequencies and time domain simulation is present. The most important region for this platform is the region close to the resonance, which is at $\omega = 0.82$. The region between 0.6 and 1.2 is thus the most important. As expected the method over predicts at low frequencies, and under predicts at high frequencies. The under prediction at high frequencies is not associated with any large responses. For the smaller sea states considerably

accurate results is achieved in the important region. For larger sea states the deviation in low frequency response increases. In all cases is seem to be a certain degree of conservatism in the important regions. The largest cutoff height gives better results for frequencies between $\omega = 0.5$ and 1.

The cutoff height of 30m seem to give reasonable results for small sea states. This indicates that the selection of cutoff height might not as important as long as it is taken high enough.
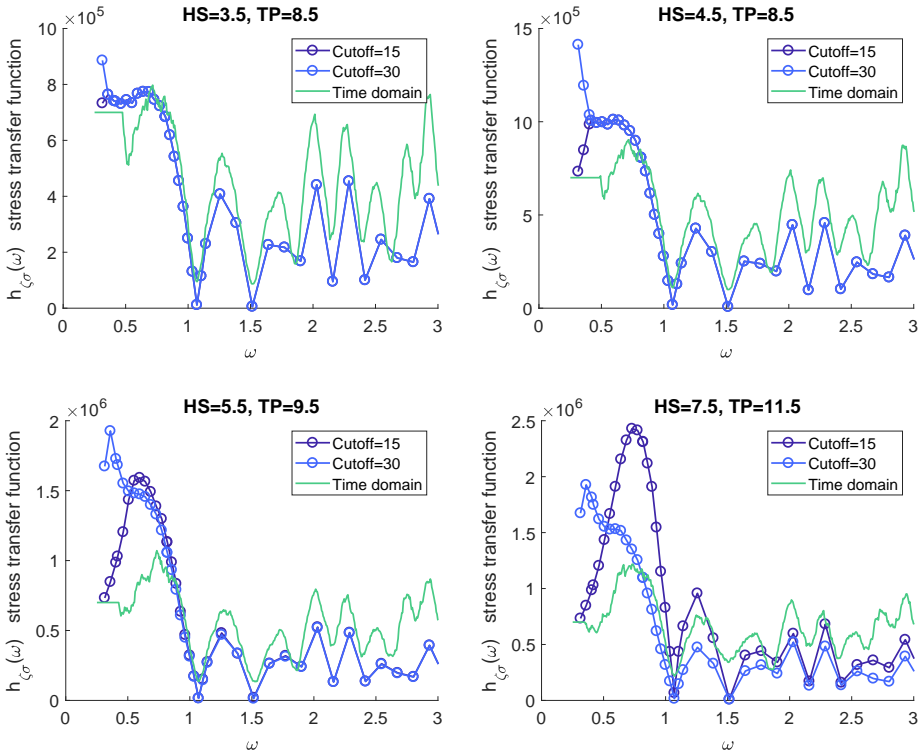
Figure 7.12: *Comparison of steepness-linearized static transfer function of stress with stochastic time domain*

Constant wave height-period ratio

The scheme of selecting wave heights outlined in Section 7.2.1.2 of having constant wave height to period ratio is here investigated in the terms static transfer functions. This can bee seen in figure 7.13.

Also in this case the overshoot in low frequencies increases for for higher sea states. The higher frequency response seem to be better approximated than for the con-

stant steepness. Thus height period ratio might be worth considering for platforms with lower natural periods.
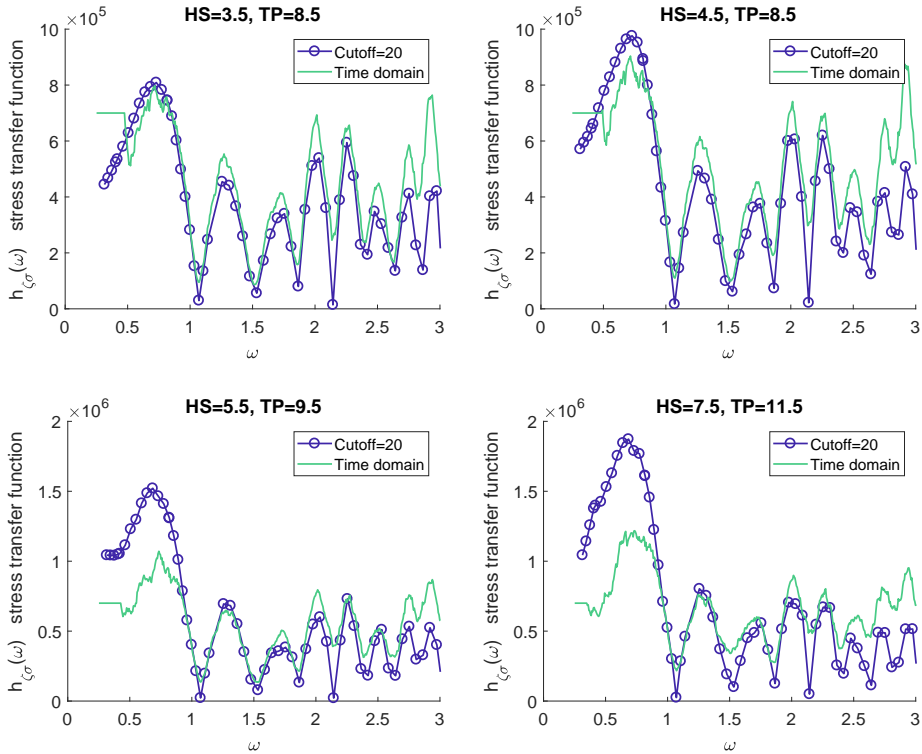
Figure 7.13: *Comparison of height-period-linearized static transfer function of stress with stochastic time domain*

JONSWAP spectrum to determine wave heights

The scheme of selecting wave heights outlined in Section 7.2.1.3 by using the square root of the spectrum and scale this to achieve a proper wave height is here inspected in terms of static stress transfer functions.

This scheme give a large peak at the peak period of the spectra. It also seem to under predict the high frequency response for all cases.
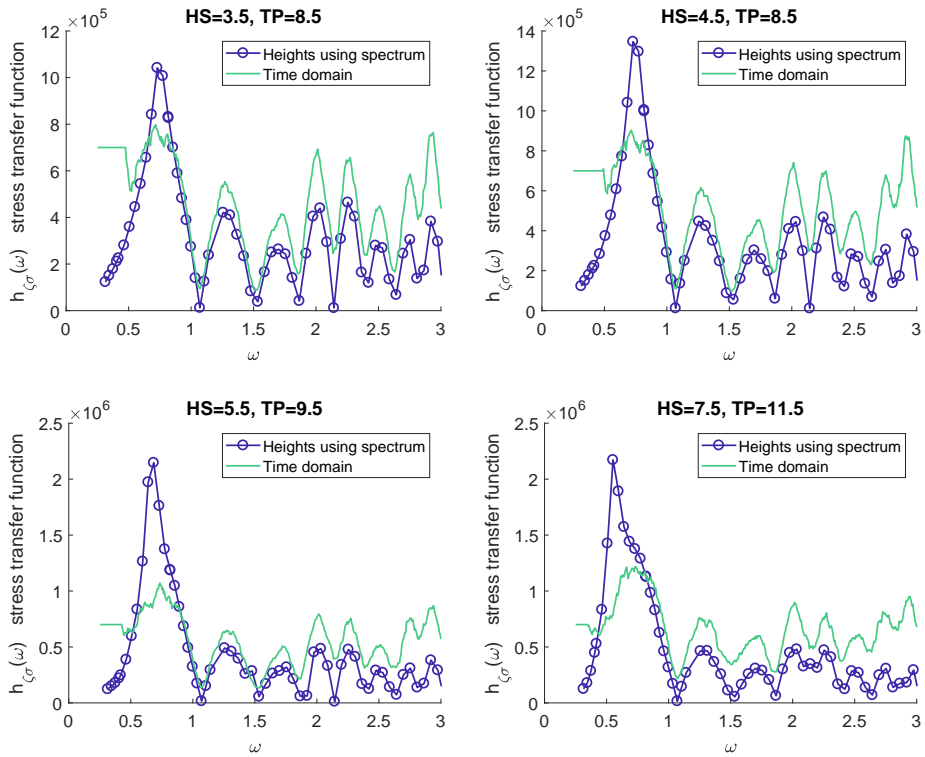
Figure 7.14: *Static stress transfer functions with JONSWAP spectrum used to generate input wave heights, compared with time domain simulations.*

Comparison of all schemes

All the schemes above are plotted together in Figure 7.15 for easier comparison.
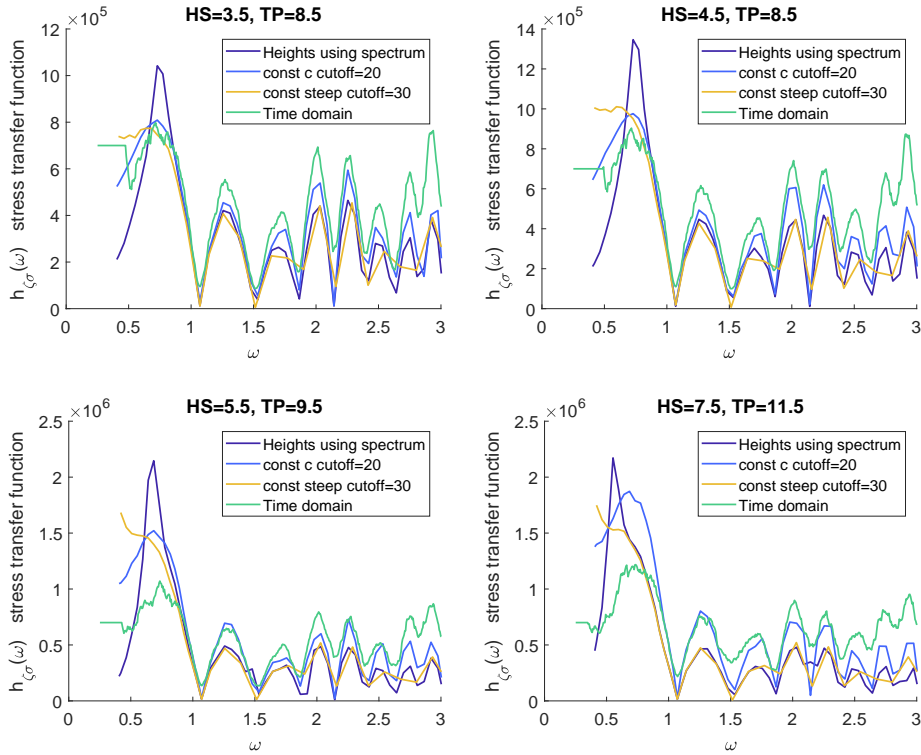
Figure 7.15: SComparison of all schemes, static transfer functions

7.2.5 Dynamic transfer functions

Due to the large degree of dynamic amplification the most important transfer function is the dynamic transfer function. It is of interest to see how the deviation in static transfer function influence the dynamic. The accuracy of the response will be largely influenced by how well the transfer function in the static and dynamic case preform at the natural frequency.

Constant steepness

The constant steepness approach show promising results for the dynamic transfer functions. Evident in Figure 7.16 is that it preforms well on low frequencies. At natural period it overshoots by a significant amount, and this is expected as it also is present in the static transfer function. The overshoot at resonance will contribute to add conservatism. At the larger sea the under prediction at high frequencies increases. This might be important to be aware of if stiffer installations

are considered.
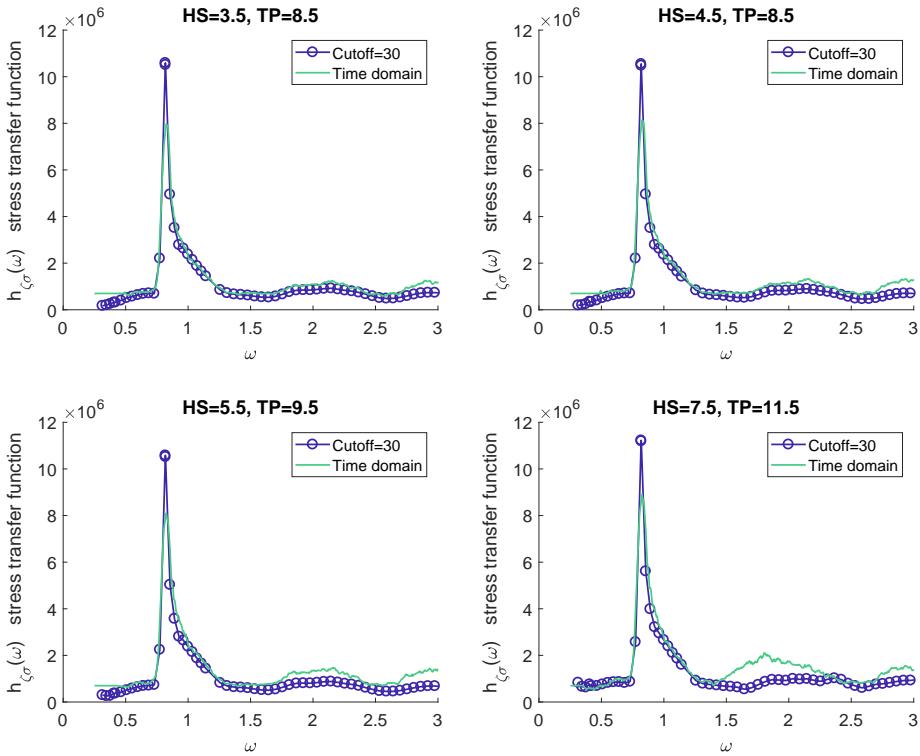
Figure 7.16: *Dynamic stress transfer functions with constant wave steepness, compared with time domain simulations.*

Constant wave height-period ratio

For constant wave height period ratio, the low frequency part is overestimated by a significant amount compared to constant steepness. This is evident in figure 7.17. However the high frequency response seem to be better approximated. In the case of stiff installations with natural periods bellow 4s this scheme might be considered.
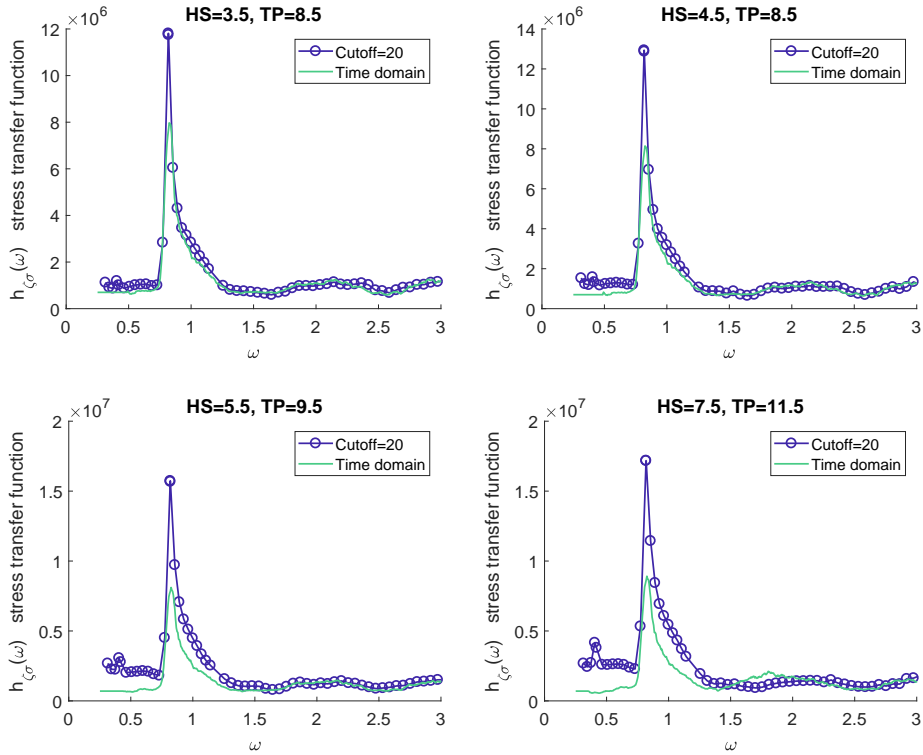
Figure 7.17: *Dynamic stress transfer functions with constant height period ratio, compared with time domain simulations.*

JONSWAP spectrum to determine wave heights

The results for this scheme can bee seen in Figure 7.18. When the JONSWAP spectrum is used to determine the input wave heights the dynamic response seem to give good results at lower sea states. However at low frequencies at higher sea states a second peak is present. This is a result of the peak in the spectrum used to determine the input wave heights. This peak will continue to increase for larger sea states and will give a large over estimate of response at the spectral peak frequency of the spectrum. This method will not be investigated any further.
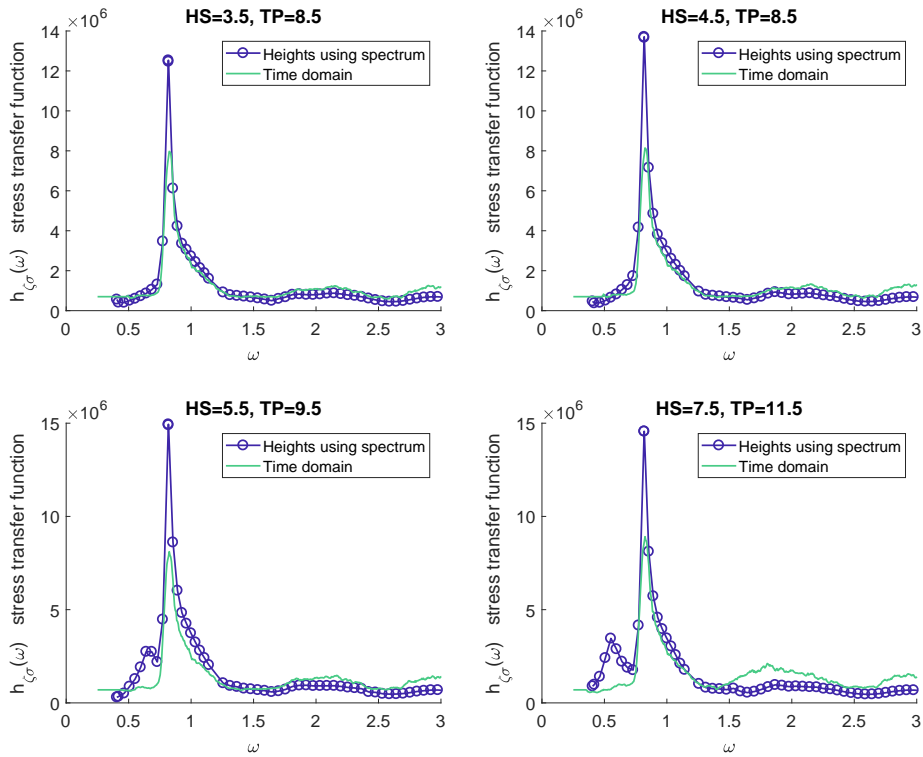
Figure 7.18: *Dynamic stress transfer functions with JONSWAP spectrum used to generate input wave heights, compared with time domain simulations.*

Comparison of all schemes

All the schemes above are plotted together in Figure 7.19 for easier comparison.
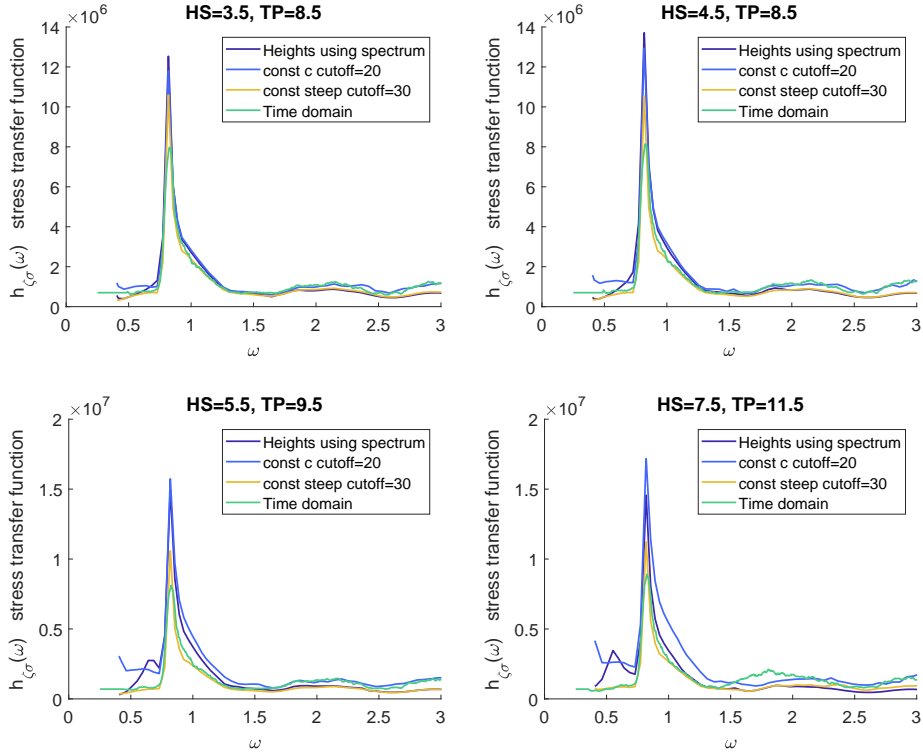
Figure 7.19: Comparison of dynamic transfer functions from all schemes

7.2.6 Calibration for every sea state

Instead of using one transfer function to represent the response for every sea state, it is here created one transfer function for each sea state. This means that the steepness and height-period parameter is calibrated for every sea state. This should result in significant improvements compared to only using one transfer function. This will in turn increase the computational demand, but still be considerably lower than the time domain simulation. In the following two sections the results are presented with colors. For numerical results in tables see appendix A.

7.2.6.1 Comparison of short term damage

The constant steepness scheme gives very promising results. It do however over predict the damage at resonance compared to the time domain simulation. For calibration of c the values are in general to large. However it does give as large amplifications in the resonant area as the the steepness.
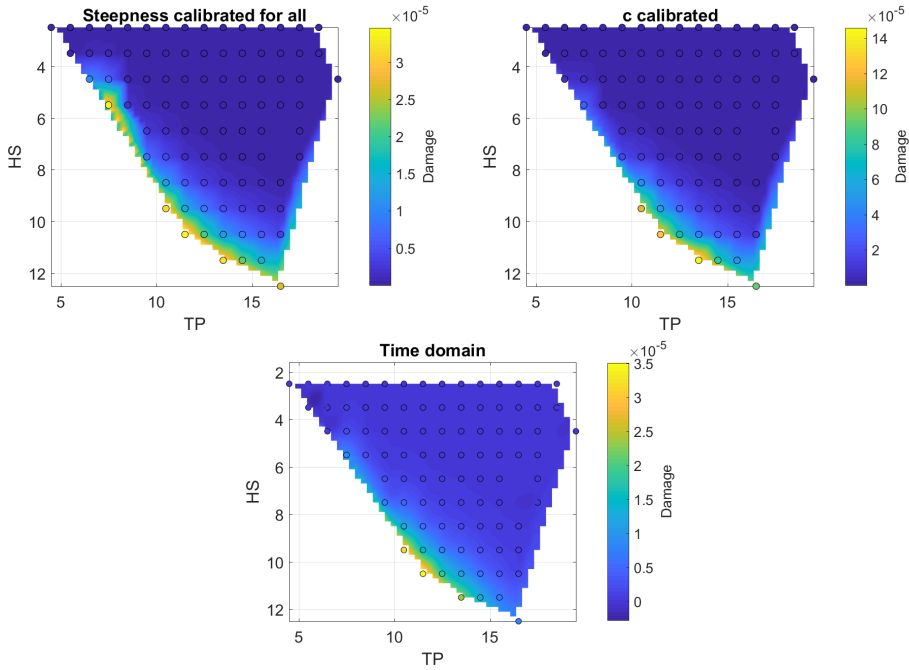
Figure 7.20: *Comparison of short term damage for different linearizations (c = H/T)*

7.2.6.2 Comparison of long term damage

In this section the long term damage is presented. This is the total damage experienced during 56 years in the Ekofisk area from each block in the scatter diagram. As indicated in the previous section the amplitudes of scheme with constant height-period ratio (c) gives larger damages, this is also the case for the long term damage. However the total damage is not to far from what is calculated in time domain simulations. The scheme with constant steepness gives total damage slightly higher than the time domain simulation. However in this case the damage is much more concentrated. The degree of conservatism might bee too small in order to rely on the steepness in the general case.
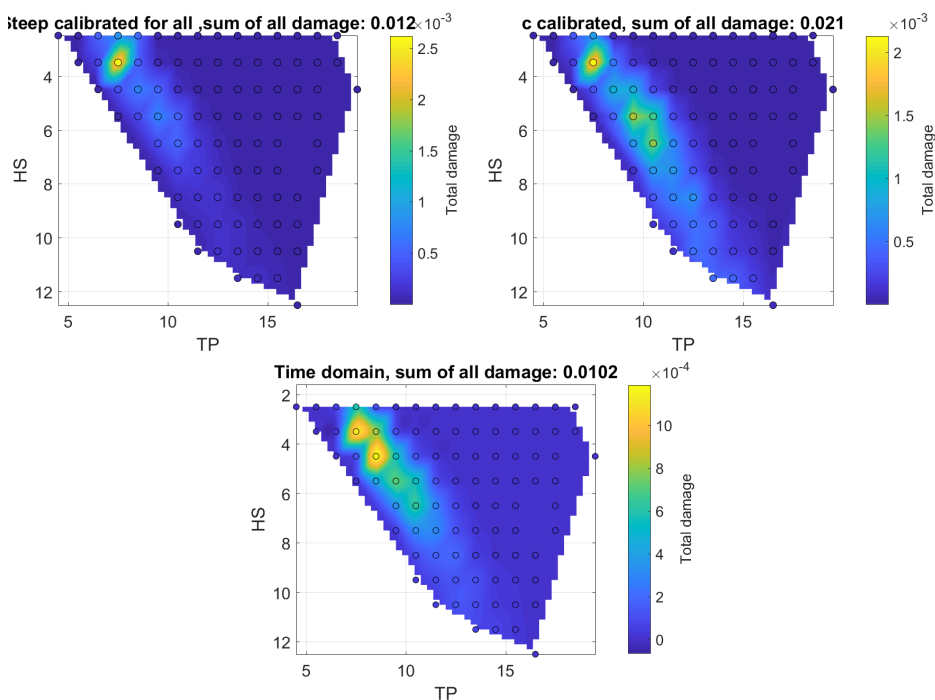
Figure 7.21: *Comparison of short term damage for different linearizations (c =
H/T)*

7.3   Linearization by changing the drag coefficient

In a general case there can hardly be possible to come up with empirical simple
mathematical relations describing the calibration of parameters such as steepness.
The main aspect leading to this is the differences from design to design. Dimen-
sional properties vary from design to design, and will influence the performance of
a certain steepness value.

Another take on the problem might be in changing the drag coefficient. A method
of linearizing the problem is illustrated in equation 7.21, by simply changing the
drag term to a linear. This involves changing the drag coefficient. The huge
benefit of this method is its local impact. It opens up for more generalized ways
of selecting appropriate values for the linearized problem since the drag coefficient
can be customized for each member.

Here one such method is outlined. This method utilizes the standard deviation of
the wave particle velocity in addition to diameter in order to select drag coefficient.
The standard deviation in particle velocity will rely on the sea state as well as depth.

$$F_D = \frac{1}{2}C_D\rho D|u|u \rightarrow F_D^{lin} = \frac{1}{2}C_{(D,L)}\rho Du \tag{7.21}$$

In equation 7.21, the $C_{(D,L)}$ is a linear drag coefficient. This coefficient should be selected such that the total force gives similar characteristics as the nonlinear. One way to select this coefficient is such that the integral of the deviation between the linear and nonlinear drag force during one cycle is minimized. However for fatigue damage the stress range is of importance, and not the deviation during a cycle. Instead of minimize the deviation for one cycle, it seem more reasonable to select the linear drag coefficient to give an equal amount of fatigue damage. By assuming that the fatigue damage can be estimated from the individual peak values of the stress process it is with certain assumptions possible to establish a drag coefficient that gives equal damage as the true drag.

By assuming that there exist a linear relationship between force peak and stress peak, equation 7.22 can be used to describe the damage from one peak.

$$D_i = \nu(F_{p,i})^m \tag{7.22}$$

Here m is the slope of the SN-curve, ν a constant, and $F_{p,i}$ force peak number i. By assuming that the velocities follows a Rayleigh distribution, and requiring that the expected value of damage from forces with linear drag term es equal to the true forces as in equation 7.23,

$$E[F_{p,L}^m] = E[F_p^m] \tag{7.23}$$

the ratio $C = \frac{C_{(D,L)}}{C_D\sigma_u}$ can be given on a closed form as in equation 7.24 [Wolfram, 1998].

$$
\begin{aligned}
C^{(m)}(K)^2 = \Bigg\{ &\frac{1}{\Gamma(1+0.5m)} \left[\sum_{p=0}^{m} \frac{m!}{(m-p)!p!}\Gamma(1+p, \frac{1}{8K^2})^{m-p}/2^{0.5p} \right. \\
&\left. + \ \gamma(1+0.5m, \frac{1}{8K^2})/K^m \right] \Bigg\}^{2/m} - \frac{1}{K^2}
\end{aligned}
\tag{7.24}
$$

Where $\Gamma()$ is the gamma function, and $\gamma(,)$ and $\Gamma(,)$ is the lower and upper incomplete gamma function given by equation 7.25 and 7.26 [Abramowitz and Stegun, 1972].

$$\gamma(a,x) = \int_0^x \exp(-t)t^{a-1}dt \tag{7.25}$$

$$\Gamma(a,x) = \int_x^\infty \exp(-t)t^{a-1}dt \tag{7.26}$$

K is given in equation 7.27

$$K = \frac{C_D \sigma_u T_P}{\pi^2 C_M D} \tag{7.27}$$

The standard deviation in wave particle velocity will obviously vary with sea state. However it will also vary with depth. Members in the deep part of the structure will have smaller standard deviation in velocity compared to the ones in the surface area. The standard deviation of velocity can be calculated according to equation 7.28. Other properties such as angle on current will also contribute to the velocity standard deviation.

$$\sigma_u^2 = \int_0^\infty e^{2kz} \omega^2 S_{\zeta\zeta}(\omega) d\omega = \int_0^\infty e^{2\frac{\omega^2 z}{g}} \omega^2 S_{\zeta\zeta}(\omega) d\omega \tag{7.28}$$

The solution procedure will then be to first calculate K from equation 7.27 and use this to calculate a drag coefficient according to equation 7.29. Both K and $C^{(m)}(K)$ has to be calculated for all members due to the standard deviation in velocity and its dependency on depth.

$$C_{(D,L)} = C^{(m)}(K) C_D \sigma_u \tag{7.29}$$

$C^{(m)}(K)$ is plotted in Figure 7.22. For the members in the surface area K will be typically above 1 for the most important sea states (region $H_S=4.5, T_P = 8.5$).
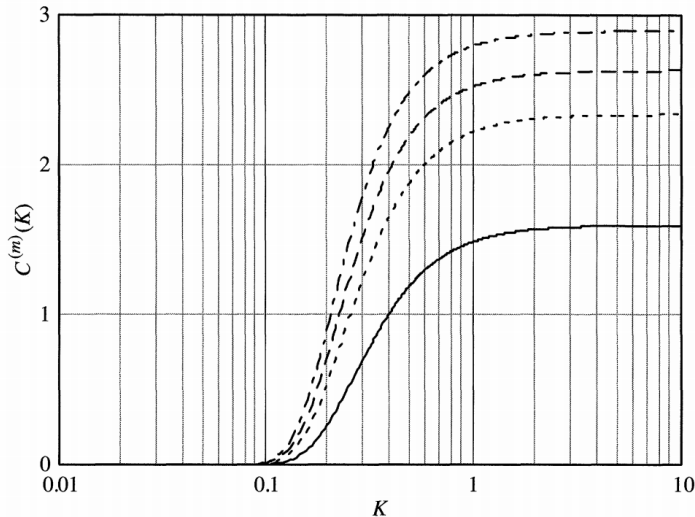
Figure 7.22: *Linearization factors for Morison's equation for estimating expected fatigue damage when the SN-slope, m=1, 3, 4 and 5 represented by full, dotted, dashed and dash-dotted lines, respectively. From: [Wolfram, 1998]*

In the above method relative velocity are not accounted for. However it might give reasonable values of the linear drag coefficient considering that the structural velocities are small compared to wave particle velocities as seen in Table 7.6.

H	T	$\dot{r}_a/u_a$
7m	13s	$\approx 10^{-3}$
3m	5s	$\approx 10^{-4}$

Table 7.6: *The ratio between structural response velocity amplitude and water particle velocity amplitude for 2 cases, with harmonic input, measured in surface area (drag coefficient of 1.15 is used for the whole structure)*

To investigate how this method compares to the other, modifications to USFOS source code has to be made. The program need to be able to change to a linear drag term, which is not a feature at the present point in time. Hence an implementation of this method is not acomplished.

Chapter 8

Conclusion

The three parameter Weibull distribution fitted by the method of moments gives adequate statistical descriptions of the short term stress processes. The parameters can be presented as smooth surfaces over the $H_S - T_P$ plane.

The damage encountered is influenced by the particular realization of each sea state. In order to ensure that the estimated damage has statistical reliability several realizations of the same sea state should be averaged.

Drag forces are found to be a lot more important than inertia forces. This is due to the small dimensions on the structural members, in addition to the large drag coefficient for chords induced by the rack.

If the response is represented by one transfer function at the center of fatigue the results are highly dependent on the initial assumptions that estimates the location of the center of fatigue. This method might give good results if the center of fatigue is estimated correctly, however this is not an straight forward process. Different aspects complicates this process. Kinked SN-curves and nonlinear relationships between wave height and stress is among them. If the center of fatigue is not located properly the method will give poor results. To add conservatism it is possible to move the estimated center of fatigue to a higher significant wave height.

It is however strongly recommended to calibrate the wave heights for every sea state. This demands more computational efforts, but is still very manageable. It gives a much better impression of how the structure is behaving at each sea state. For this particular jack-up this method gives conservative results, and in general the calibration procedure must be considered to give good results. If the cutoff height selected is to low, the calibration procedure might not be possible for sea states with larger significant wave heights.

Both steepness and constant height-period ratio has shown promising results. The

constant wave height-period ratio is giving more accurate results for periods of less than 4s, and should be considered for stiffer drag dominated structures.

Another aspect is the rapid improvement in computational capacity. This makes time domain simulations more and more affordable. The method used for the realization of the waves allows for less wave components and hence saving a lot of simulation time. More computational time must however be expected by using second order irregular wave kinematics instead of first order.

Chapter 9

Recommendations for further work

Other critical spots for stress concentrations than the joint selected might be critical. There is a high possibility that a critical spot might be on rack or in the gearing system used to elevate and lock the racks in place. This will require detailed finite element modeling of the rack and a gear system. The dimensional properties of gears are such that 3 dimensional solid elements should be used for modeling. This is not always supported software wise in the offshore industry, which usually sticks to plates and beams.

The linearization techniques might also be viewed in the context of heading. By dividing the heading in different sectors, and perhaps calculate the calibrated steepness for each heading.

The spectrum used here is a sharply peaked JONSWAP spectrum. It might be interesting to look into the case of a double peaked spectrum. This perhaps introduces new difficulties regarding the linearization process.

A equivalent drag coefficient might be another way to approach the problem. This will however require software to support such linear drag terms. It will open up for a far more detailed linearization process, and may also by simple mathematical relations.

An extended analysis might also be carried out to insure sufficient statistical accuracy in terms of realizations. This can be carried out by averaging several realizations of the same sea state.

What is the might most important aspect to get more insight into, is however, the effect of current. As indicated in the beginning of the thesis, the current may amplify the amplitudes of the forces significantly.

Bibliography

Aarsnes, L. H. [2015], *Estimation of Extreme Response on a Jack-up Platform by Application of Stochastic Methods*, Department of Marine Technology NTNU.

Abramowitz, M. and Stegun, I. A. [1972], *Handbook of Mathematical Functions with Formulas, Graphs, and Mathematical Tables*, U.S. Department of Commerce, NIST.

Almar-Næss, A. [1985], *Fatigue Handbook: Offshore Steel Structures*, 1 edn, Tapir.

Box, G. E. P., Jenkins, G. M. and Reinsel, G. C. [1994], *Time Series Analysis: Forecasting and Control*, Prentice Hall.

Conte, C. P. [2016], *Random vibrations*, UC Dan Diego Jacobs School of Engineering.

DNV GL [2014*a*], *DNV-RP-C205: Environmental Conditions and Environmental Loads*, july edn, DNV GL.

DNV GL [2014*b*], *DNVGL-RP-C203: Fatigue design of offshore steel structures*, july edn, DNV GL.

DNV GL [2015], *DNVGL-RP-C104: Self-elevating units*, july edn, DNV GL.

Faltinsen, O. M. [1993], *Sea Loads on Ships and Offshore Structures*, 1 edn, Cambridge University Press.

Goncalves, A. [2017], 'Mail correspondence'. Received; 10 May 2017.

Haver, S. [2016], *Stochastic Description of Ocean Waves and Response Analysis and Prediction of Extremes*, NTNU.

Haver, S. [2017], *Metocean Modelling and Prediction of Extremes, Draft version 1*, Univeristy in Stavangerm NTNU.

Hilber, H. M. and Hughes, T. J. R. [1978], *Collocation, Dissipation and 'Overshoot' for Time Integration Schemes in Structural Dynamics*, Earthquake Engineering and Structural Dynamics 6 p. 99-118.

Hughes, T. J. R. [2000], *The Finite Element Method Linear Static and Dynamic Finite Element Analysis*, 1 edn, Dover.

ISO [2007], *ISO 19902 Petroleum and natural gas industries – Fixed steel offshore structures*, International Organization for Standardization.

Langen, I. and Sigbjornsson, R. [1986], *Dynamisk Analyse av marine konstruksjoner*, Tapir.

Larsen, C. M. [2014], *TMR4182 Marine dynamics*, january edn, Department of Marine Technology.

Marintek [2001], *USFOS Getting Started*, SINTEF group.

Marintek [2010], *USFOS Hydrodynmaics, Theory, Description of use, Verification*, SINTEF group.

Myrhaug, D. [2007], *TMR 4180 Marin Dynamikk uregelmessig sjø*, NTNU.

Myrhaug, D. [2016], *TMR4235: Stochastic Theory of Sea Loads. Statistics of Narrow Band Processes and Equivalent Linearization*, Department of Marine Technology NTNU.

Newland, D. E. [2005], *Random Vibrations, Spectral and Wavelet Analysis*, 3 edn, Dover Publications.

NORSOK [2007], *N-003*.

Søreide, T. H., Amdahl, J., Eberg, E., Holmås, T. and Øyvind Hellan [1993], *USFOS - A computer Program for Progressive Collapse Analysis of Steel Offshore Structures. Theory Manual*, SINTEF Division of Structural Engineering.

Tahery, H. M. [2015], *Investigation of which sea states yield the dominating contribution to fatigue accumulation in offshore structure*, Department of marine technology, NTNU.

WAFO-group [2011], *WAFO - A Matlab Toolbox for Analysis of Random Waves and Loads - A Tutorial*, Math. Stat., Center for Math. Sci., Lund Univ.

Wolfram, J. [1998], *On alternative approaches to linearization and Morison's equation for wave forces*, Department of Civil and Offshore Engineering, Heriot- Watt University, Edinburgh EH9 1.

Appendices

Linearization and time domain results and tables

In this appendix the numerical results are presented in tables. These tables are in the same format as the scatter diagram.

A.1 Calibration ratios

Table A.1: Steepness, defined as $\frac{H}{T^2}$

$0<HS<1$ \ $2<TP<3$	2.5	3.5	4.5	5.5	6.5	7.5	8.5	9.5	10.5	11.5	12.5	13.5	14.5	15.5	16.5	17.5	18.5	19.5	20.5	Cutoff
0.5																				
1.5																				
2.5			1.57E-01	1.84E-01	1.55E-01	6.75E-02	5.37E-02	3.99E-02	4.22E-02	3.63E-02	3.60E-02	3.09E-02	2.72E-02	2.41E-02	2.25E-02	2.15E-02	2.13E-02	0		
3.5				2.55E-01	2.09E-01	1.07E-01	4.86E-02	6.10E-02	5.92E-02	5.11E-02	4.75E-02	4.01E-02	3.45E-02	3.03E-02	2.82E-02	2.69E-02	2.67E-02	0		
4.5					2.75E-01	1.43E-01	6.72E-02	7.98E-02	7.53E-02	6.39E-02	5.83E-02	5.03E-02	4.35E-02	3.82E-02	3.54E-02	3.37E-02	0	3.60E-02		
5.5						1.76E-01	9.39E-02	1.02E-01	9.40E-02	7.92E-02	7.05E-02	6.02E-02	5.29E-02	4.69E-02	4.33E-02	4.12E-02				
6.5								1.19E-01	1.09E-01	9.15E-02	8.17E-02	6.98E-02	6.13E-02	5.49E-02	0	4.85E-02				
7.5								1.37E-01	1.25E-01	1.04E-01	9.28E-02	7.93E-02	6.97E-02	6.25E-02	6.64E-02	5.59E-02				
8.5									1.46E-01	1.21E-01	1.06E-01	9.10E-02	7.93E-02	7.12E-02	7.38E-02					
9.5									1.63E-01	1.37E-01	1.20E-01	1.02E-01	8.94E-02	7.88E-02	8.24E-02					
10.5										1.53E-01	1.34E-01	1.13E-01	9.97E-02	8.89E-02	0					
11.5												1.30E-01	1.12E-01	9.99E-02	1.03E-01					
12.5																				

Table A.2: Height period ratio, defined as $\frac{H}{T}$

$0<HS<1$ \ $2<TP<3$	2.5	3.5	4.5	5.5	6.5	7.5	8.5	9.5	10.5	11.5	12.5	13.5	14.5	15.5	16.5	17.5	18.5	19.5	20.5	Cutoff
0.5																				
1.5																				
2.5			7.78E-01	1.01E+00	9.36E-01	4.71E-01	4.39E-01	4.07E-01	4.75E-01	4.53E-01	4.89E-01	4.54E-01	4.28E-01	3.95E-01	3.79E-01	3.71E-01	3.80E-01	0		
3.5				1.35E+00	1.24E+00	7.22E-01	4.08E-01	6.14E-01	6.61E-01	6.24E-01	6.32E-01	5.85E-01	5.40E-01	4.98E-01	4.81E-01	4.74E-01	4.85E-01	0		
4.5					1.62E+00	9.85E-01	5.82E-01	7.83E-01	8.34E-01	7.86E-01	7.77E-01	7.16E-01	6.69E-01	6.22E-01	6.02E-01	5.94E-01	0	6.64E-01		
5.5						1.20E+00	7.76E-01	1.00E+00	1.05E+00	9.69E-01	9.42E-01	8.62E-01	8.04E-01	7.51E-01	7.27E-01	7.20E-01				
6.5								1.17E+00	1.21E+00	1.12E+00	1.09E+00	1.00E+00	9.35E-01	8.76E-01	0	8.38E-01				
7.5								1.35E+00	1.38E+00	1.28E+00	1.24E+00	1.14E+00	1.07E+00	1.00E+00	1.14E+00	9.67E-01				
8.5									1.76E+00	1.59E+00	1.50E+00	1.36E+00	1.27E+00	1.18E+00	1.27E+00					
9.5									1.98E+00	1.78E+00	1.68E+00	1.53E+00	1.40E+00	1.30E+00	1.42E+00					
10.5										2.00E+00	1.89E+00	1.71E+00	1.57E+00	1.47E+00	0					
11.5												2.41E+00	2.03E+00	1.78E+00	2.50E+00					
12.5																				

A.2 Short term sea state

Table A.3: *Calibrated using steepness*

2<TP<3 / 0<HS<1	2.5	3.5	4.5	5.5	6.5	7.5	8.5	9.5	10.5	11.5	12.5	13.5	14.5	15.5	16.5	17.5	18.5	19.5	20.5	Cutoff
2.5			1.67E-10	7.26E-09	6.02E-08	7.65E-08	2.31E-09	1.34E-09	6.60E-10	3.91E-10	1.97E-10	1.10E-10	6.21E-11	3.74E-11	2.32E-11	1.62E-11				2.20E-07
3.5				1.40E-07	1.07E-06	8.39E-07	5.73E-08	2.15E-08	1.18E-08	5.53E-09	3.20E-09	1.62E-09	8.57E-10	4.88E-10	3.02E-10	1.92E-10	1.41E-10			2.15E-06
4.5				1.03E-05	6.52E-06	3.33E-07	1.34E-07	7.17E-08	3.14E-08	1.74E-08	9.13E-09	5.00E-09	2.96E-09	1.82E-09	1.19E-09	0		8.14E-10		1.74E-05
5.5				3.38E-05	6.52E-06	1.76E-06	6.47E-07	3.40E-07	1.50E-07	8.22E-08	4.12E-08	2.39E-08	1.40E-08	5.89E-08	8.93E-09	6.00E-09	0			3.68E-05
6.5						2.42E-06	1.22E-07	5.21E-07	1.61E-06	3.03E-07	1.54E-07	9.33E-08	3.11E-07	2.08E-07	0	2.53E-08				4.80E-06
7.5						7.65E-06	3.92E-06	1.22E-06	1.61E-06	9.41E-07	5.10E-07	3.11E-07	2.08E-07	2.08E-07	9.41E-08					1.52E-05
8.5							1.22E-06	5.19E-06	2.89E-06	1.60E-06	1.04E-06	6.78E-07	4.67E-07							2.41E-05
9.5								3.19E-05	5.19E-06	8.27E-06	4.48E-06	3.02E-06	1.97E-06	1.36E-06						6.49E-05
10.5									1.40E-05	2.08E-05	1.18E-05	8.15E-06	5.69E-06	3.75E-06						8.48E-05
11.5									3.46E-05		3.22E-05	2.19E-05	1.56E-05							6.97E-05
12.5														2.66E-05						2.66E-05
0	0	0	1.67E-10	1.47E-07	1.14E-05	4.12E-05	2.23E-06	1.09E-05	4.96E-05	5.61E-05	3.33E-05	5.08E-05	3.46E-05	2.42E-05	3.22E-05	1.27E-07	1.57E-10	8.14E-10	0	0.000347

Table A.4: *Time domain simulations*

2<TP<3 / 0<HS<1	2.5	3.5	4.5	5.5	6.5	7.5	8.5	9.5	10.5	11.5	12.5	13.5	14.5	15.5	16.5	17.5	18.5	19.5	20.5	Cutoff
2.5			2.22E-09	3.96E-09	1.18E-08	4.54E-08	1.56E-08	5.56E-09	4.30E-09	3.47E-09	2.85E-09	2.56E-09	2.28E-09	2.00E-09	1.81E-09	1.68E-09	1.62E-09			1.07E-07
3.5				1.36E-08	7.68E-08	3.59E-07	1.02E-07	2.70E-08	1.74E-08	1.10E-08	7.28E-09	5.51E-09	4.28E-09	3.30E-09	2.77E-09	2.42E-09	2.26E-09			6.35E-07
4.5				4.83E-07	7.68E-08	2.05E-06	1.41E-07	8.55E-08	4.58E-08	1.68E-08	1.10E-08	7.14E-09	5.04E-09	4.03E-09	1.17E-08	4.03E-09	0.00E+00	3.38E-09		3.44E-06
5.5						9.19E-06	2.42E-06	6.18E-07	3.72E-07	9.50E-08	5.72E-08	3.32E-08	1.88E-08	8.54E-09	0.00E+00					1.30E-05
6.5						2.28E-06	1.37E-06	6.72E-07	3.31E-07	1.94E-07	1.06E-07	5.70E-08	2.21E-08							5.03E-06
7.5						7.35E-06	2.12E-06	2.12E-06	1.04E-06	5.96E-07	3.18E-07	1.65E-07	6.14E-08							1.61E-05
8.5							1.27E-05	6.00E-06	2.99E-06	1.72E-06	9.03E-07	4.54E-07	2.53E-07							2.50E-05
9.5							3.18E-05	7.68E-06	4.57E-06	2.36E-06	1.20E-06	6.63E-07								6.37E-05
10.5								1.54E-05	6.00E-06	5.91E-06	1.09E-05	3.00E-06	1.62E-06							7.45E-05
11.5								3.51E-05	1.80E-05	2.37E-05	1.33E-05	6.96E-06	0.00E+00							4.40E-05
12.5														8.47E-06						8.47E-06
0	0	0	2.22E-09	1.75E-08	5.72E-07	3.1E-06	1.04E-05	5.08E-05	5.95E-05	3.02E-05	4.18E-05	2.29E-05	1.19E-05	1.1E-05	1E-07	3.88E-09	3.38E-09	0	0.000254

Table A.5: *Constant wave height-period ratio*

2<TP<3 / 0<HS<1	2.5	3.5	4.5	5.5	6.5	7.5	8.5	9.5	10.5	11.5	12.5	13.5	14.5	15.5	16.5	17.5	18.5	19.5	20.5	Cutoff
2.5			1.74E-10	4.73E-09	4.67E-08	5.39E-08	5.86E-09	3.04E-09	2.14E-09	1.07E-09	7.17E-10	3.59E-10	1.93E-10	1.03E-10	5.97E-11	3.64E-11	2.56E-11			1.19E-07
3.5				8.39E-08	6.52E-07	6.41E-07	3.70E-08	3.70E-08	2.46E-08	1.20E-08	7.30E-09	3.60E-09	1.85E-09	9.68E-10	5.78E-10	3.64E-10	2.66E-10			1.57E-06
4.5				6.22E-06	6.82E-07	5.67E-06	4.30E-07	2.25E-07	1.55E-07	7.33E-08	4.35E-08	2.21E-08	1.23E-08	6.98E-09	4.23E-09	2.69E-09	0	1.86E-09		1.29E-05
5.5						2.71E-05	2.16E-06	1.35E-06	8.60E-07	4.05E-07	2.30E-07	1.11E-07	6.10E-08	3.42E-08	1.42E-08	6.13E-08				3.24E-05
6.5						4.91E-06	3.20E-06	1.47E-06	1.10E-06	5.50E-07	2.55E-07	1.49E-07	0	2.41E-07						1.14E-05
7.5						1.66E-05	1.04E-05	4.89E-06	2.86E-06	1.47E-06	8.71E-07	5.50E-07								3.79E-05
8.5							4.54E-05	2.00E-05	1.10E-05	5.78E-06	3.50E-06	2.17E-06	1.38E-06							8.93E-05
9.5							1.13E-04		2.92E-05	1.58E-05	9.67E-06	6.07E-06	4.03E-06							2.30E-04
10.5								1.24E-04	7.08E-05	3.99E-05	2.53E-05	1.69E-05	1.13E-05							2.88E-04
11.5									1.46E-04	8.03E-05	4.99E-05	0								2.76E-04
12.5														9.24E-05						9.24E-05
0	0	0	1.74E-10	8.86E-08	6.92E-06	3.35E-05	2.66E-06	2.31E-05	5.08E-05	0.000173	0.000203	0.000115	0.000209	0.000112	7.58E-05	0.000109	3.2E-07	2.91E-10	1.86E-09	0.001072

A.3   Long term sea state (56 years)

Table A.6: *Calibrated using steepness*

Table A.7: *Time domain simulations*

Table A.8: *Constant height-period ratio*

Stress range distributions from 93 sea states
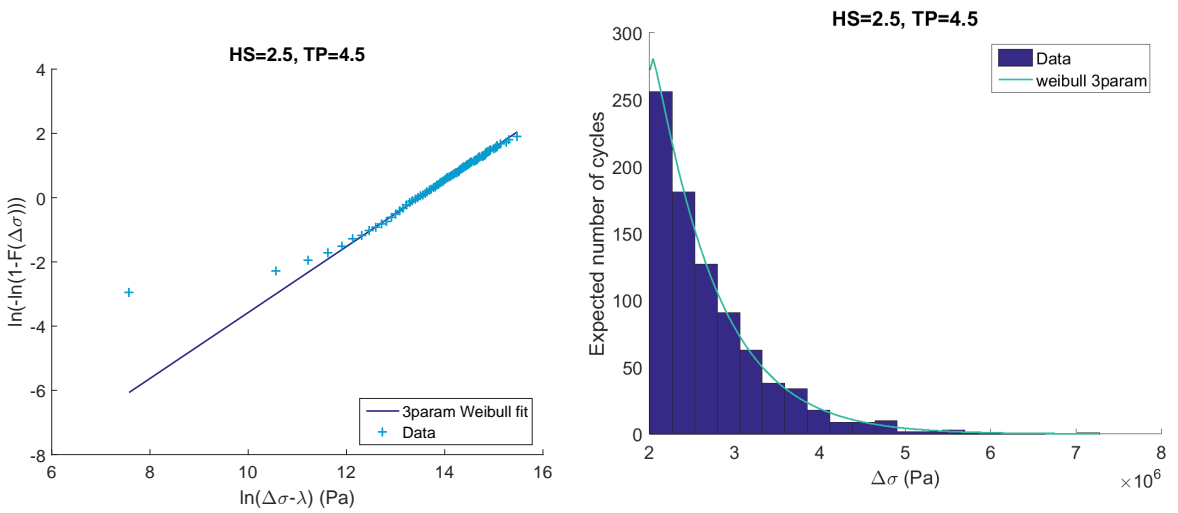
Figure B.1: *Probability distributions of stress range during 3h realizations HS:2.5 TP:4.5*
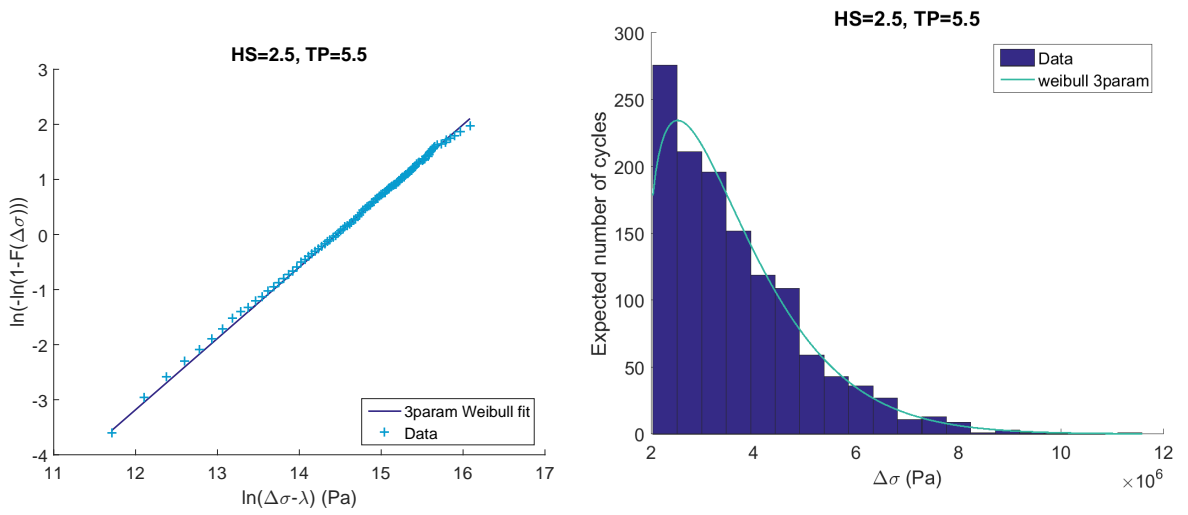
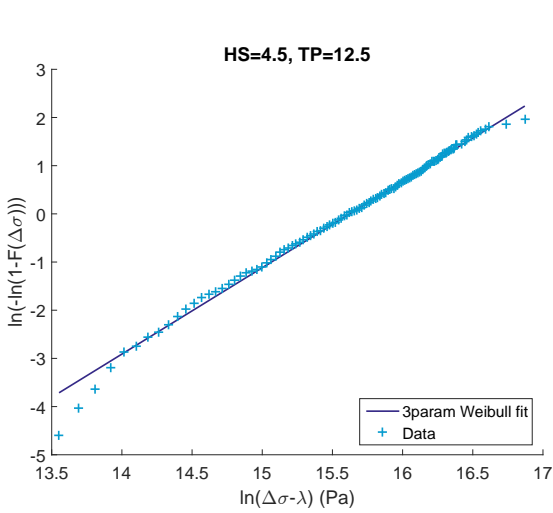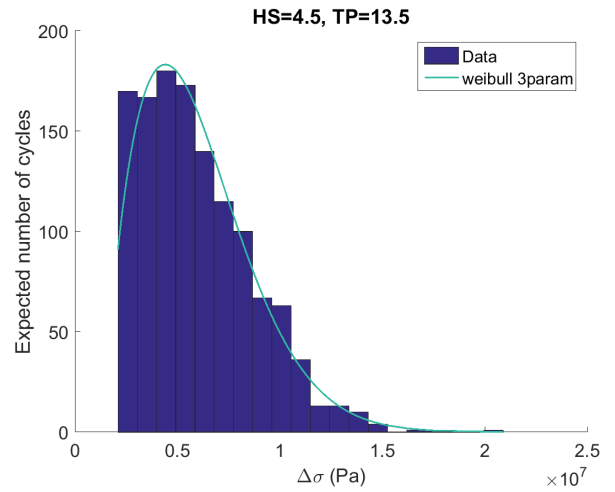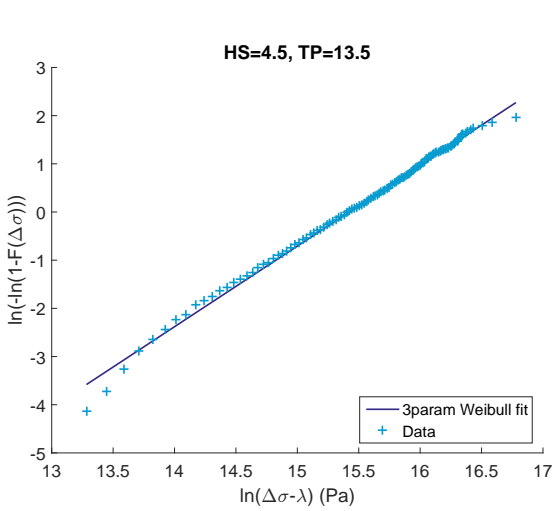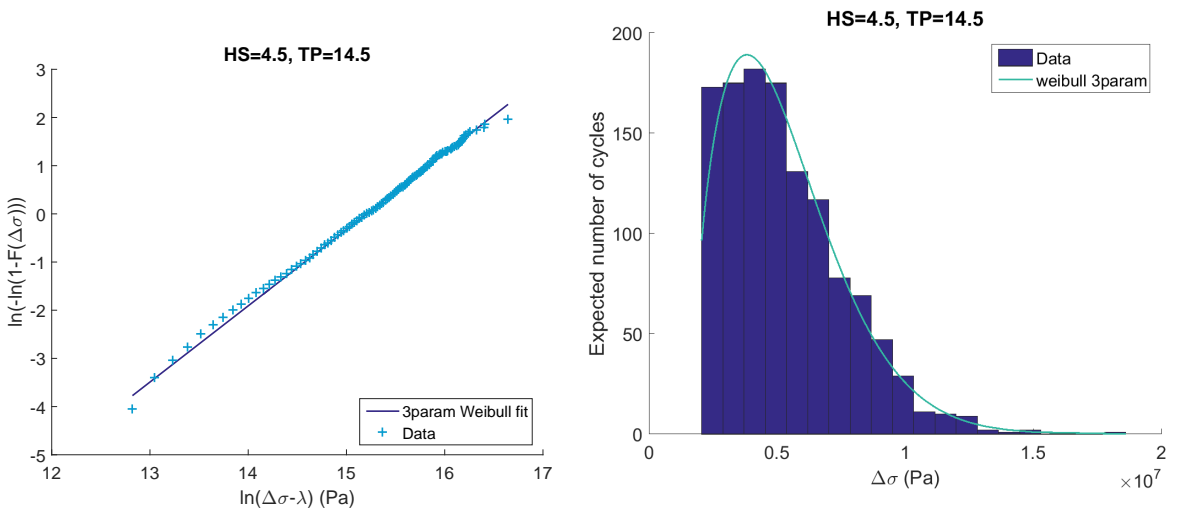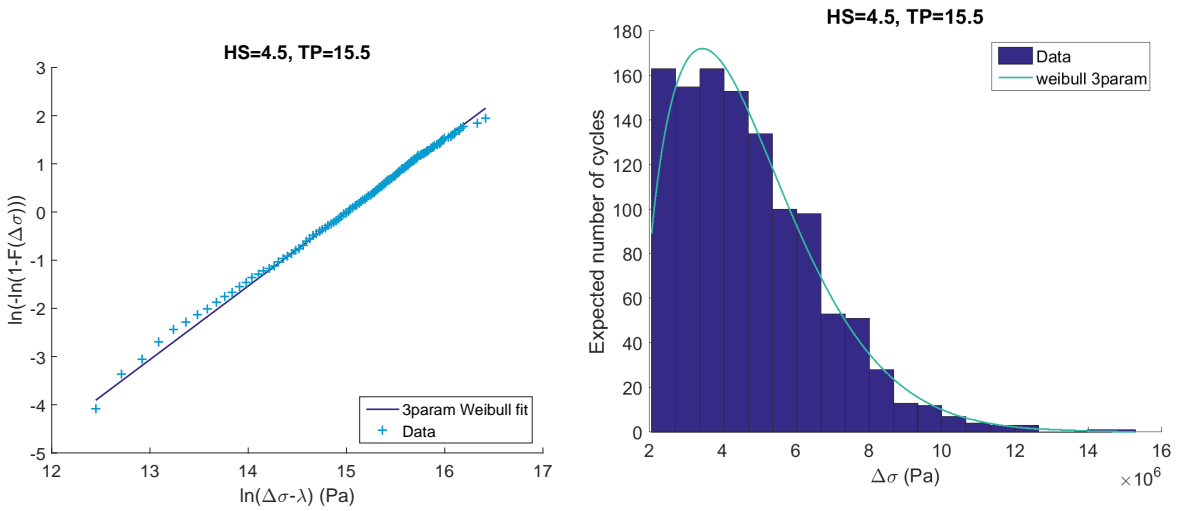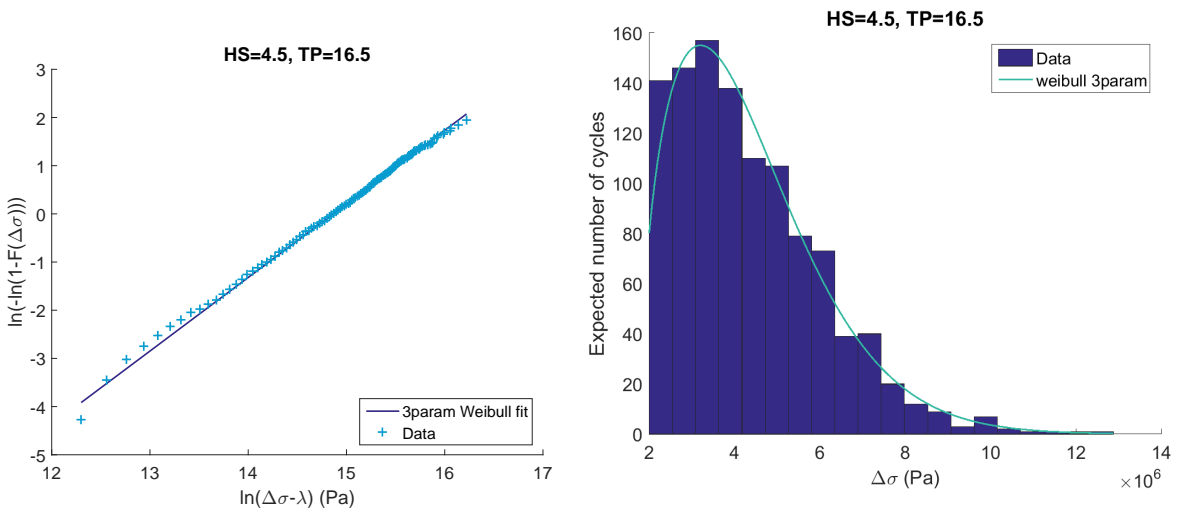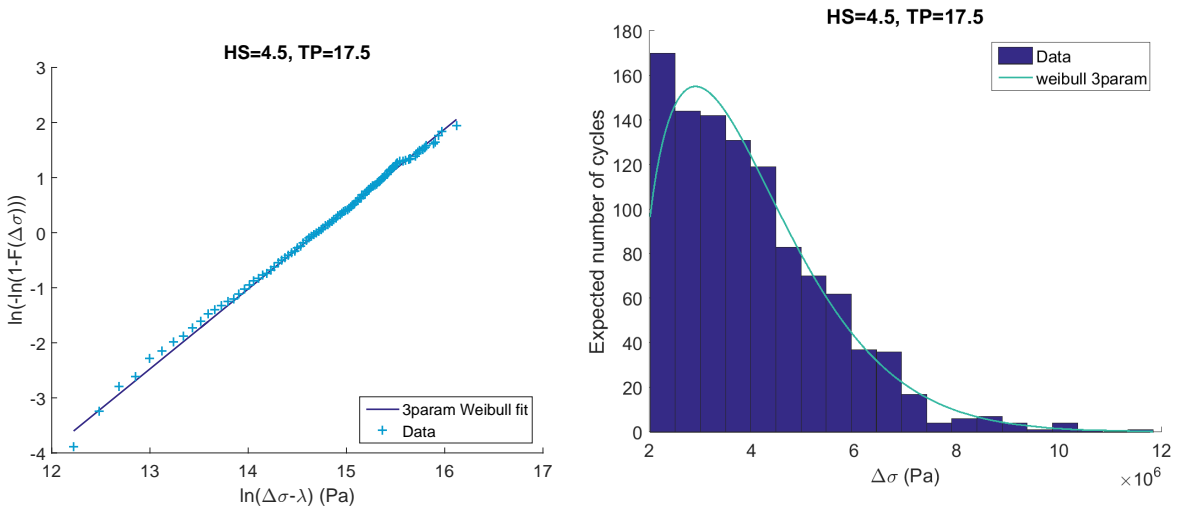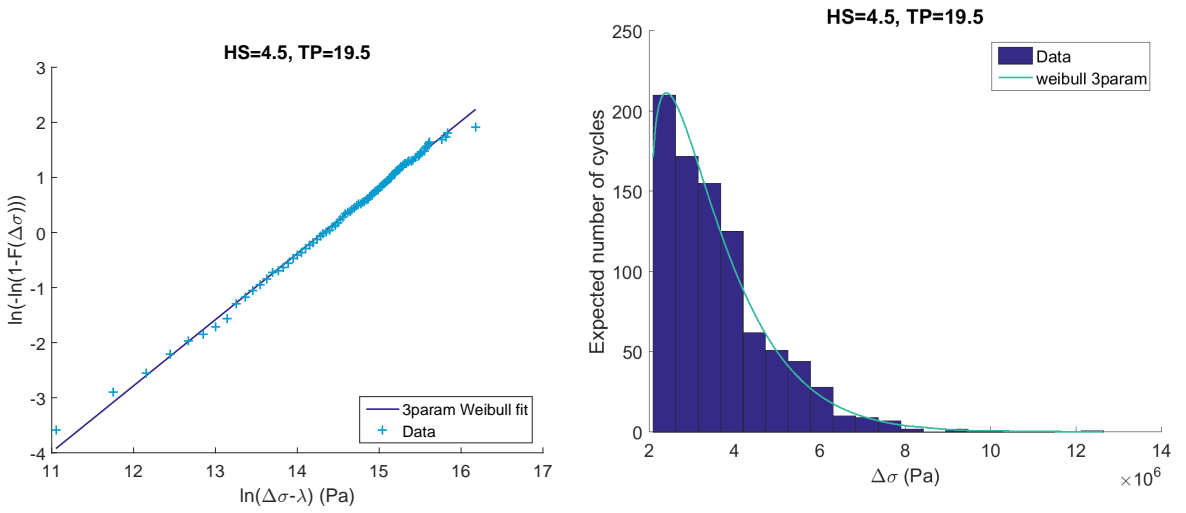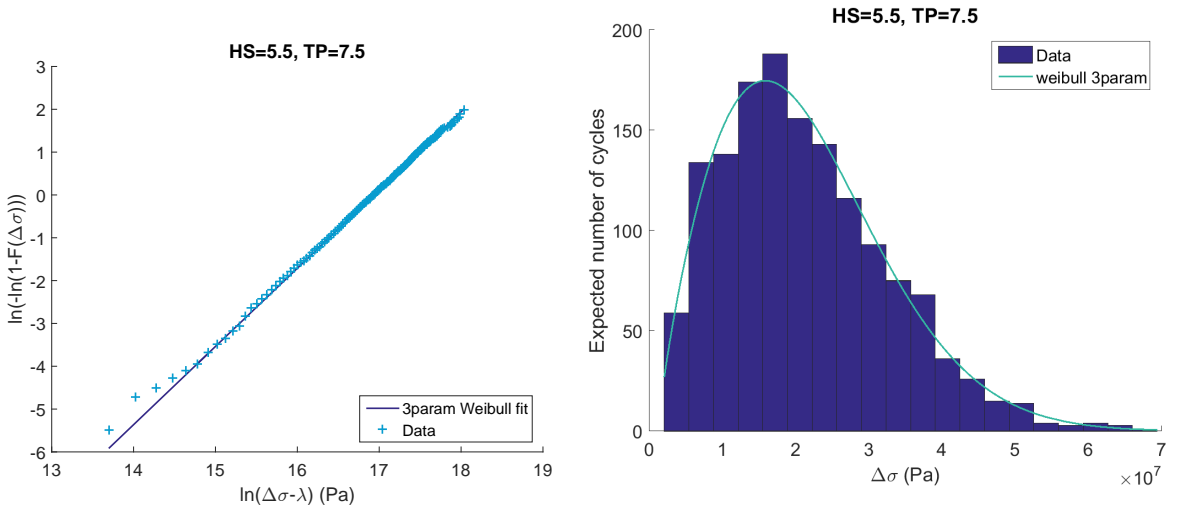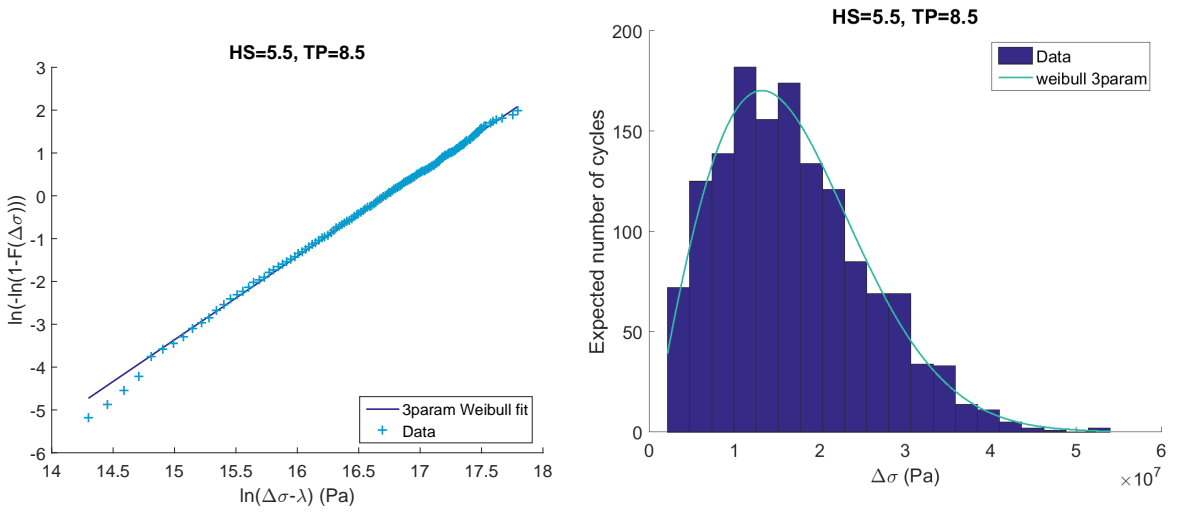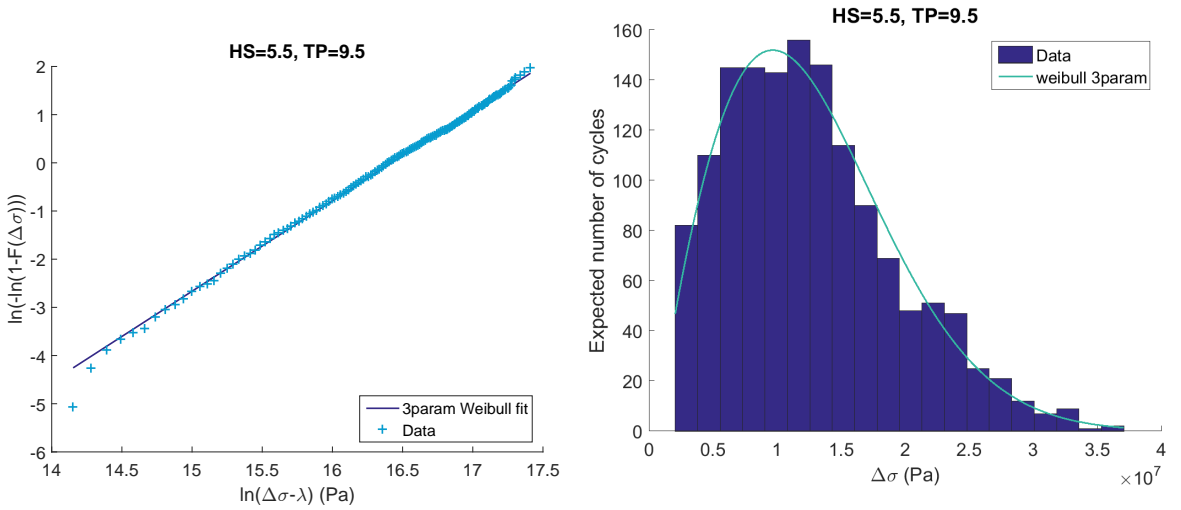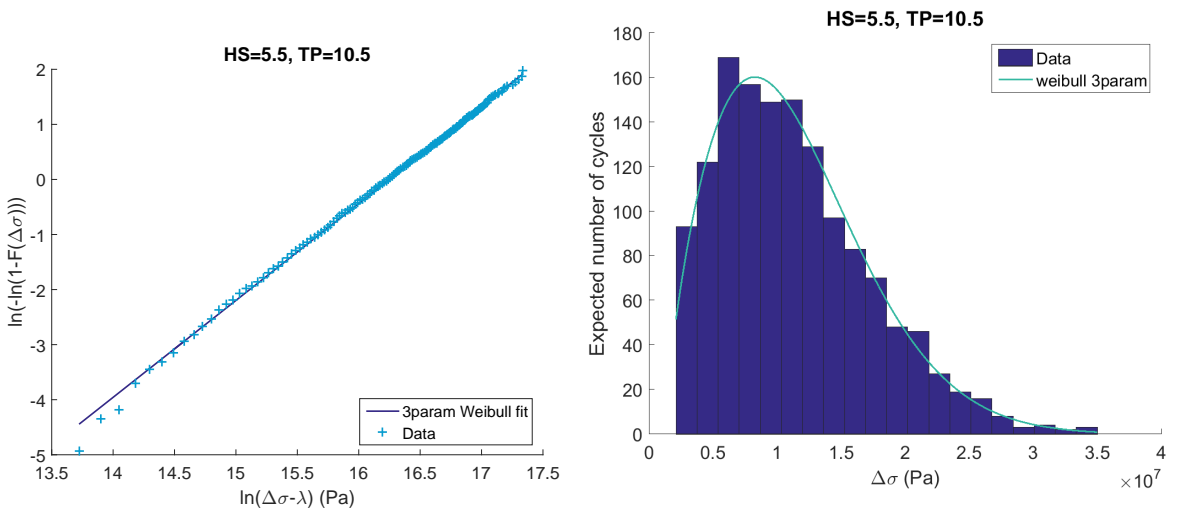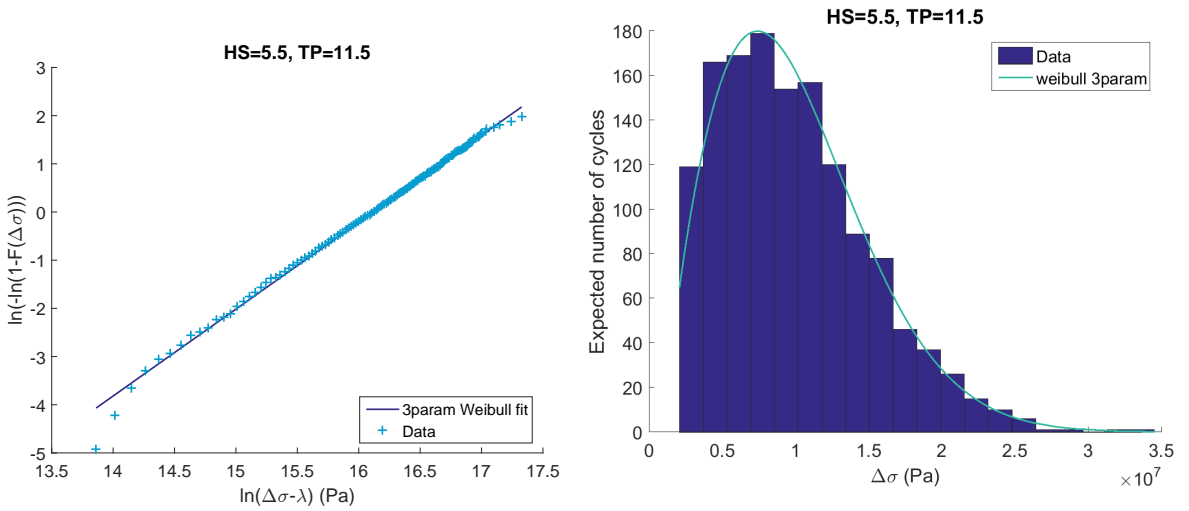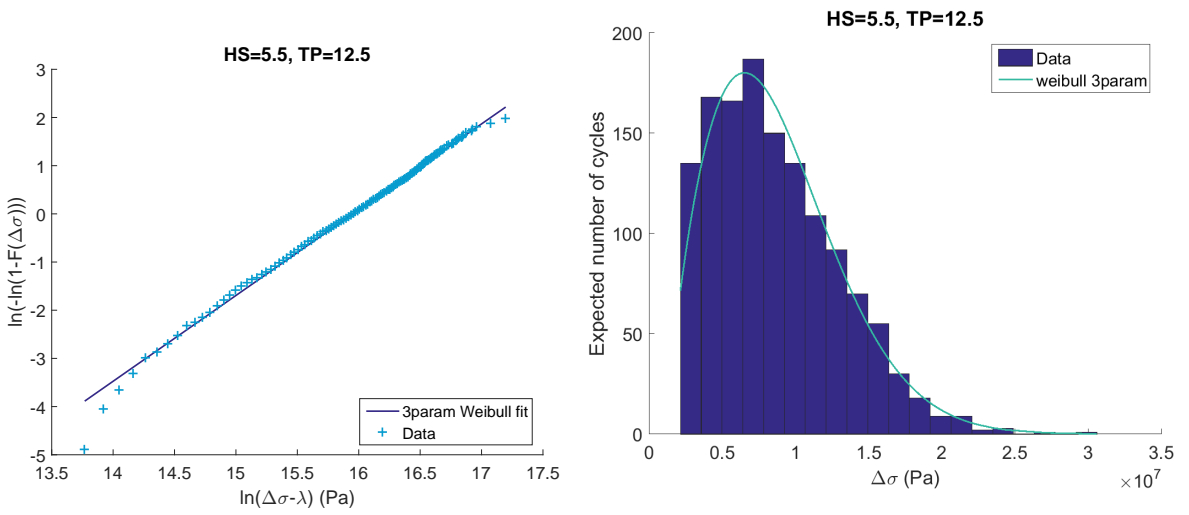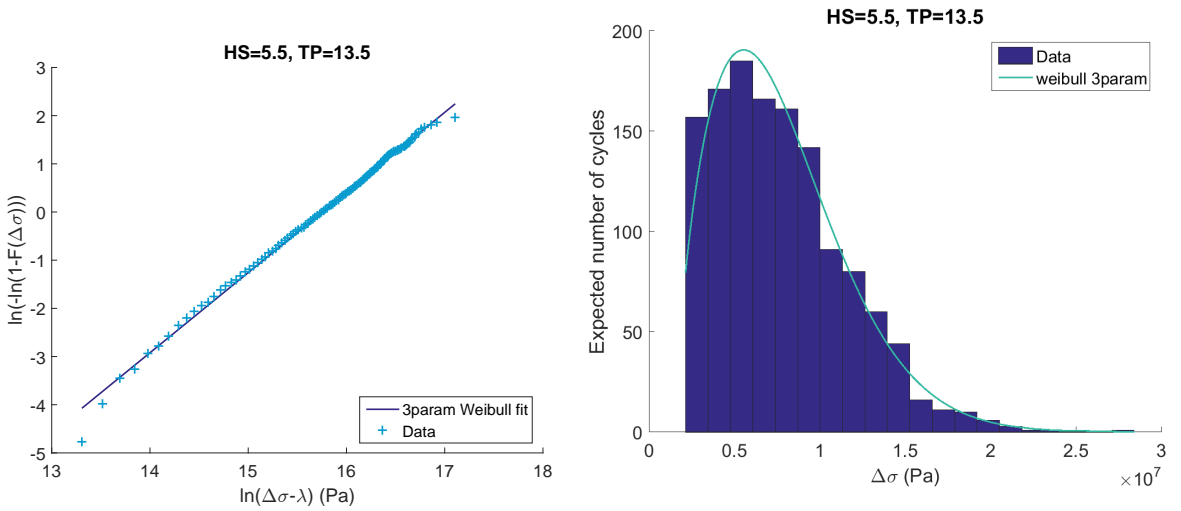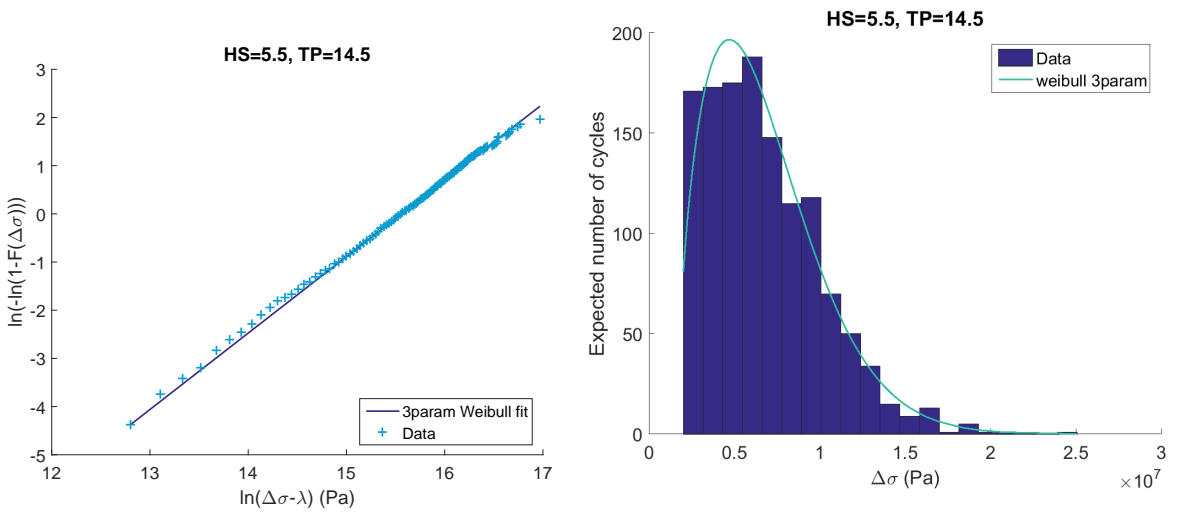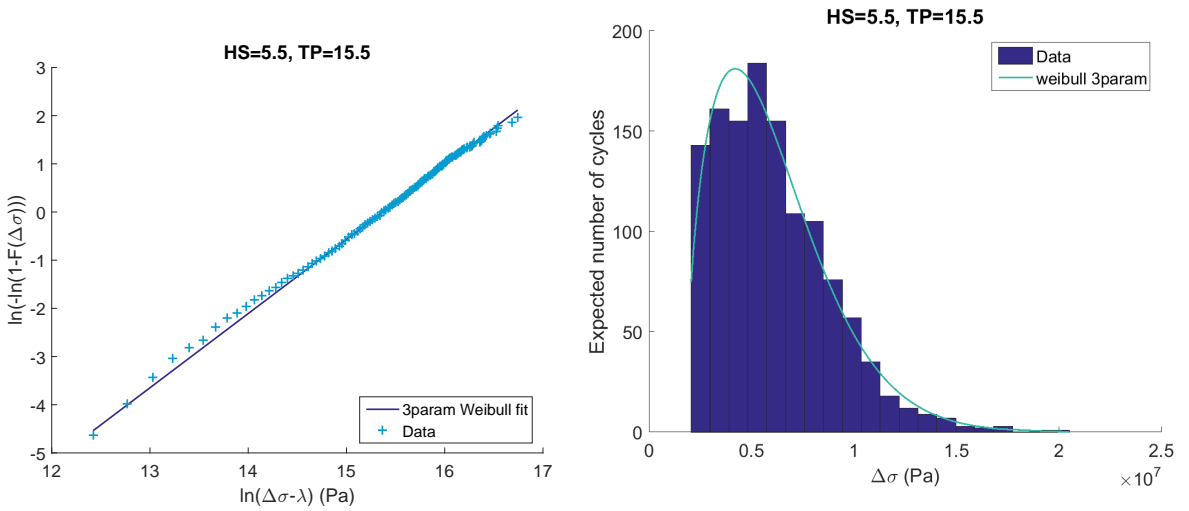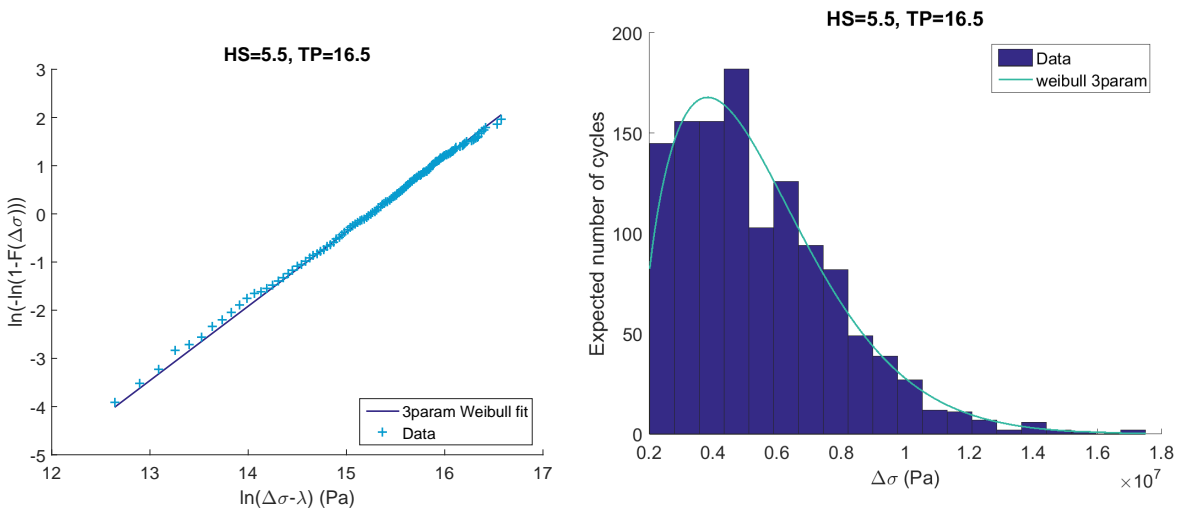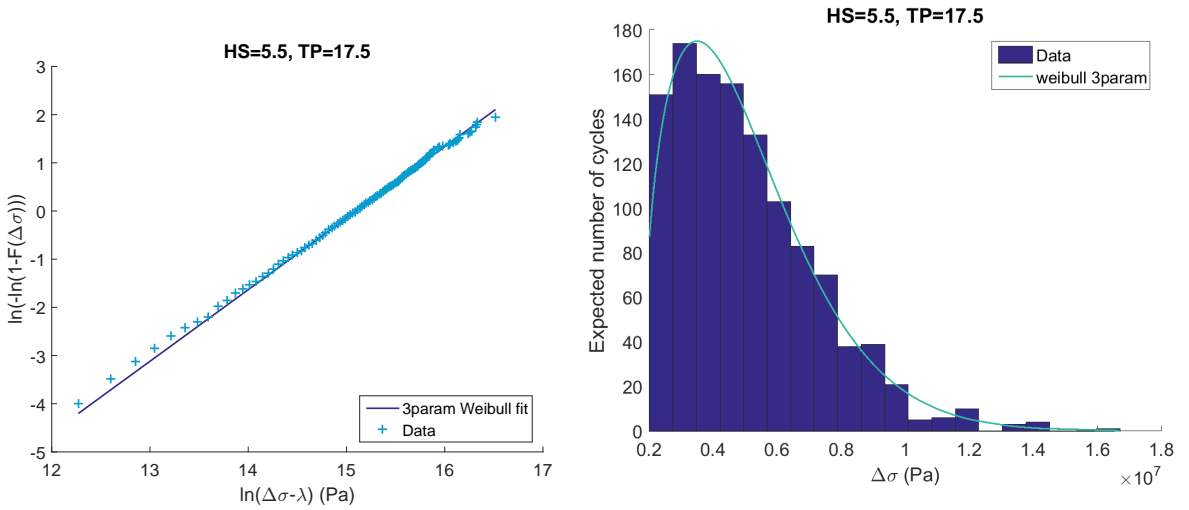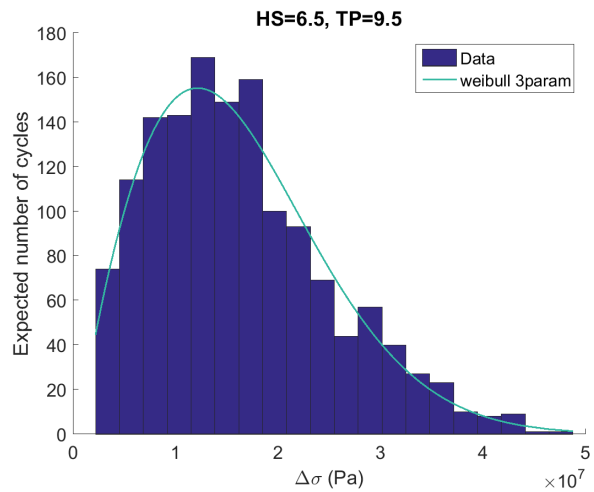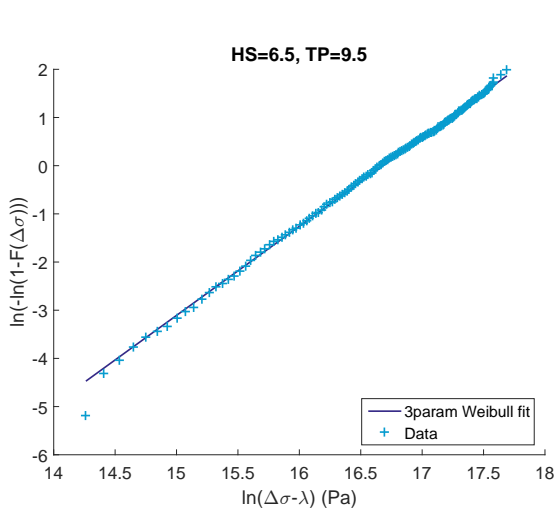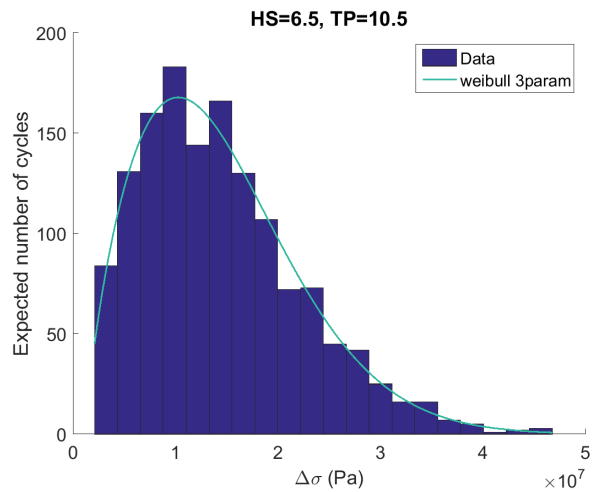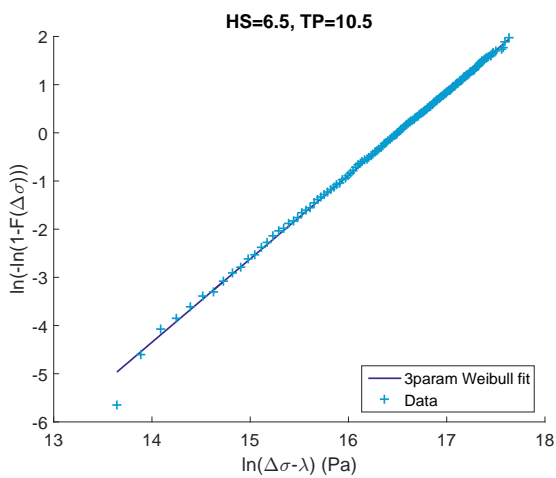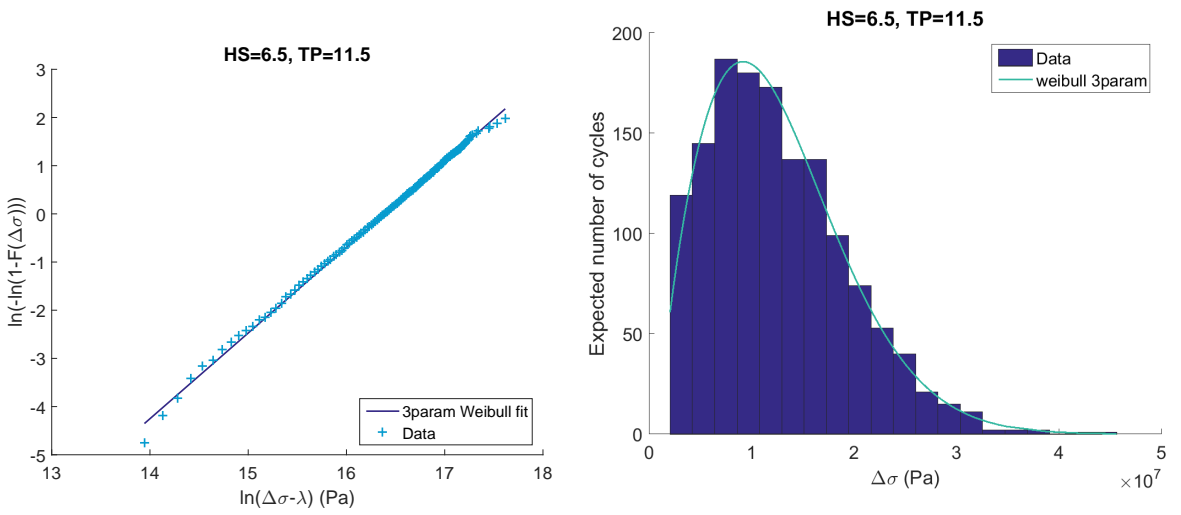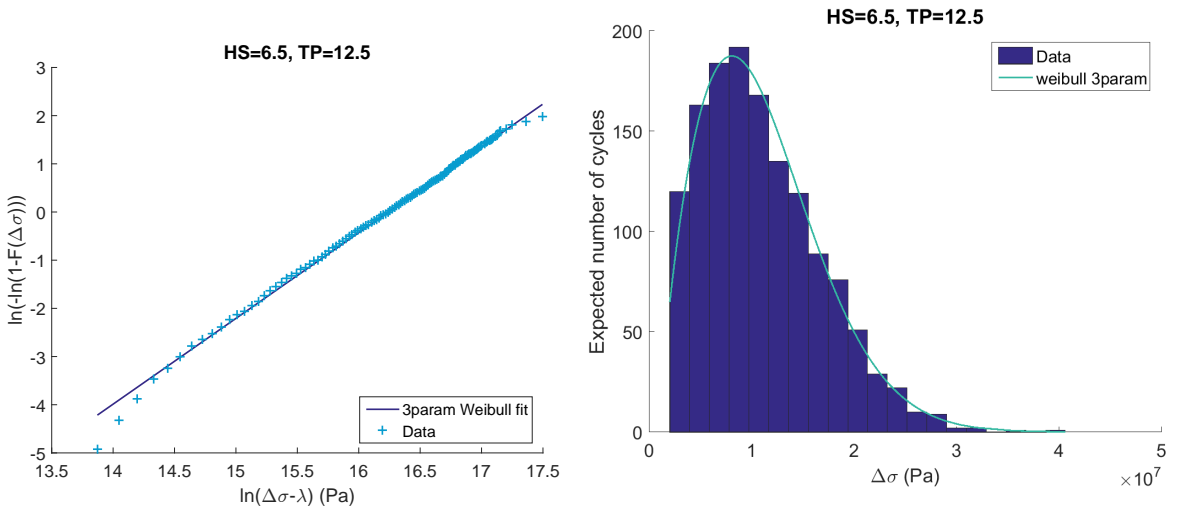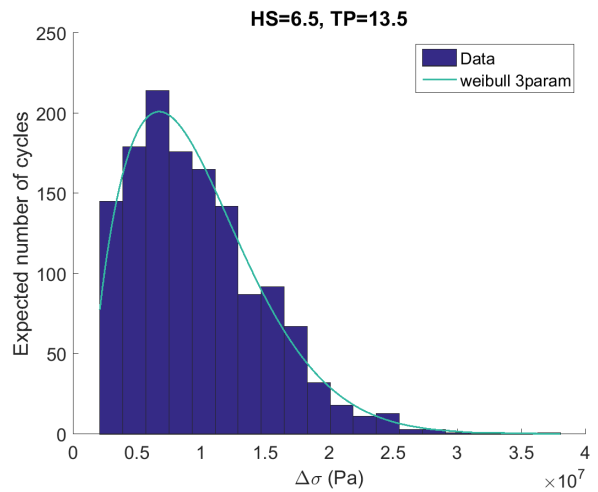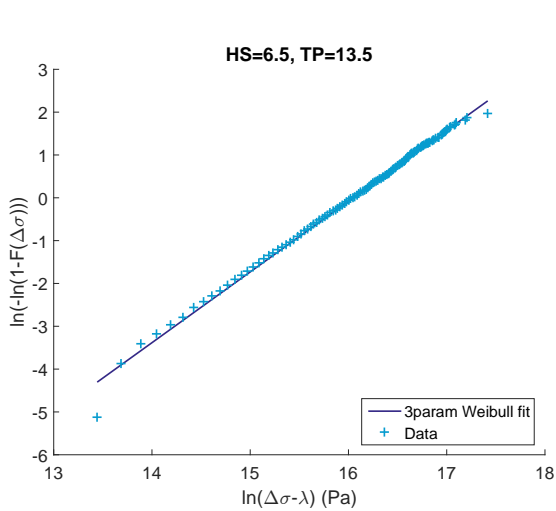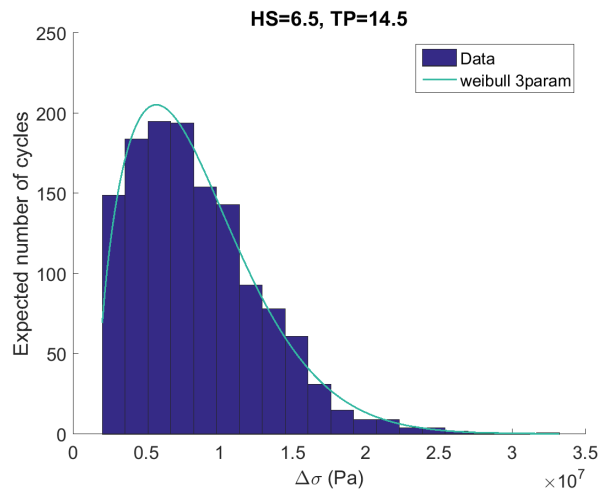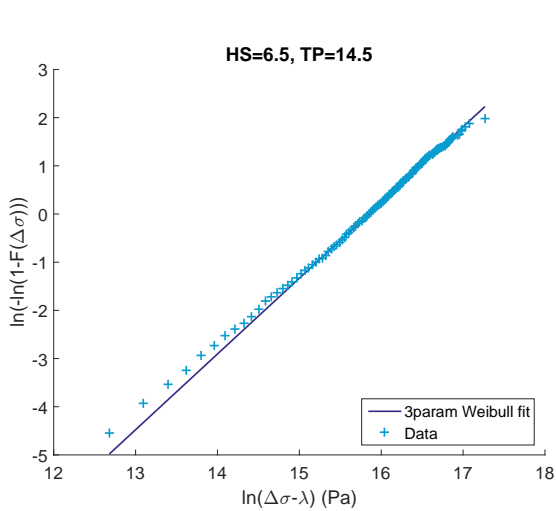**Figure B.2:** *Probability distributions of stress range during 3h realizations HS:2.5 TP:5.5*
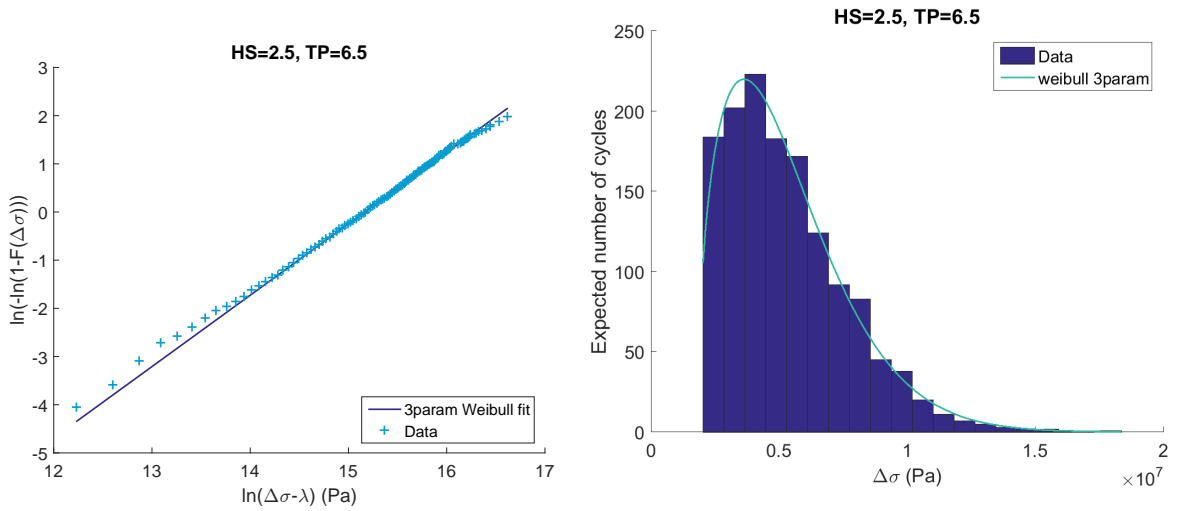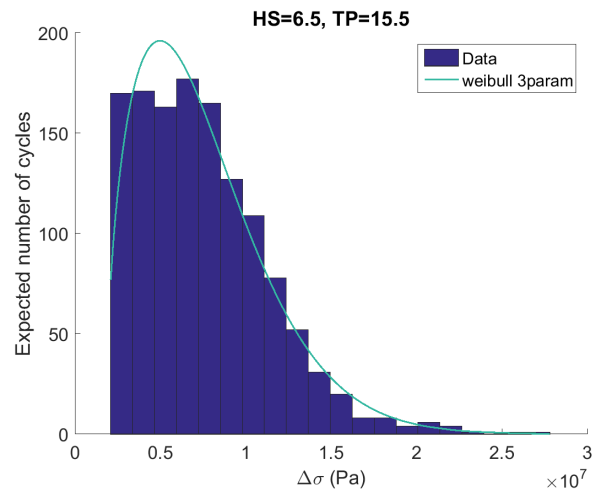

Figure B.3: *Probability distributions of stress range during 3h realizations HS:2.5 TP:6.5*
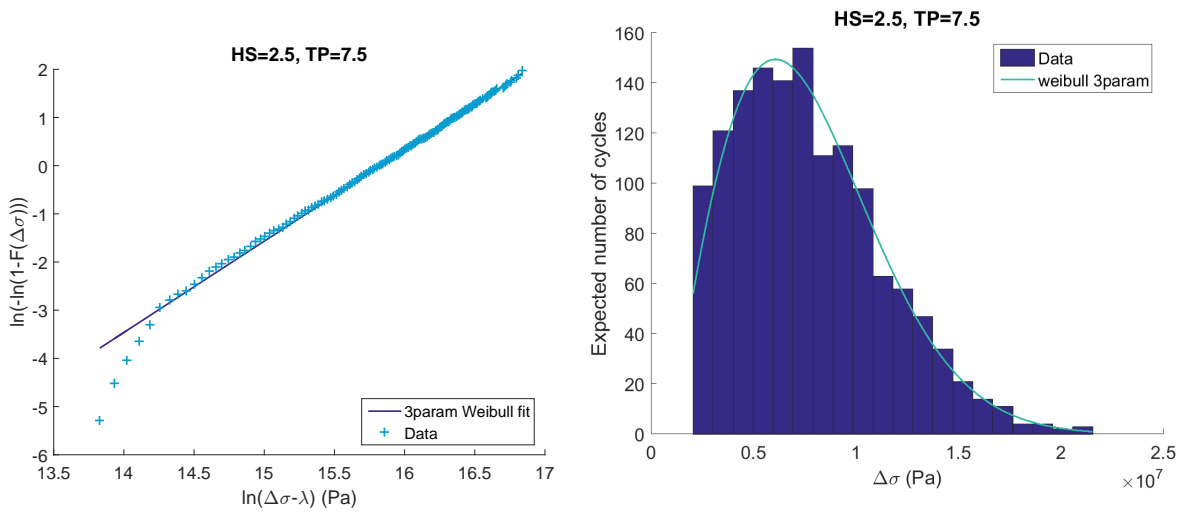
Figure B.4: *Probability distributions of stress range during 3h realizations HS:2.5 TP:7.5*
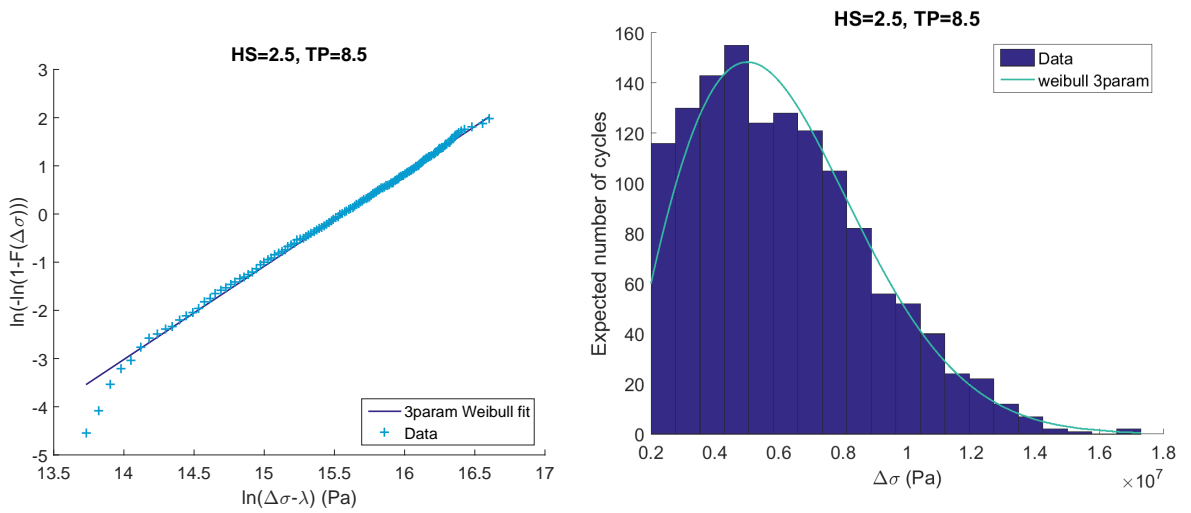
Figure B.5: *Probability distributions of stress range during 3h realizations HS:2.5 TP:8.5*
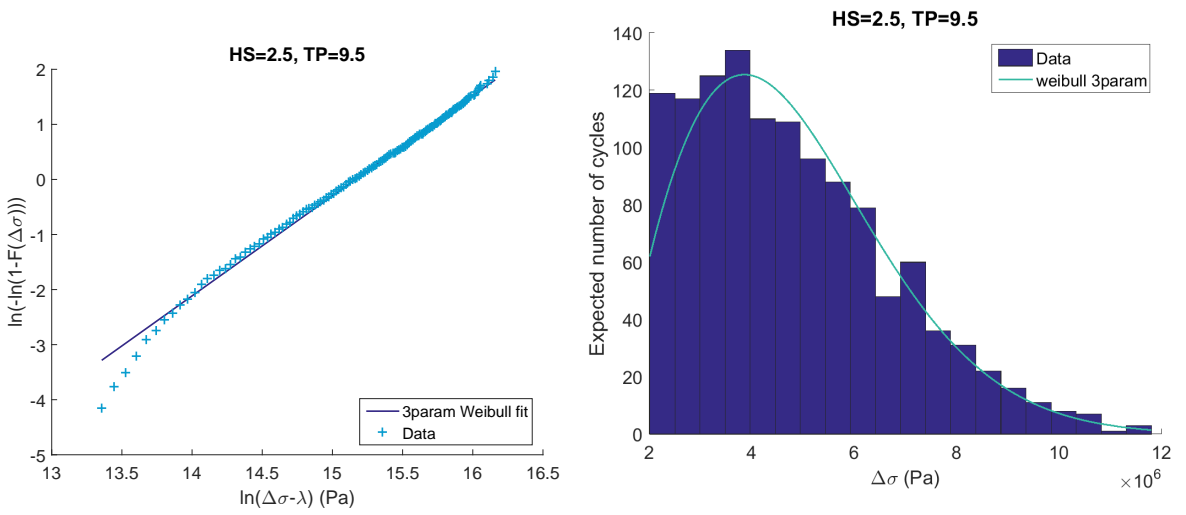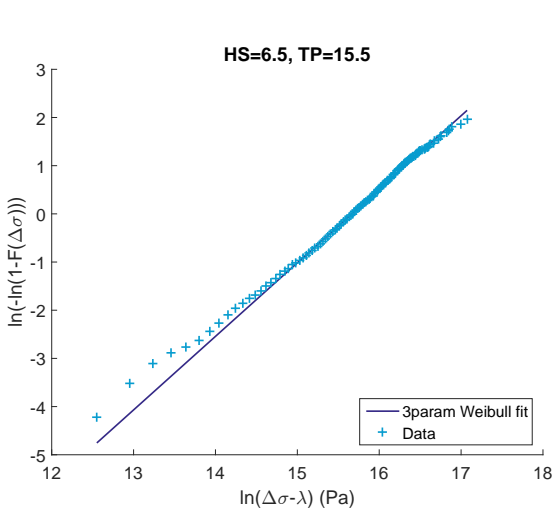
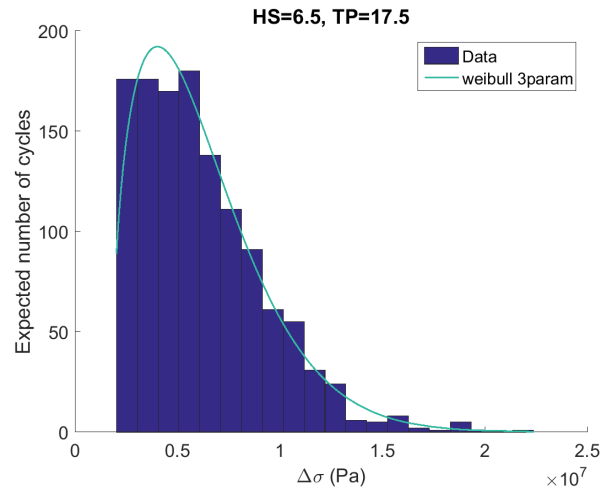**Figure B.6:** *Probability distributions of stress range during 3h realizations HS:2.5 TP:9.5*
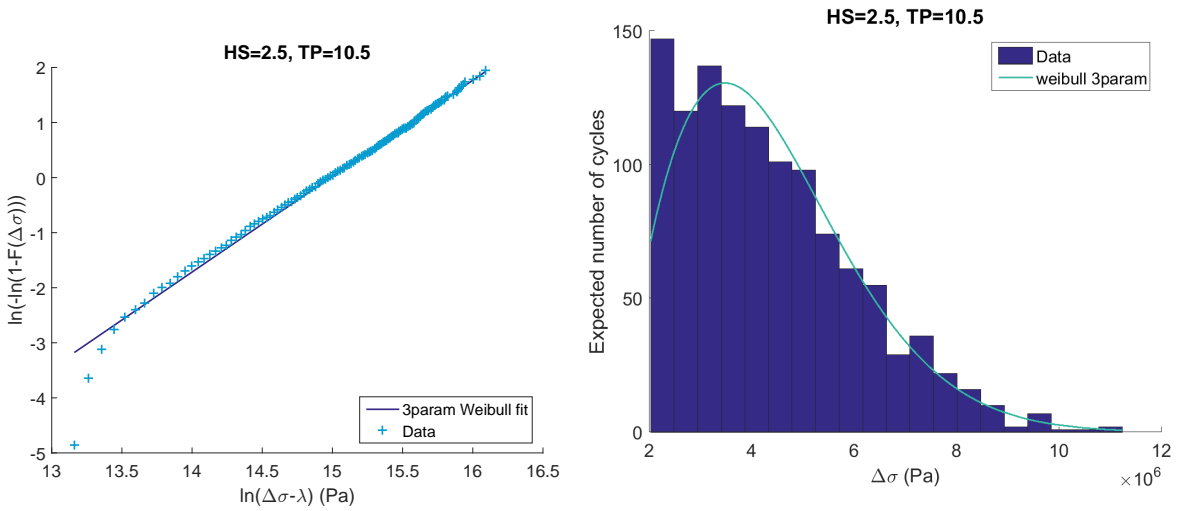
Figure B.7: *Probability distributions of stress range during 3h realizations HS:2.5 TP:10.5*
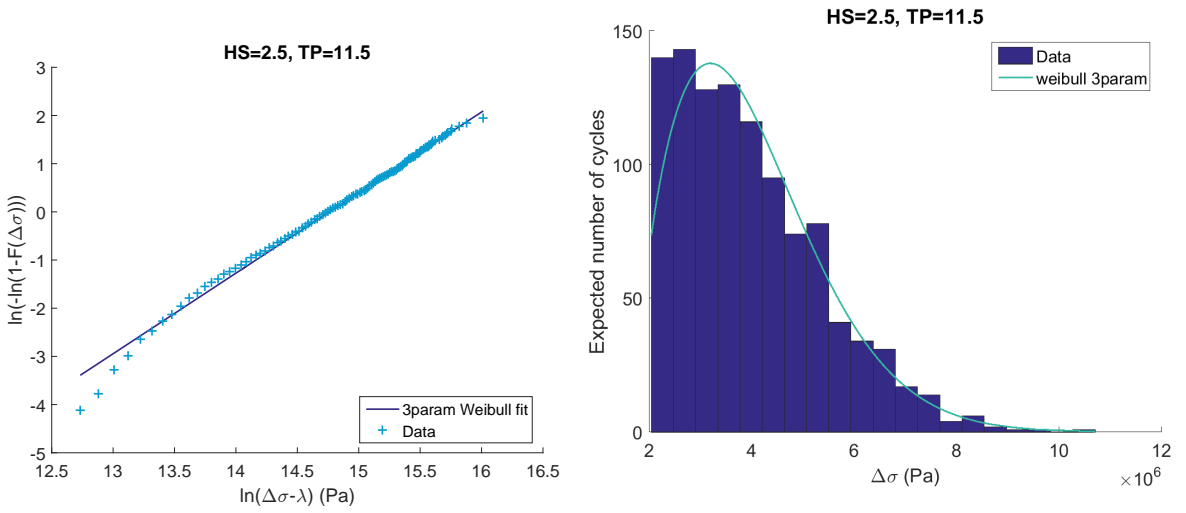
Figure B.8: *Probability distributions of stress range during 3h realizations HS:2.5 TP:11.5*
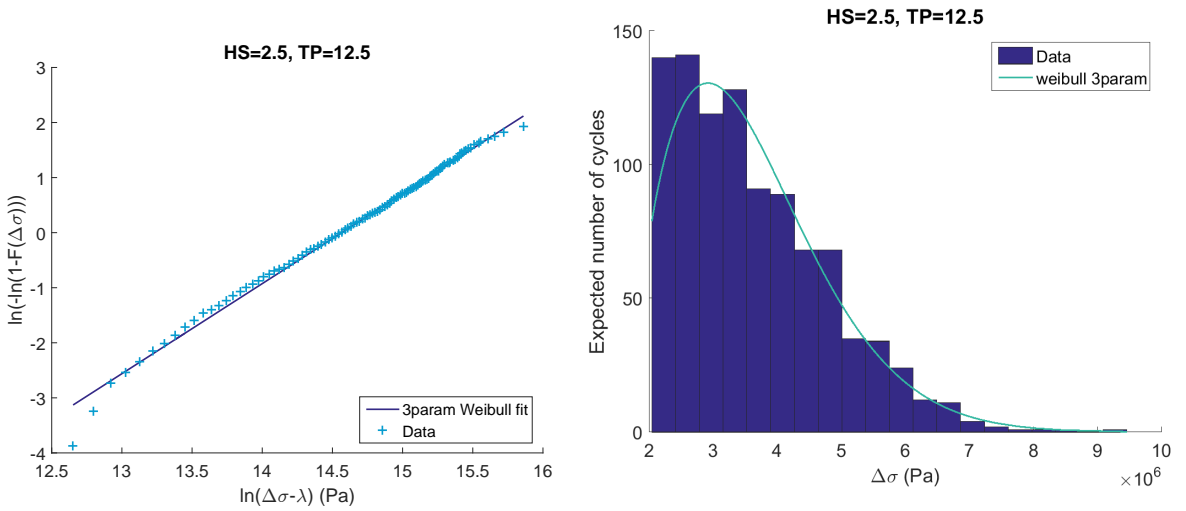
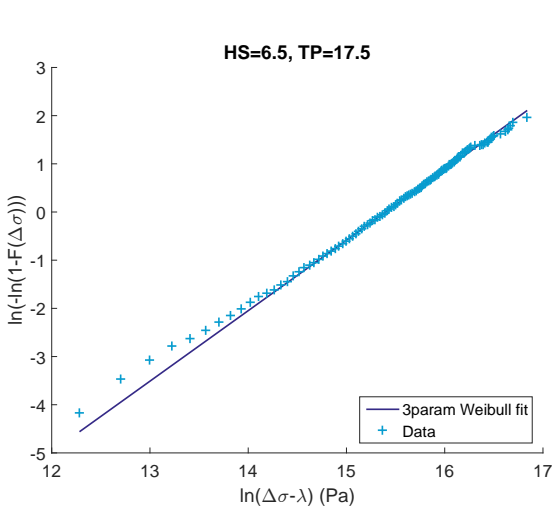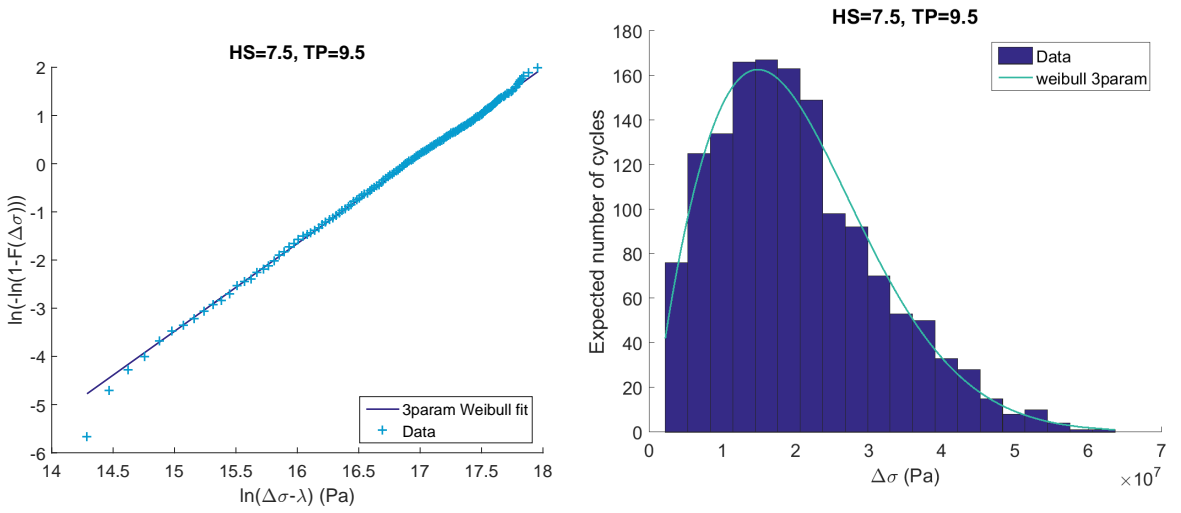**Figure B.9:** *Probability distributions of stress range during 3h realizations HS:2.5 TP:12.5*
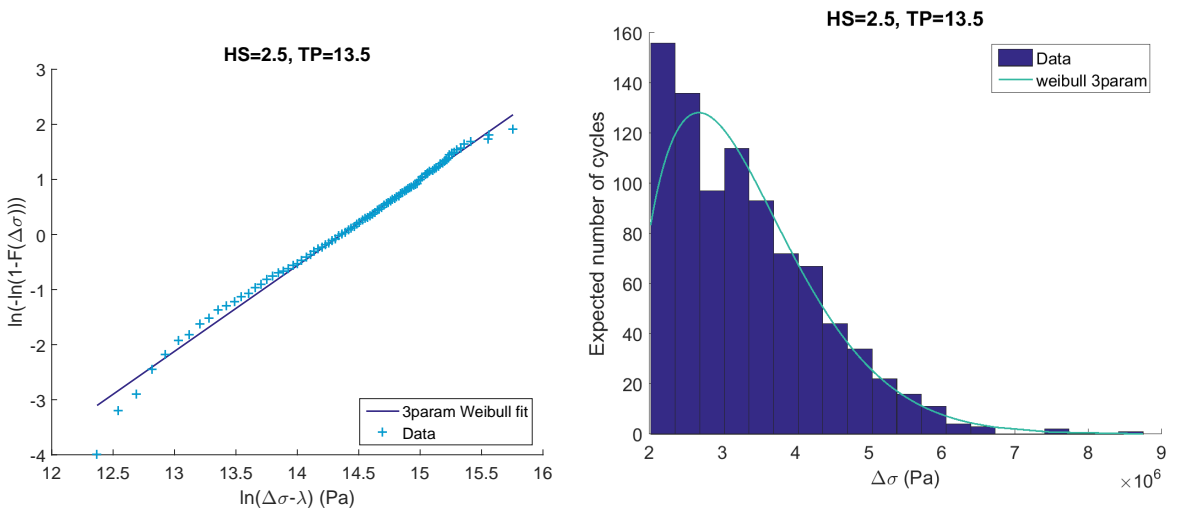
Figure B.10: *Probability distributions of stress range during 3h realizations HS:2.5 TP:13.5*
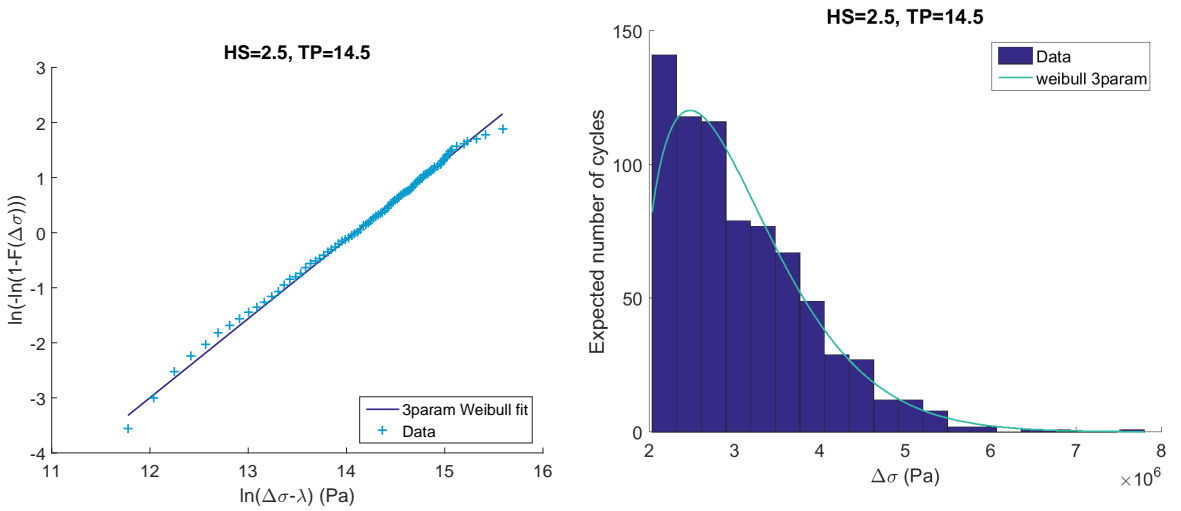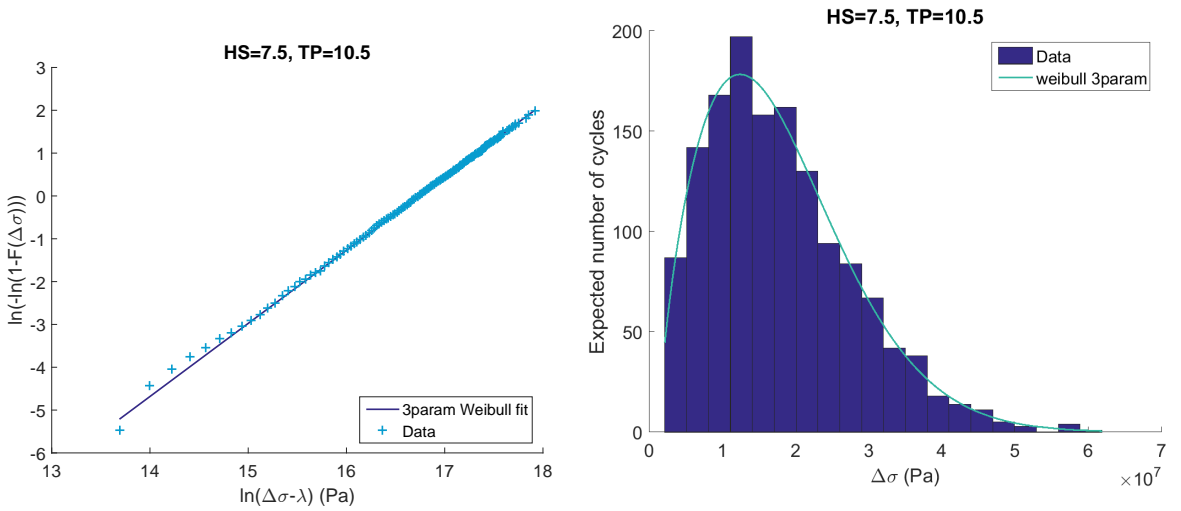

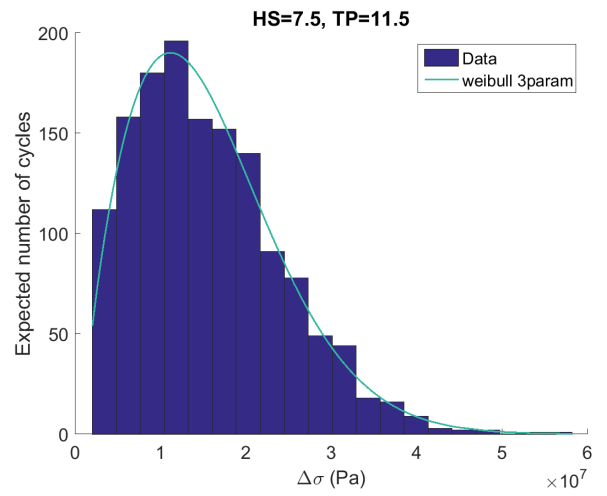***Figure B.11:*** *Probability distributions of stress range during 3h realizations HS:2.5 TP:14.5*
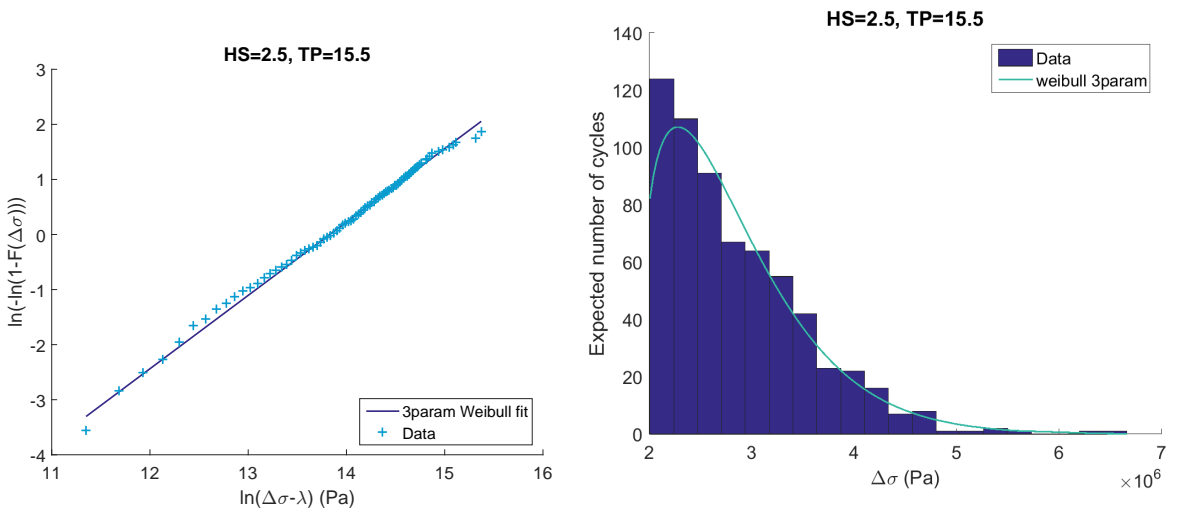
Figure B.12: *Probability distributions of stress range during 3h realizations HS:2.5 TP:15.5*
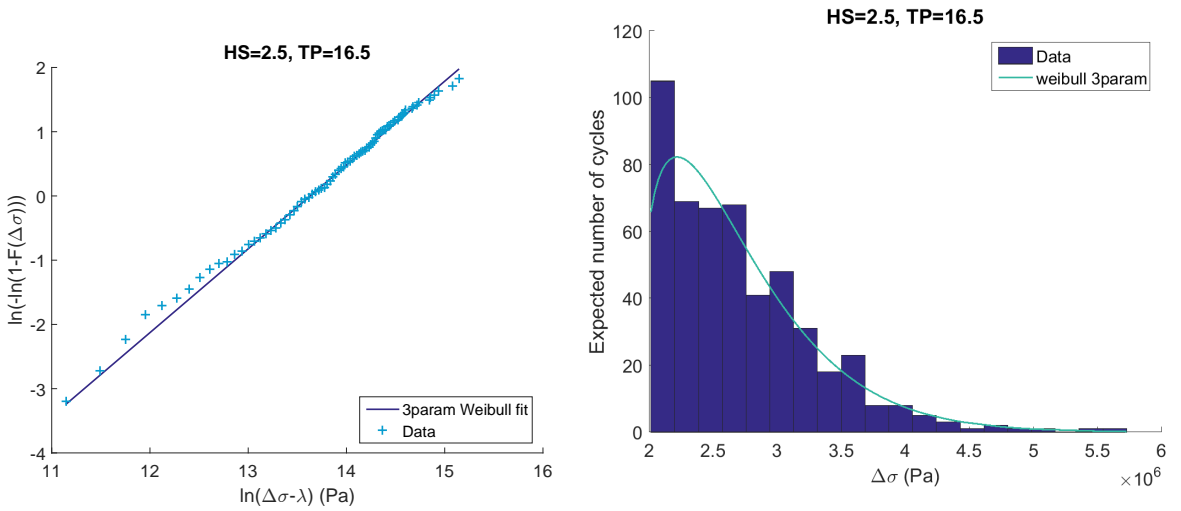
Figure B.13: *Probability distributions of stress range during 3h realizations HS:2.5 TP:16.5*
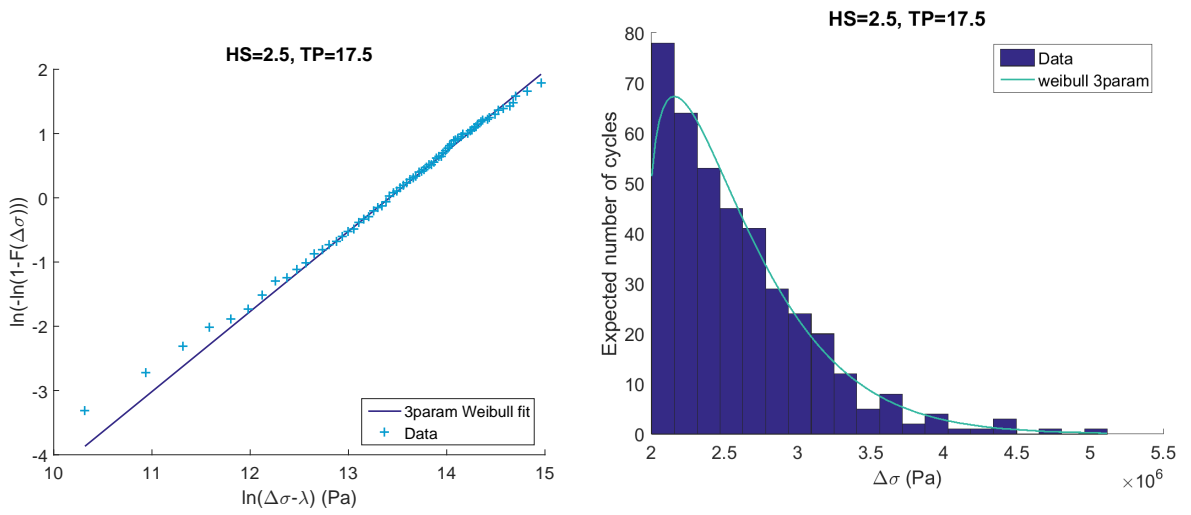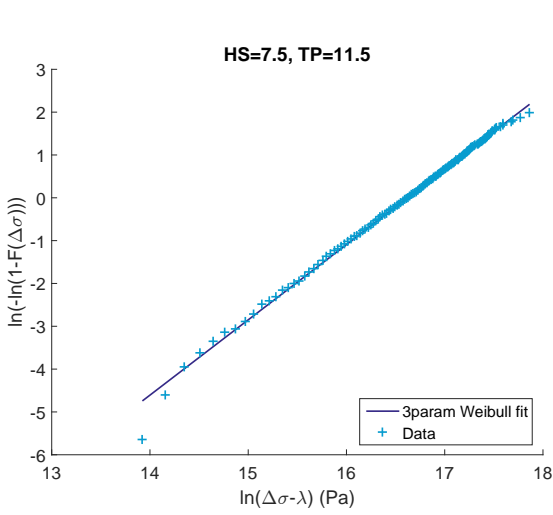
Figure B.14: *Probability distributions of stress range during 3h realizations HS:2.5 TP:17.5*
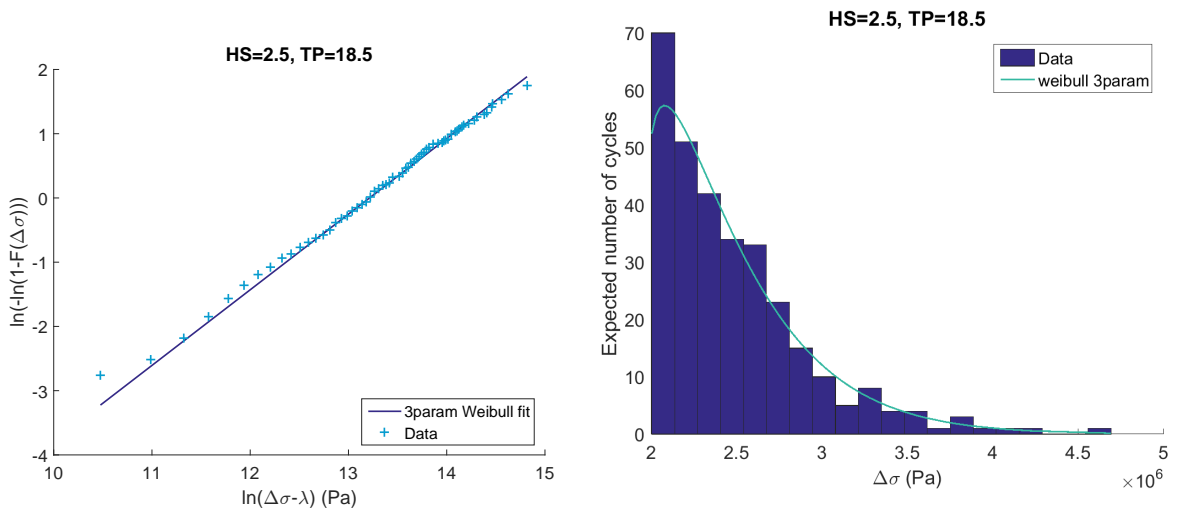
Figure B.15: *Probability distributions of stress range during 3h realizations HS:2.5 TP:18.5*
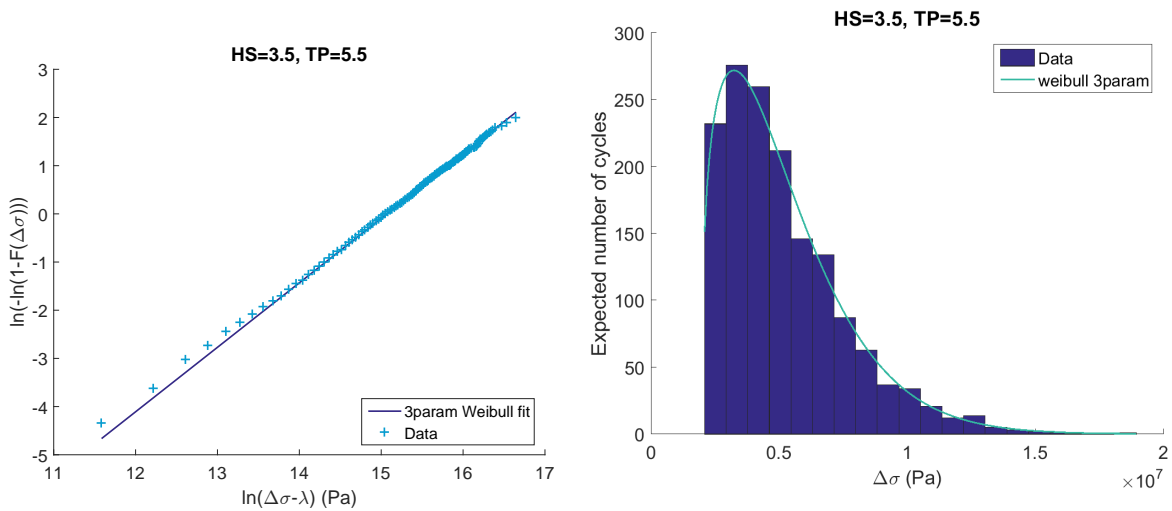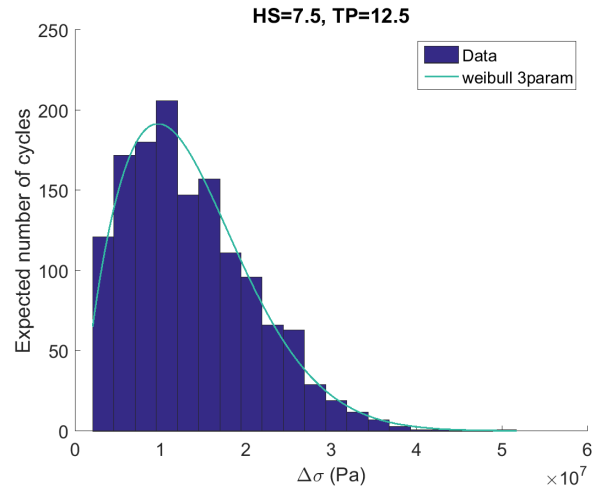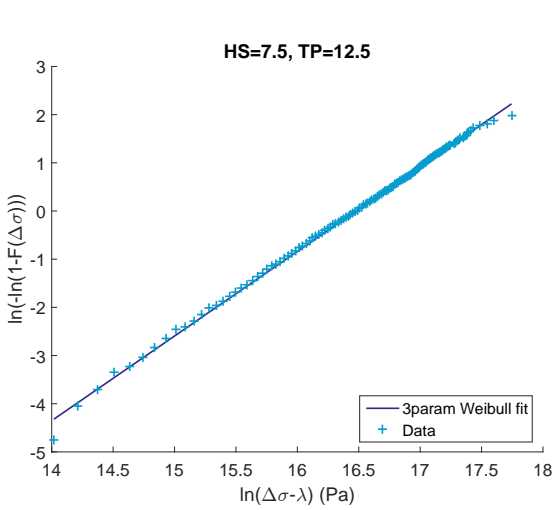
Figure B.16: *Probability distributions of stress range during 3h realizations HS:3.5 TP:5.5*
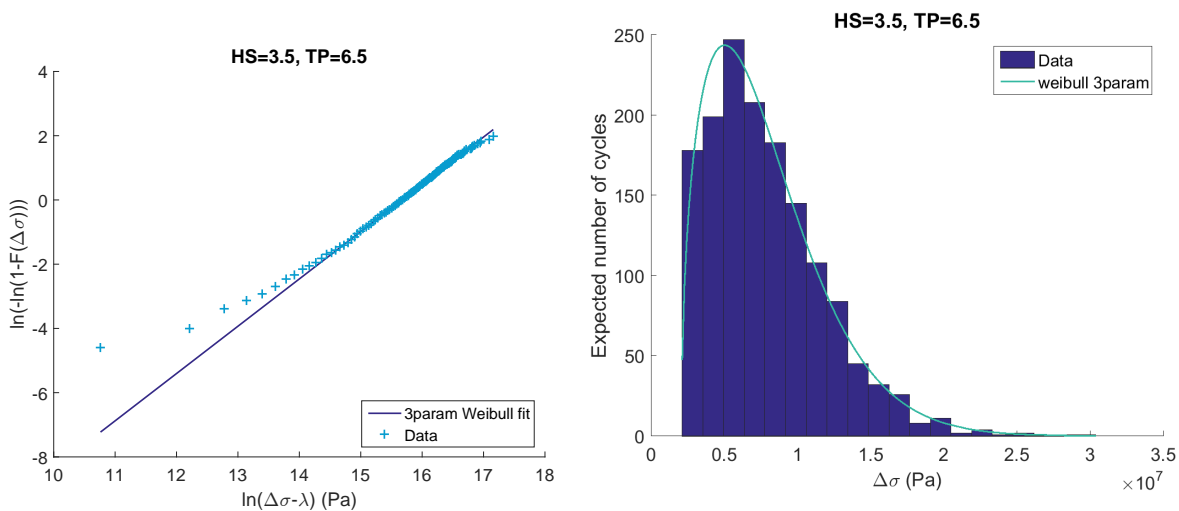
Figure B.17: *Probability distributions of stress range during 3h realizations HS:3.5 TP:6.5*
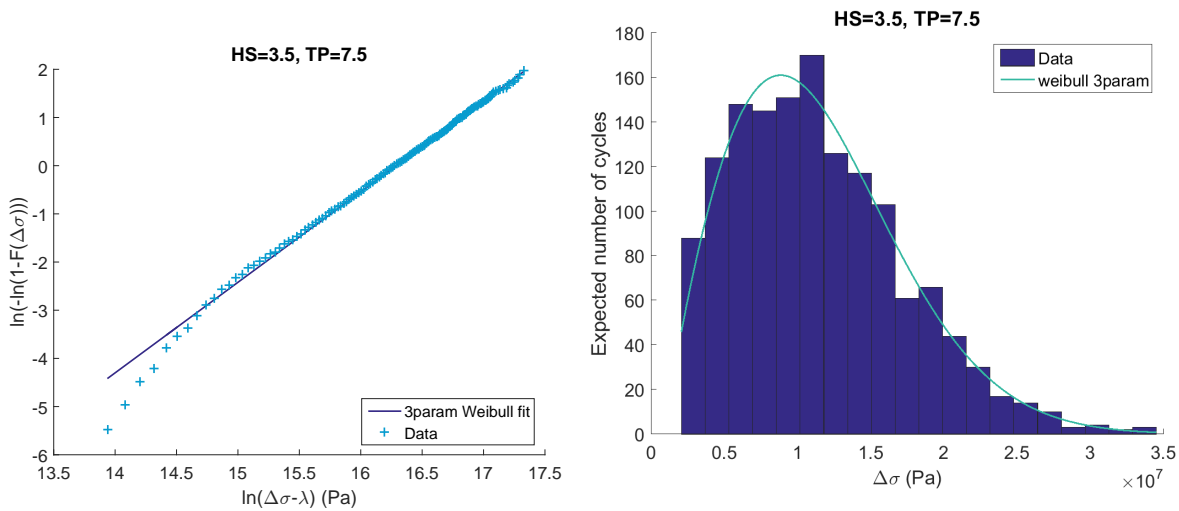
Figure B.18: *Probability distributions of stress range during 3h realizations HS:3.5 TP:7.5*
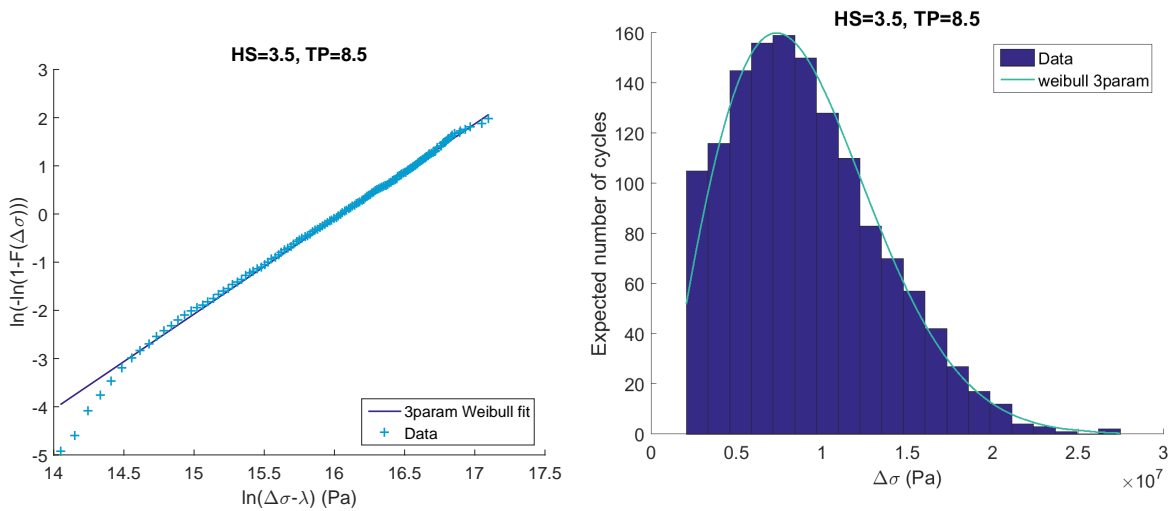
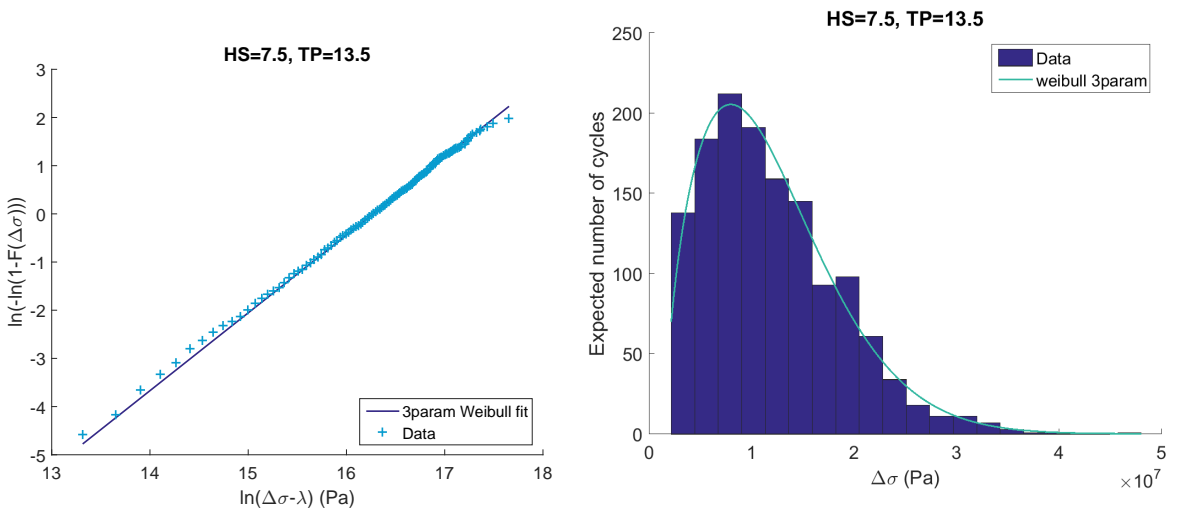**Figure B.19:** *Probability distributions of stress range during 3h realizations HS:3.5 TP:8.5*
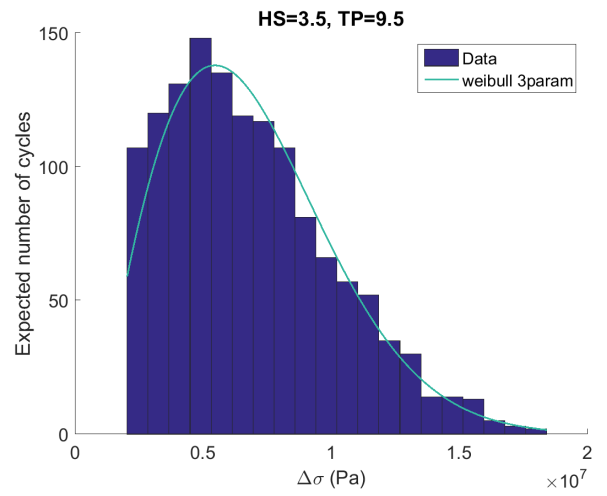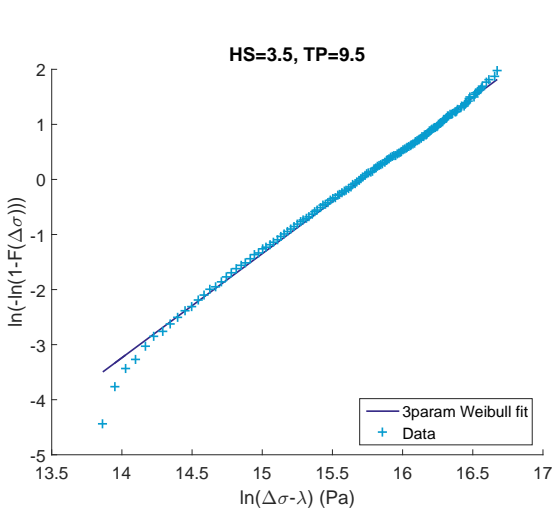
Figure B.20: *Probability distributions of stress range during 3h realizations HS:3.5 TP:9.5*
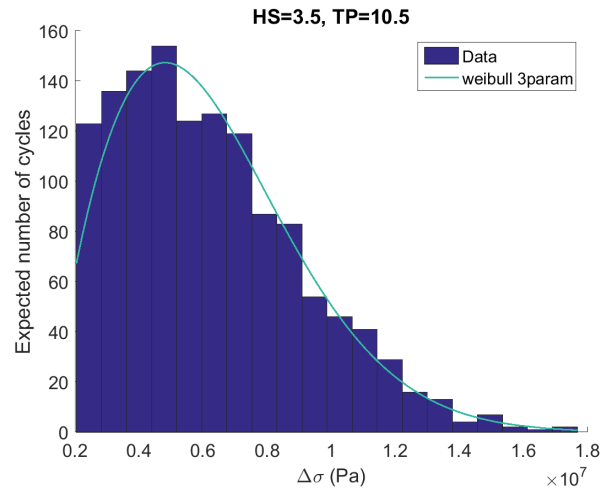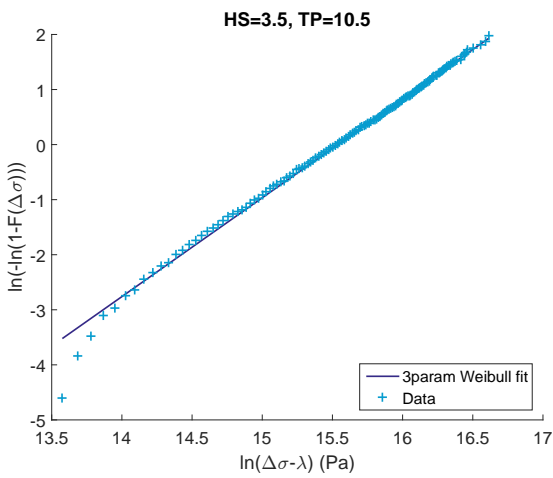
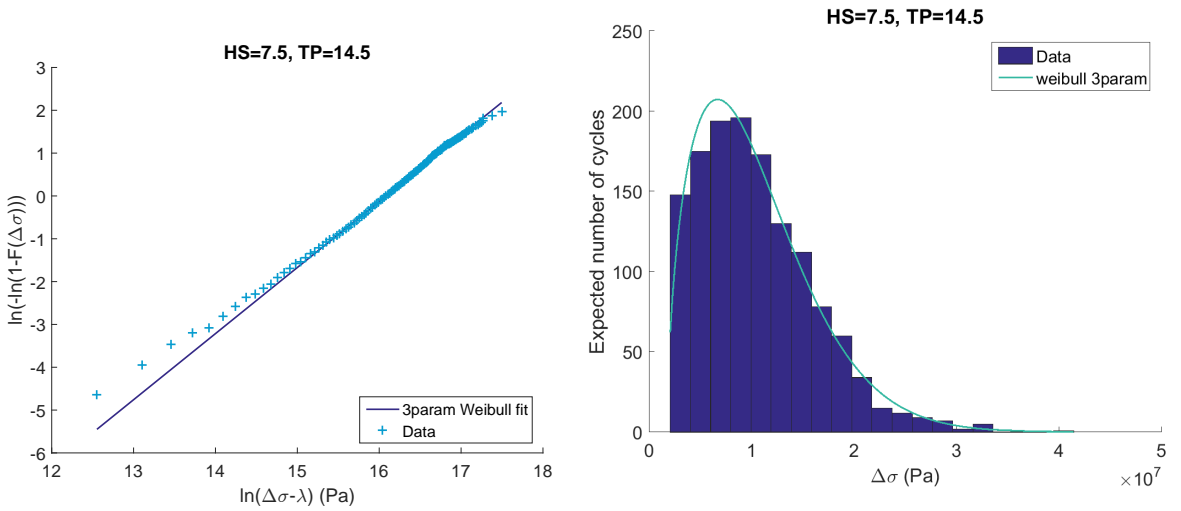**Figure B.21:** *Probability distributions of stress range during 3h realizations HS:3.5 TP:10.5*
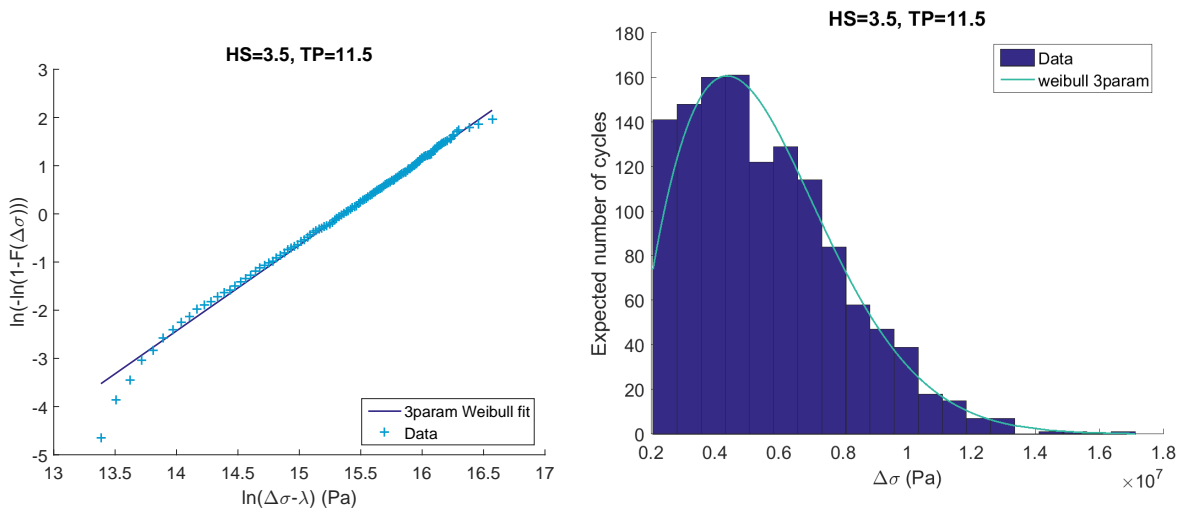
Figure B.22: *Probability distributions of stress range during 3h realizations HS:3.5 TP:11.5*
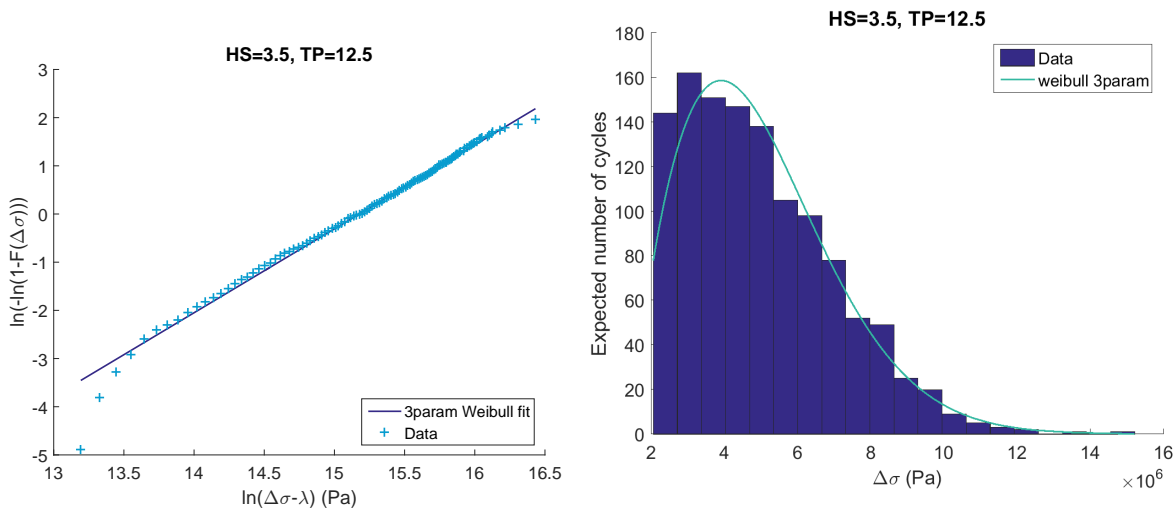
Figure B.23: *Probability distributions of stress range during 3h realizations HS:3.5 TP:12.5*
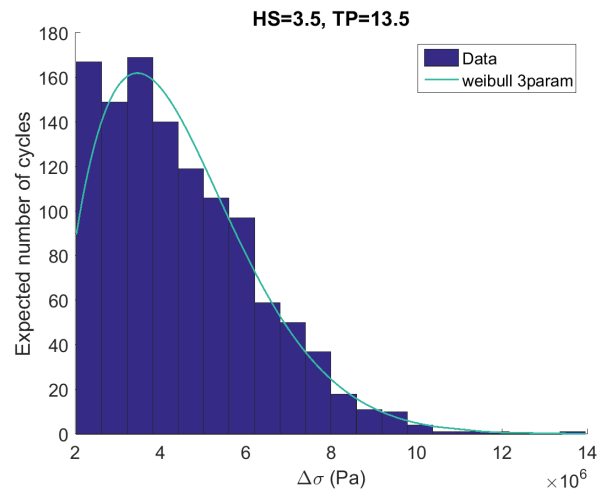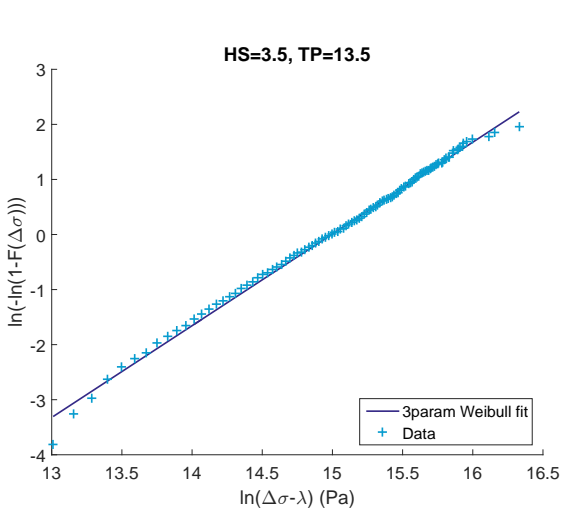
Figure B.24: *Probability distributions of stress range during 3h realizations HS:3.5 TP:13.5*
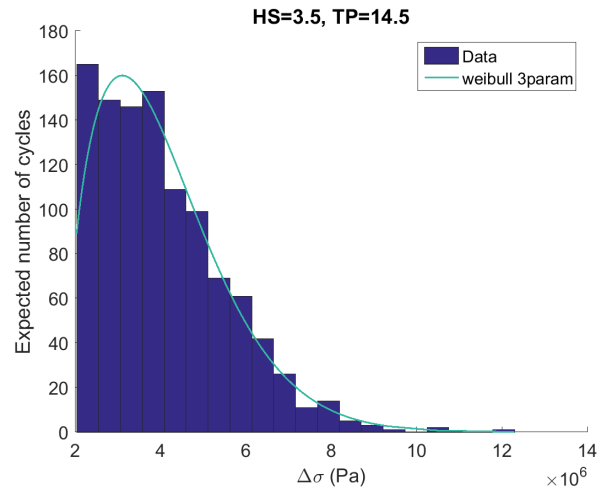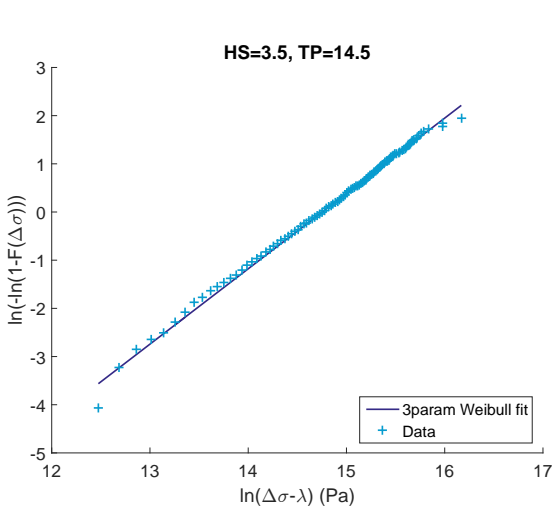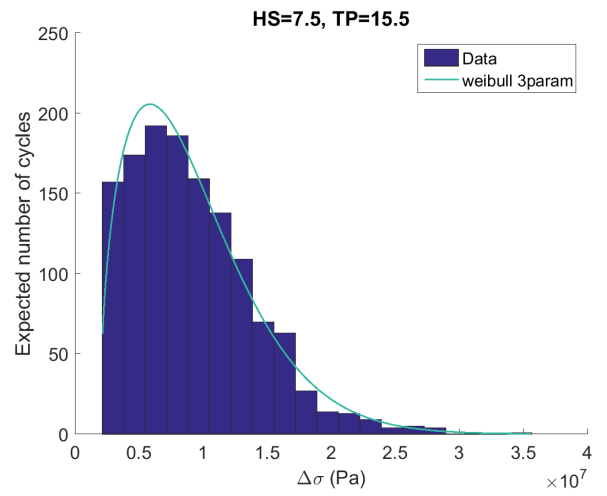

Figure B.25: *Probability distributions of stress range during 3h realizations HS:3.5 TP:14.5*
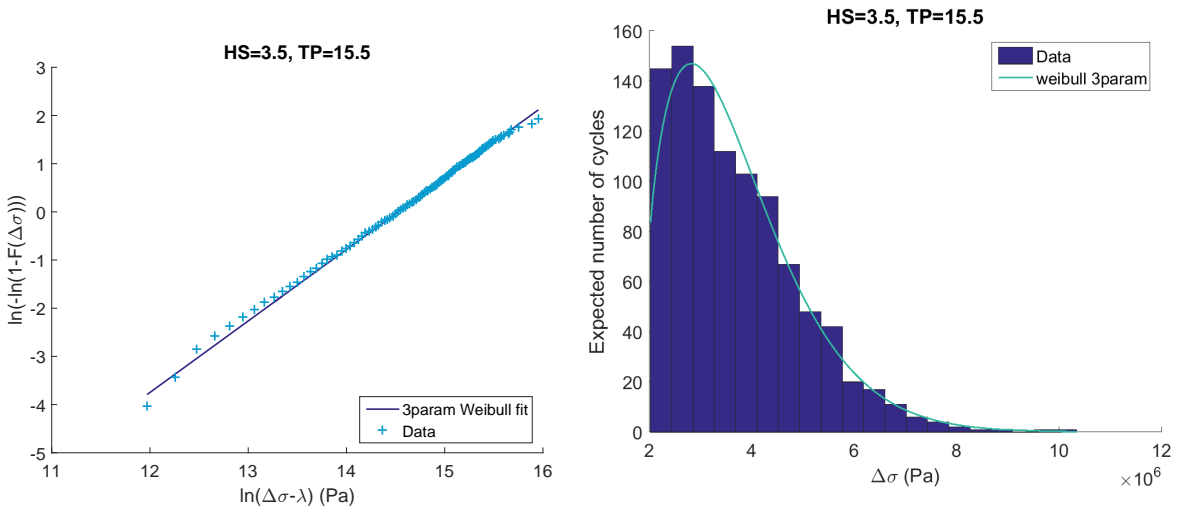
Figure B.26: *Probability distributions of stress range during 3h realizations HS:3.5 TP:15.5*
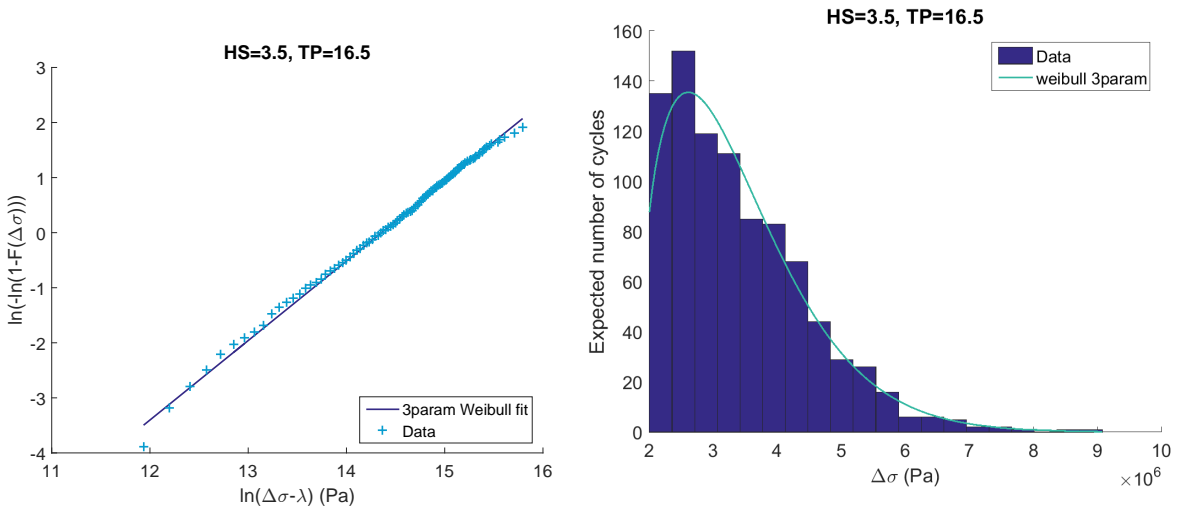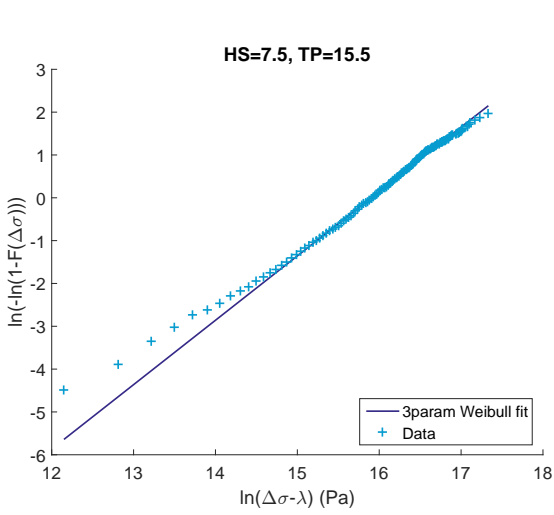

Figure B.27: *Probability distributions of stress range during 3h realizations HS:3.5 TP:16.5*
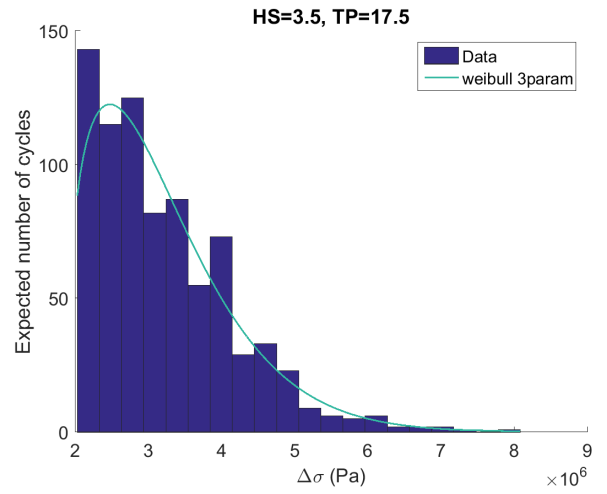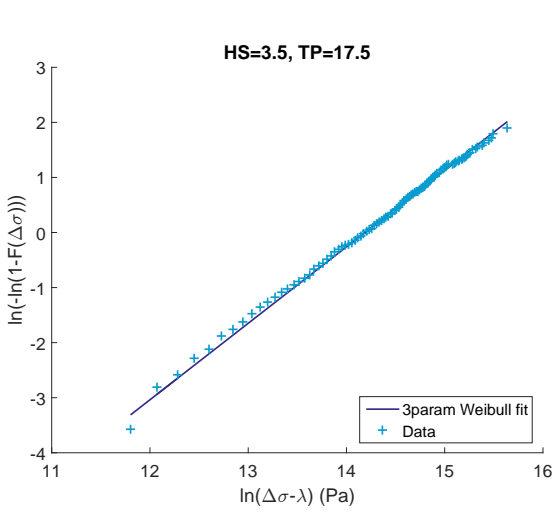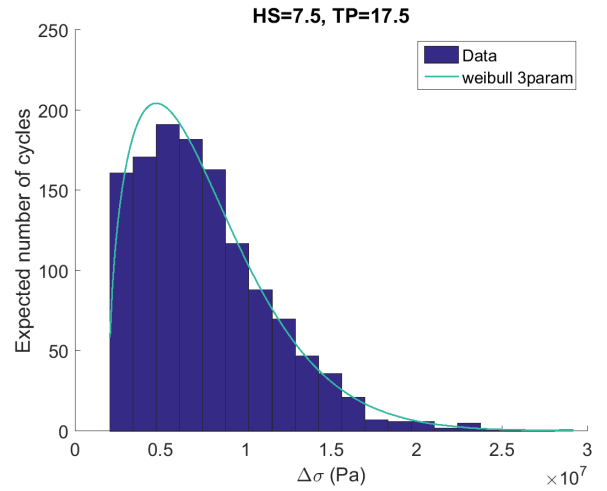
Figure B.28: *Probability distributions of stress range during 3h realizations HS:3.5 TP:17.5*
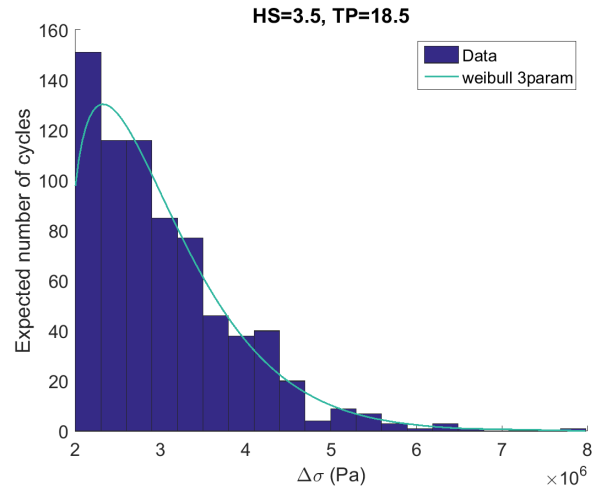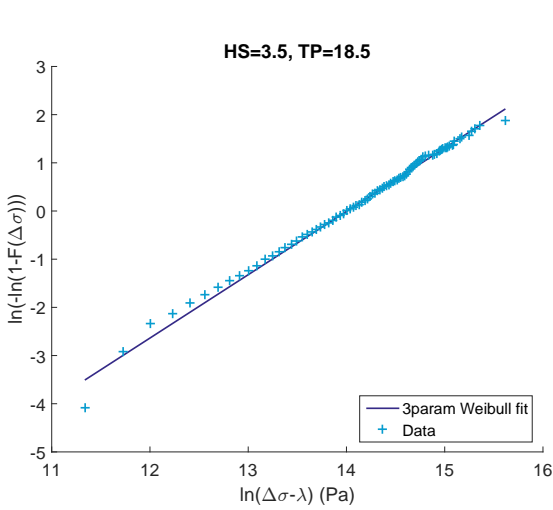
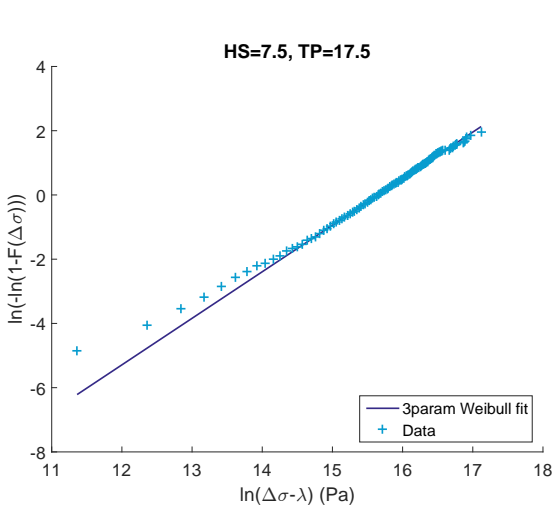**Figure B.29:** *Probability distributions of stress range during 3h realizations HS:3.5 TP:18.5*
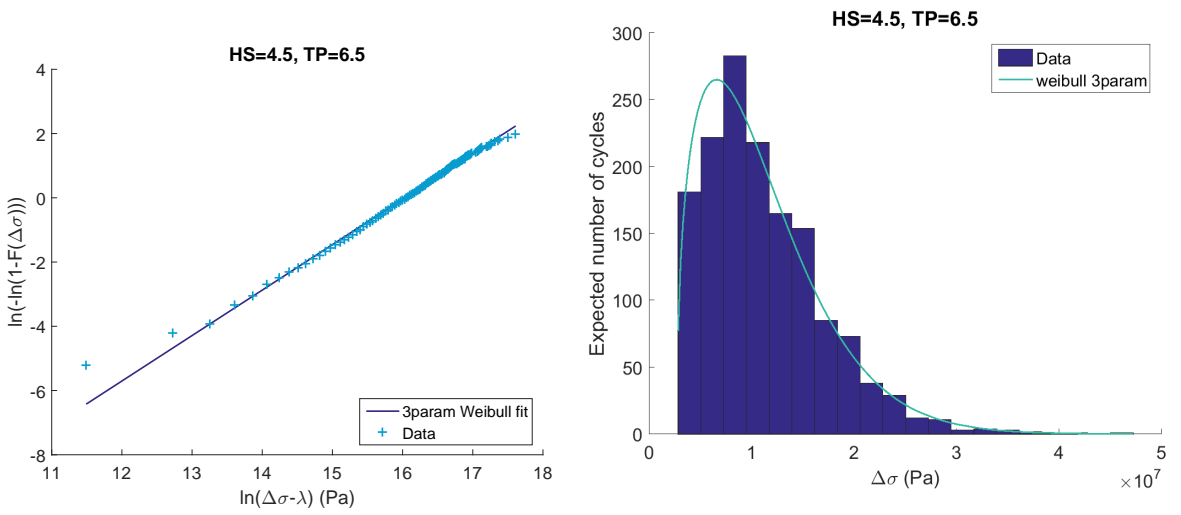
Figure B.30: *Probability distributions of stress range during 3h realizations HS:4.5 TP:6.5*
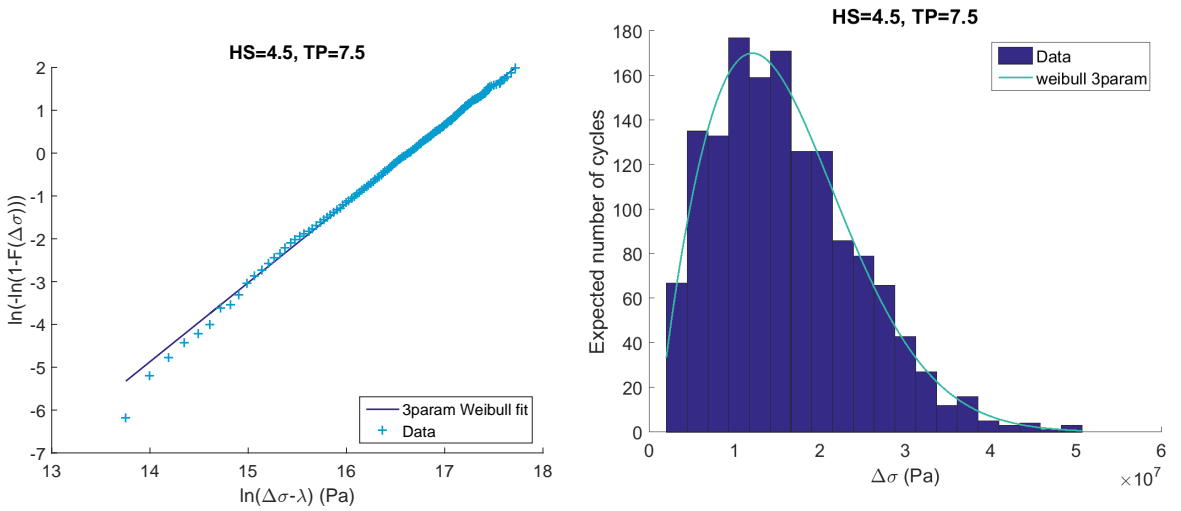
Figure B.31: *Probability distributions of stress range during 3h realizations HS:4.5 TP:7.5*
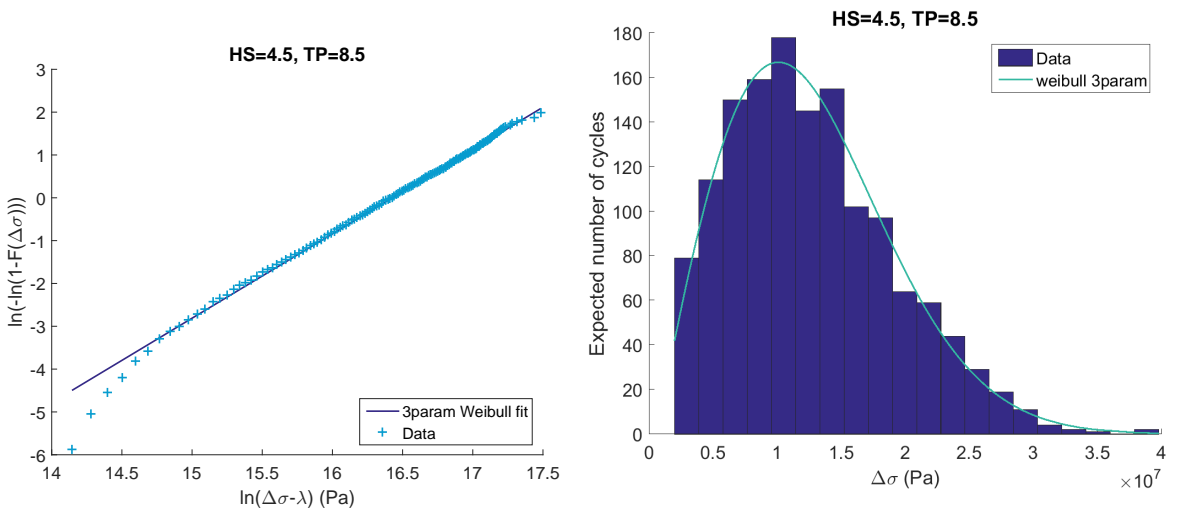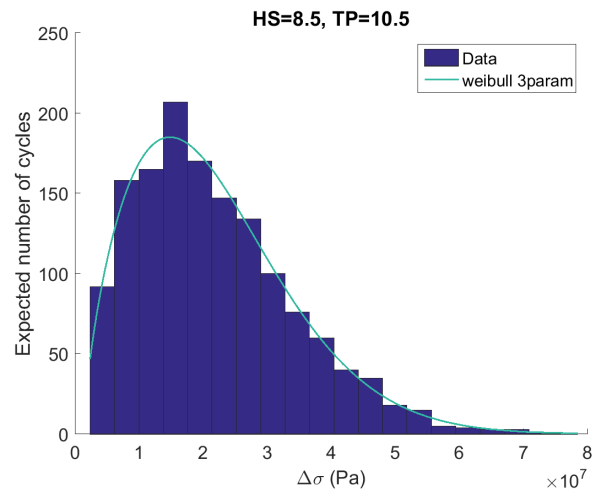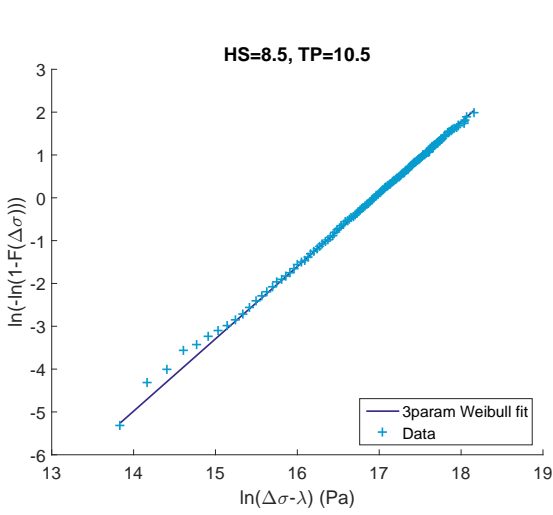
Figure B.32: *Probability distributions of stress range during 3h realizations HS:4.5 TP:8.5*
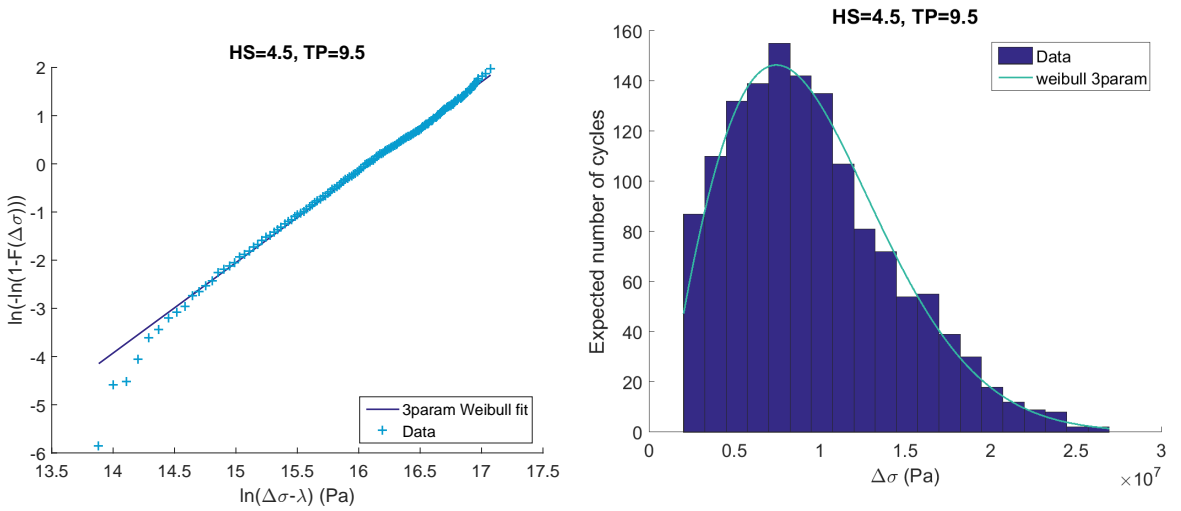
Figure B.33: *Probability distributions of stress range during 3h realizations HS:4.5 TP:9.5*
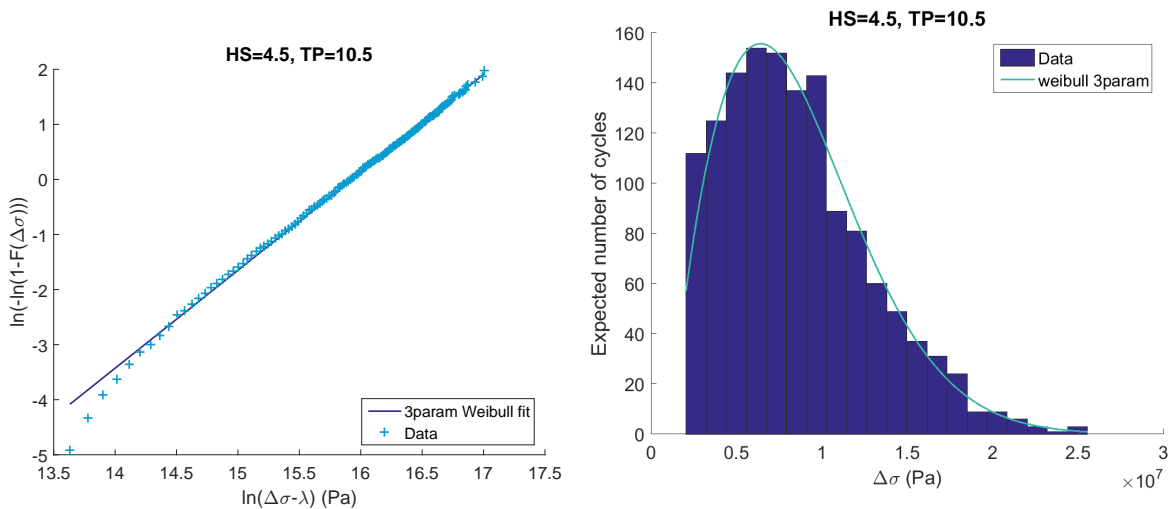
Figure B.34: *Probability distributions of stress range during 3h realizations HS:4.5 TP:10.5*
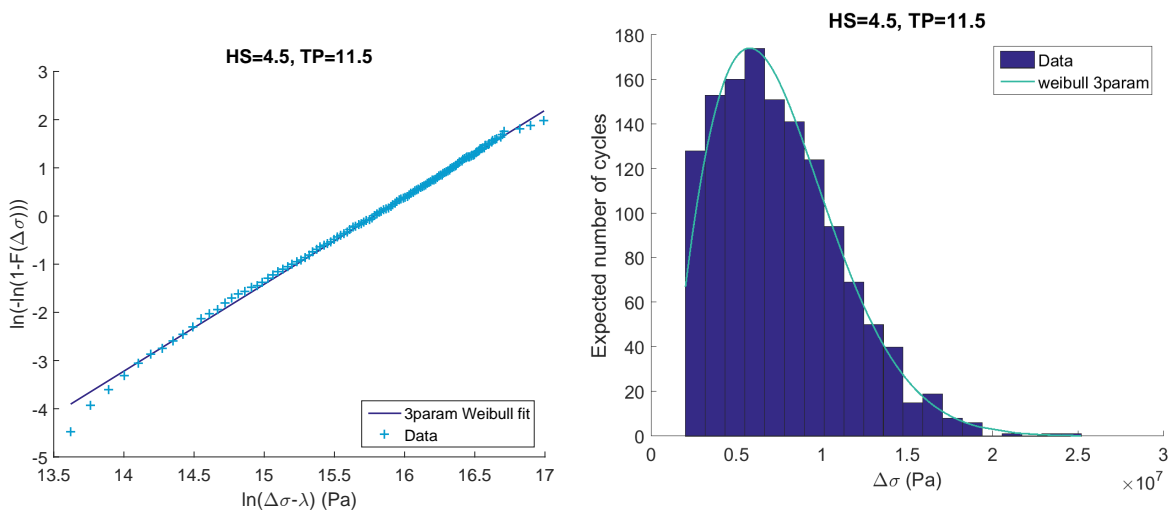
Figure B.35: *Probability distributions of stress range during 3h realizations HS:4.5 TP:11.5*
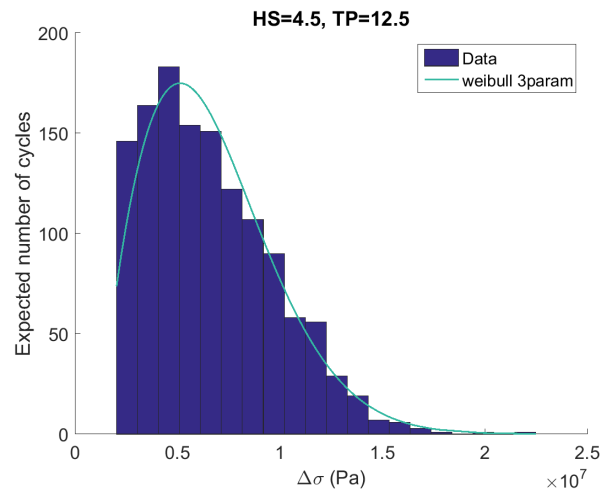
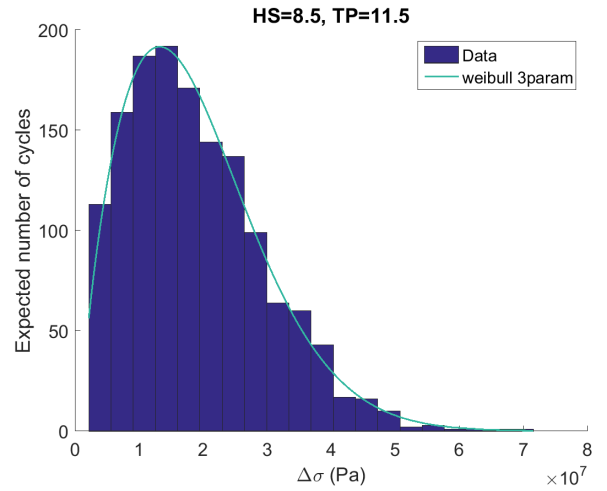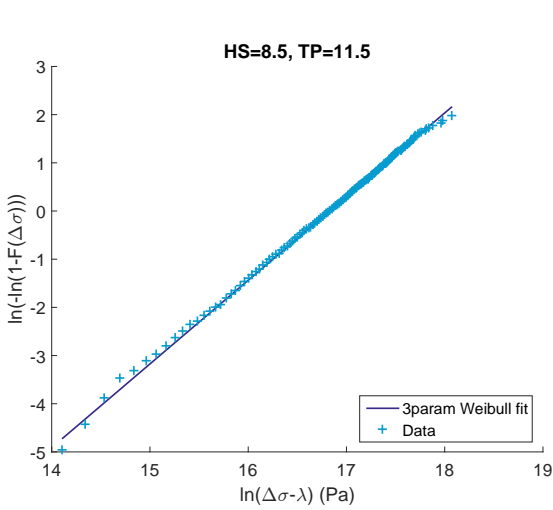**Figure B.36:** *Probability distributions of stress range during 3h realizations HS:4.5 TP:12.5*

Figure B.37: *Probability distributions of stress range during 3h realizations HS:4.5 TP:13.5*

Figure B.38: *Probability distributions of stress range during 3h realizations HS:4.5 TP:14.5*
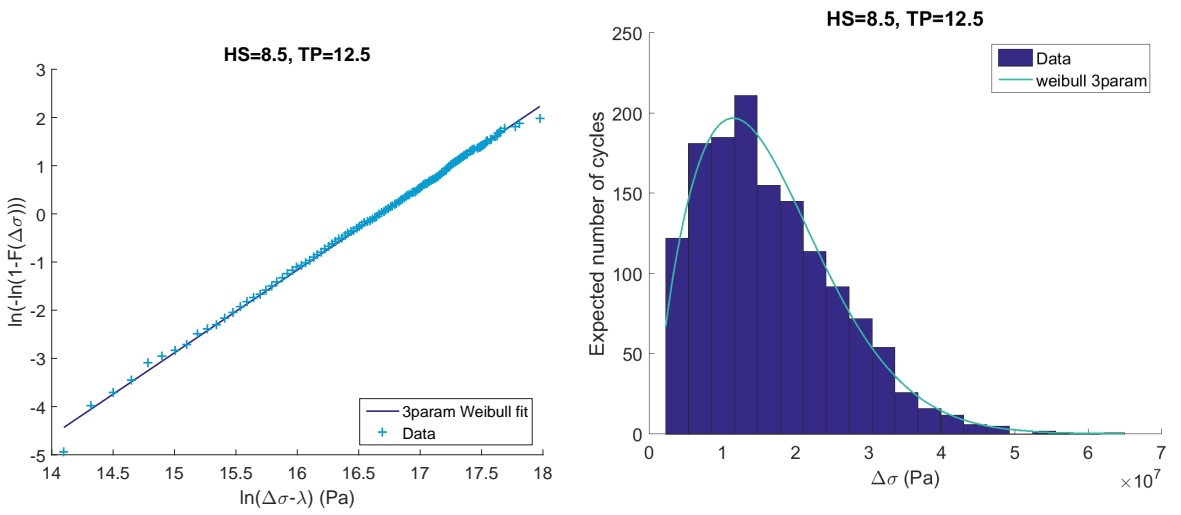

Figure B.39: *Probability distributions of stress range during 3h realizations HS:4.5 TP:15.5*

Figure B.40: *Probability distributions of stress range during 3h realizations HS:4.5 TP:16.5*

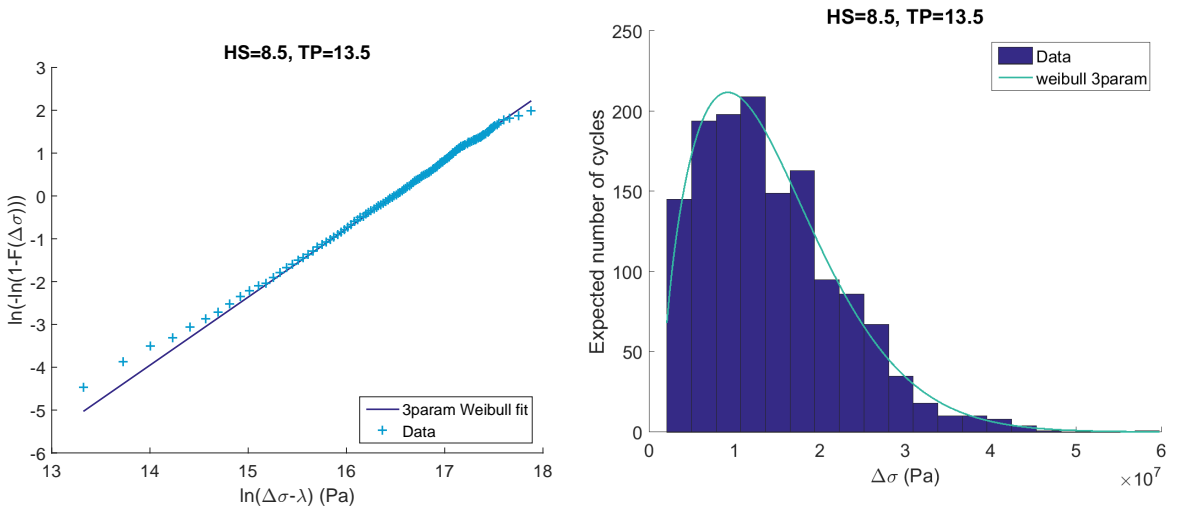**Figure B.41:** *Probability distributions of stress range during 3h realizations HS:4.5 TP:17.5*

Figure B.42: *Probability distributions of stress range during 3h realizations HS:4.5 TP:19.5*

Figure B.43: *Probability distributions of stress range during 3h realizations HS:5.5 TP:7.5*
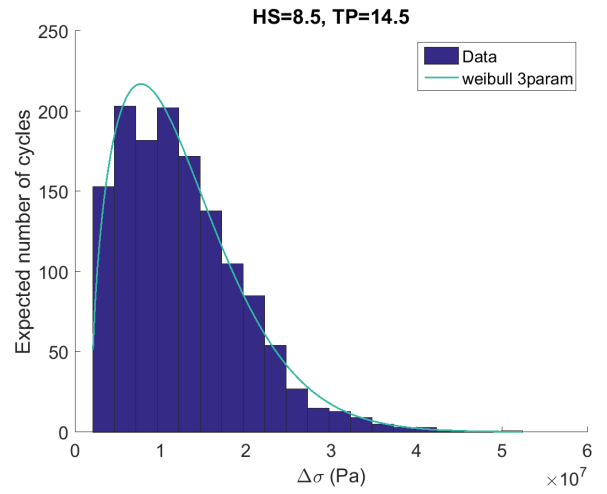
Figure B.44: *Probability distributions of stress range during 3h realizations HS:5.5 TP:8.5*

Figure B.45: *Probability distributions of stress range during 3h realizations HS:5.5 TP:9.5*
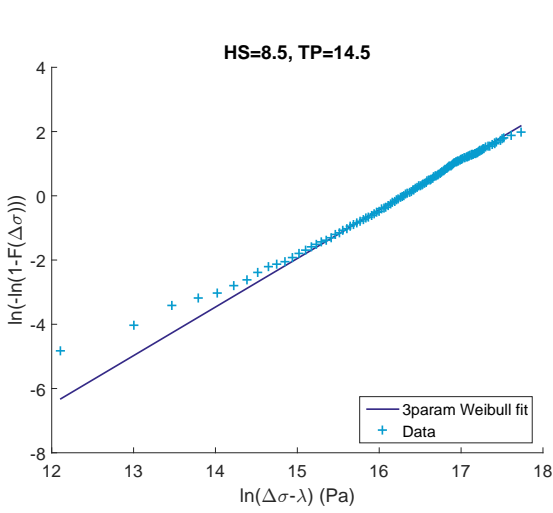
Figure B.46: *Probability distributions of stress range during 3h realizations HS:5.5 TP:10.5*

Figure B.47: *Probability distributions of stress range during 3h realizations HS:5.5 TP:11.5*

Figure B.48: *Probability distributions of stress range during 3h realizations HS:5.5 TP:12.5*
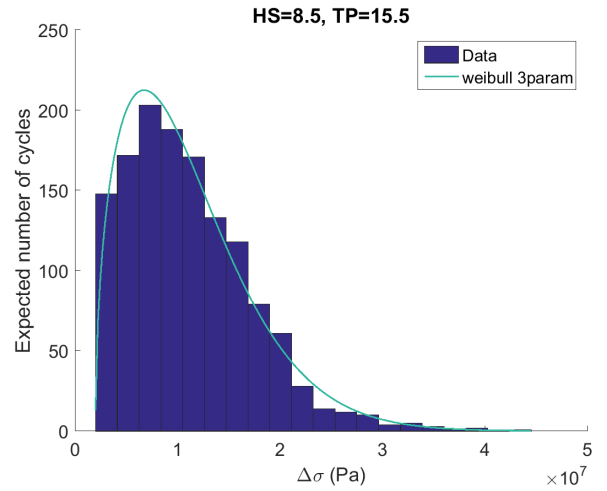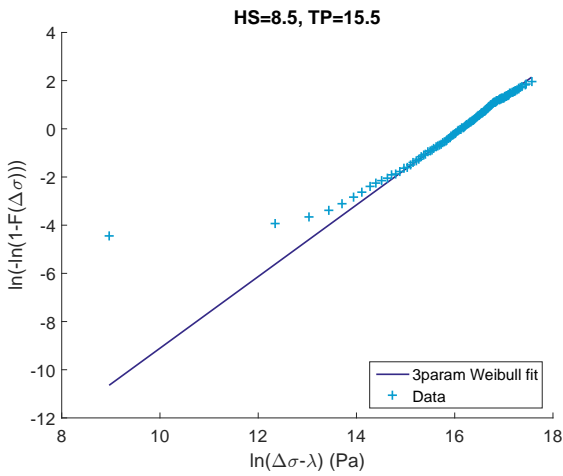

Figure B.49: *Probability distributions of stress range during 3h realizations HS:5.5 TP:13.5*

Figure B.50: *Probability distributions of stress range during 3h realizations HS:5.5 TP:14.5*

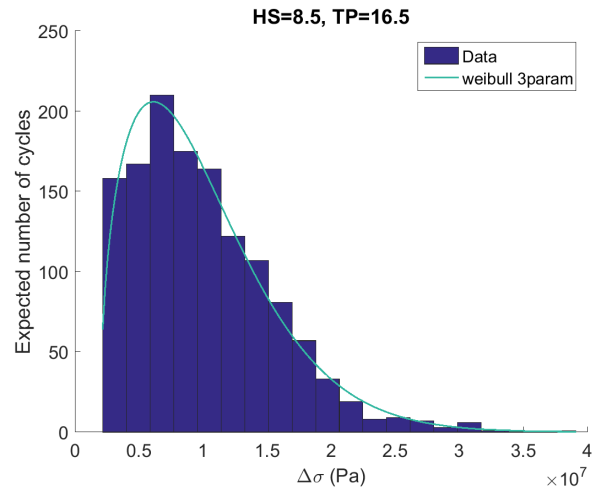**Figure B.51:** *Probability distributions of stress range during 3h realizations HS:5.5 TP:15.5*

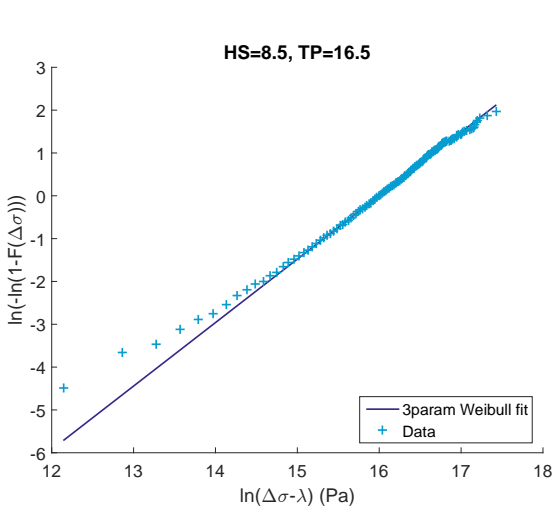**Figure B.52:** *Probability distributions of stress range during 3h realizations HS:5.5 TP:16.5*

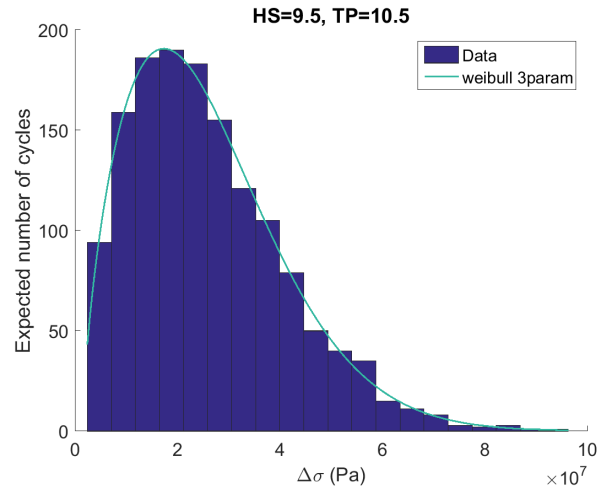**Figure B.53:** *Probability distributions of stress range during 3h realizations HS:5.5 TP:17.5*
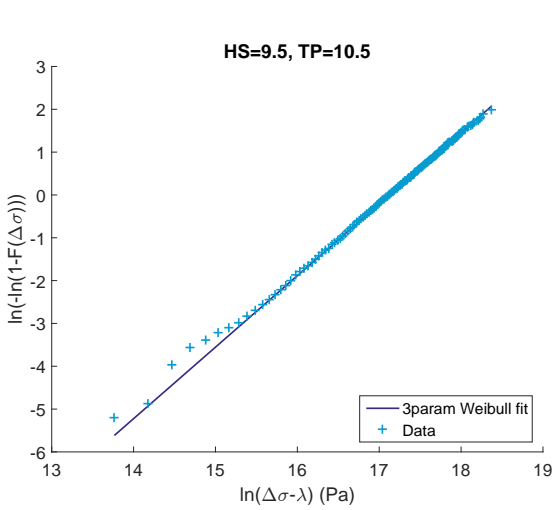
Figure B.54: *Probability distributions of stress range during 3h realizations HS:6.5 TP:9.5*

Figure B.55: *Probability distributions of stress range during 3h realizations HS:6.5 TP:10.5*

Figure B.56: *Probability distributions of stress range during 3h realizations HS:6.5 TP:11.5*

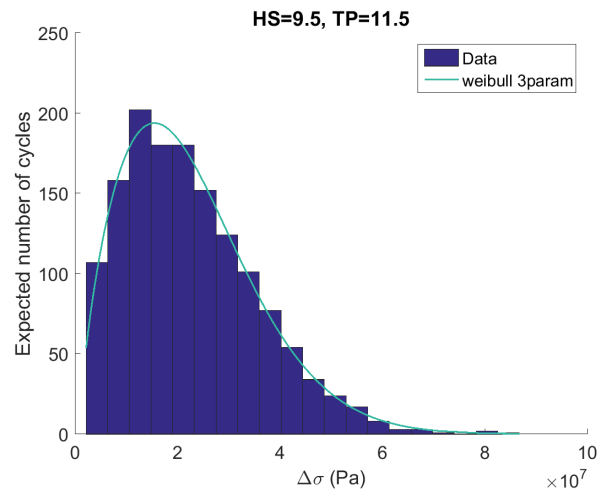**Figure B.57:** *Probability distributions of stress range during 3h realizations HS:6.5 TP:12.5*

Figure B.58: *Probability distributions of stress range during 3h realizations HS:6.5 TP:13.5*
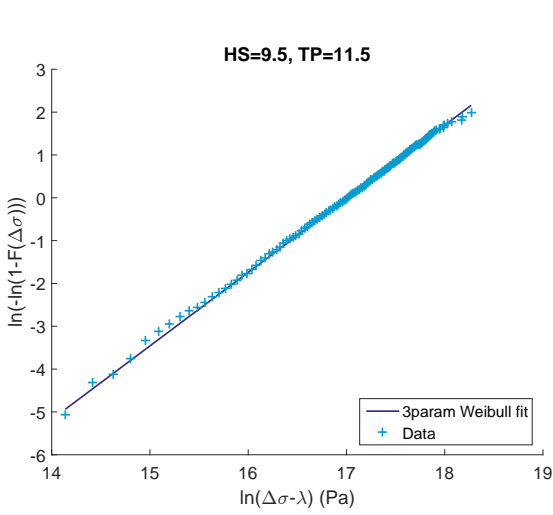

Figure B.59: *Probability distributions of stress range during 3h realizations HS:6.5 TP:14.5*

Figure B.60: *Probability distributions of stress range during 3h realizations HS:6.5 TP:15.5*
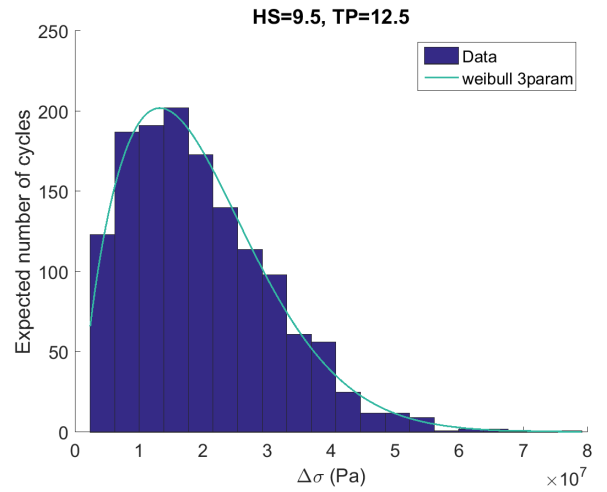

Figure B.61: *Probability distributions of stress range during 3h realizations HS:6.5 TP:17.5*
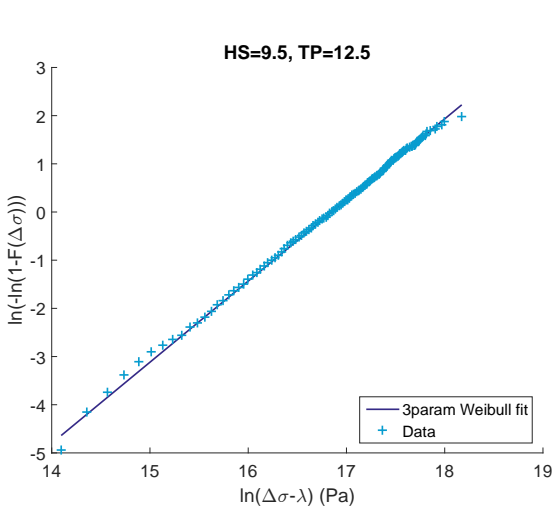
Figure B.62: *Probability distributions of stress range during 3h realizations HS:7.5 TP:9.5*

Figure B.63: *Probability distributions of stress range during 3h realizations HS:7.5 TP:10.5*

Figure B.64: *Probability distributions of stress range during 3h realizations HS:7.5 TP:11.5*
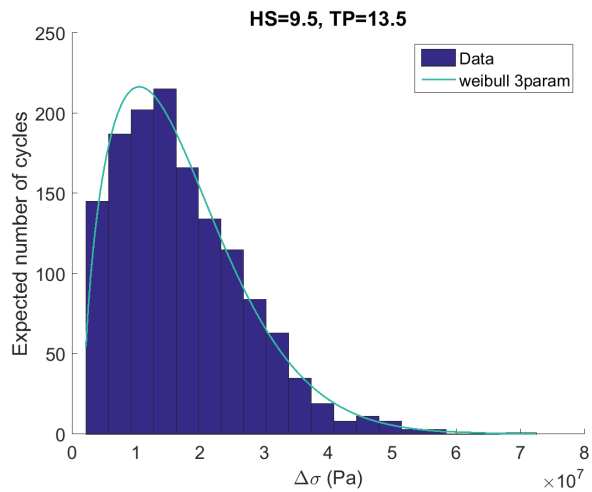

Figure B.65: *Probability distributions of stress range during 3h realizations HS:7.5 TP:12.5*

Figure B.66: *Probability distributions of stress range during 3h realizations HS:7.5 TP:13.5*
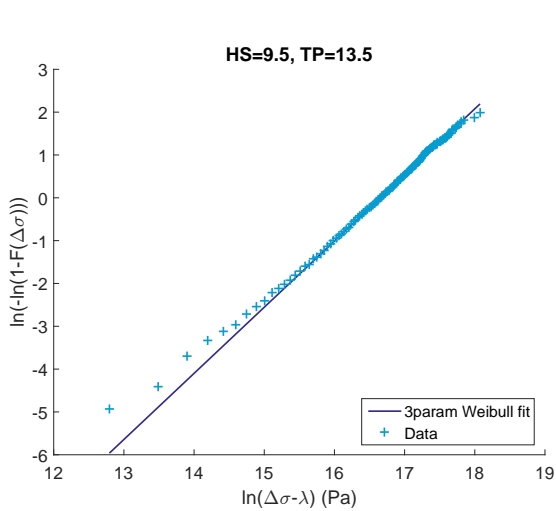

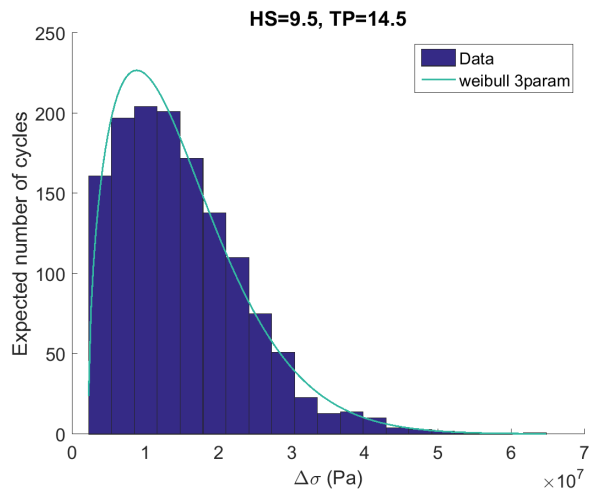**Figure B.67:** *Probability distributions of stress range during 3h realizations HS:7.5 TP:14.5*
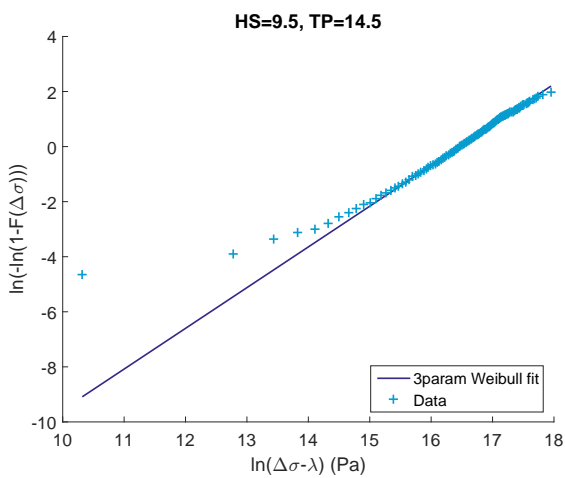
Figure B.68: *Probability distributions of stress range during 3h realizations HS:7.5 TP:15.5*

Figure B.69: *Probability distributions of stress range during 3h realizations HS:7.5 TP:17.5*

Figure B.70: *Probability distributions of stress range during 3h realizations HS:8.5 TP:10.5*

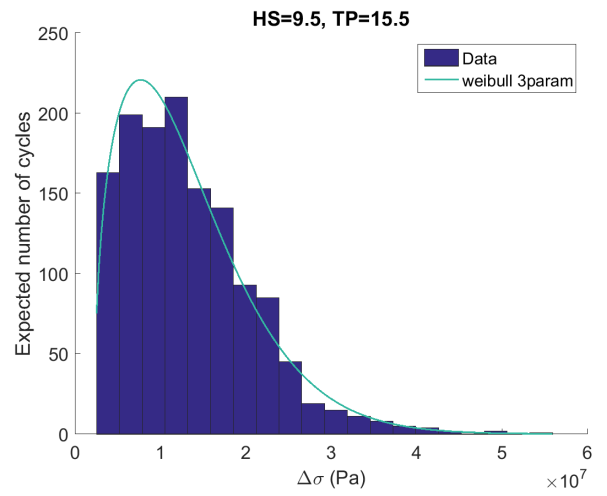**Figure B.71:** *Probability distributions of stress range during 3h realizations HS:8.5 TP:11.5*
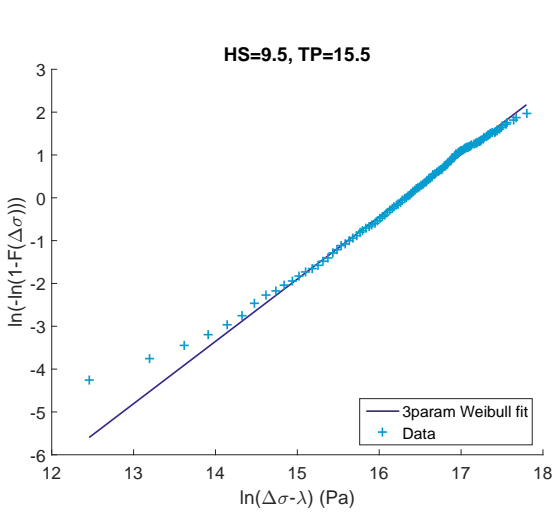
Figure B.72: *Probability distributions of stress range during 3h realizations HS:8.5 TP:12.5*

Figure B.73: *Probability distributions of stress range during 3h realizations HS:8.5 TP:13.5*

Figure B.74: *Probability distributions of stress range during 3h realizations HS:8.5 TP:14.5*
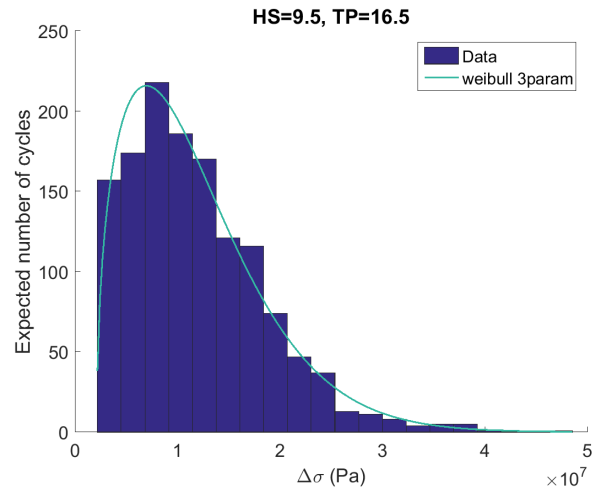

Figure B.75: *Probability distributions of stress range during 3h realizations HS:8.5 TP:15.5*

Figure B.76: *Probability distributions of stress range during 3h realizations HS:8.5 TP:16.5*

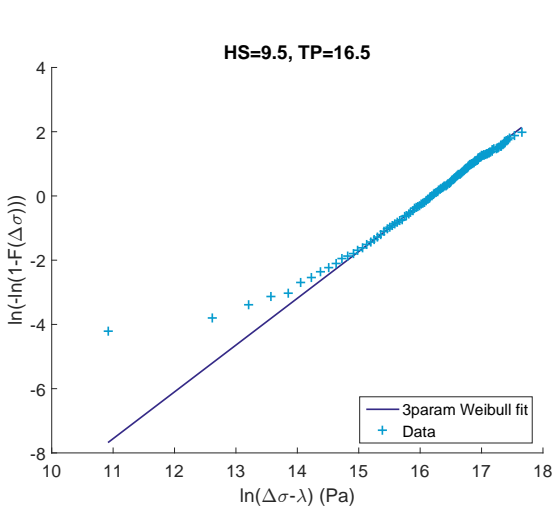**Figure B.77:** *Probability distributions of stress range during 3h realizations HS:9.5 TP:10.5*

Figure B.78: *Probability distributions of stress range during 3h realizations HS:9.5 TP:11.5*

Figure B.79: *Probability distributions of stress range during 3h realizations HS:9.5 TP:12.5*

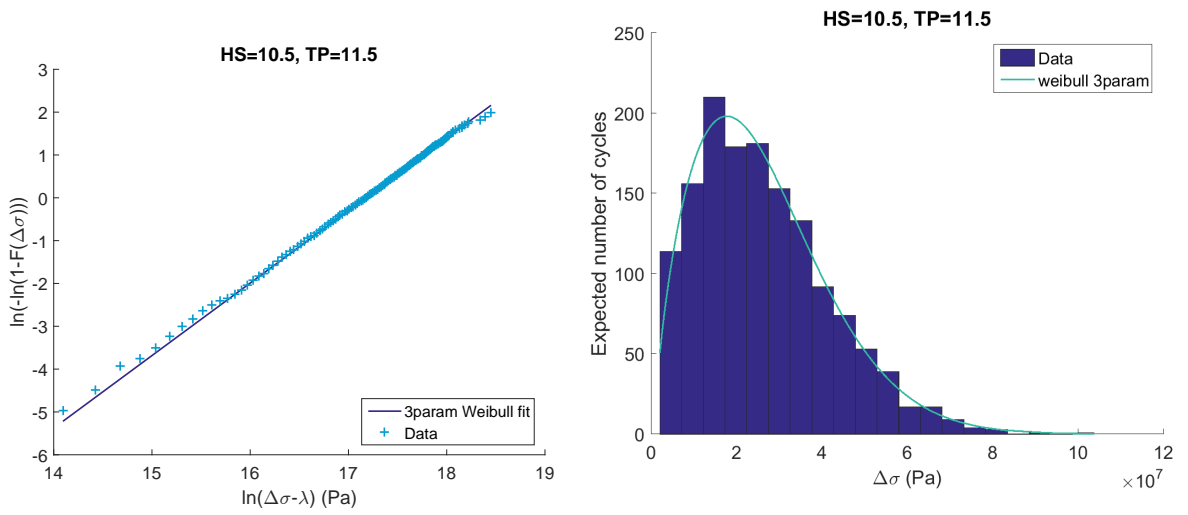**Figure B.80:** *Probability distributions of stress range during 3h realizations HS:9.5 TP:13.5*

Figure B.81: *Probability distributions of stress range during 3h realizations HS:9.5 TP:14.5*
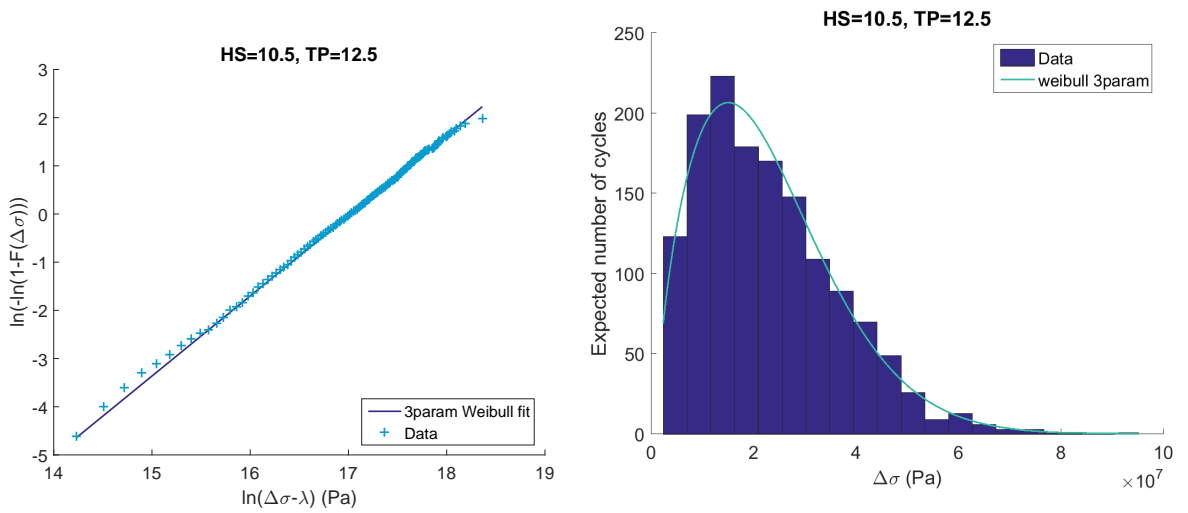
Figure B.82: *Probability distributions of stress range during 3h realizations HS:9.5 TP:15.5*

Figure B.83: *Probability distributions of stress range during 3h realizations HS:9.5 TP:16.5*

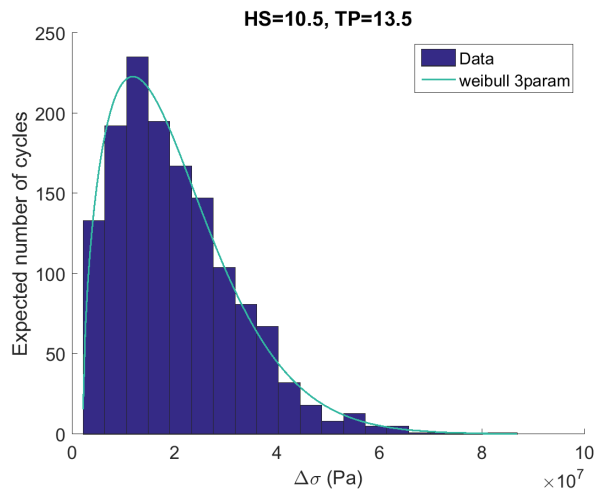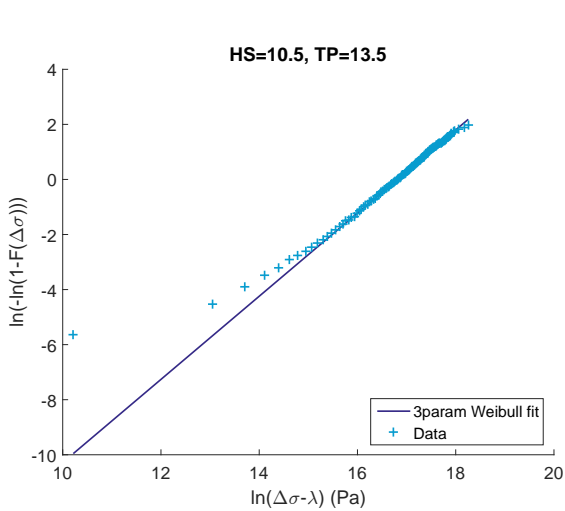**Figure B.84:** *Probability distributions of stress range during 3h realizations HS:10.5 TP:11.5*

Figure B.85: *Probability distributions of stress range during 3h realizations HS:10.5 TP:12.5*
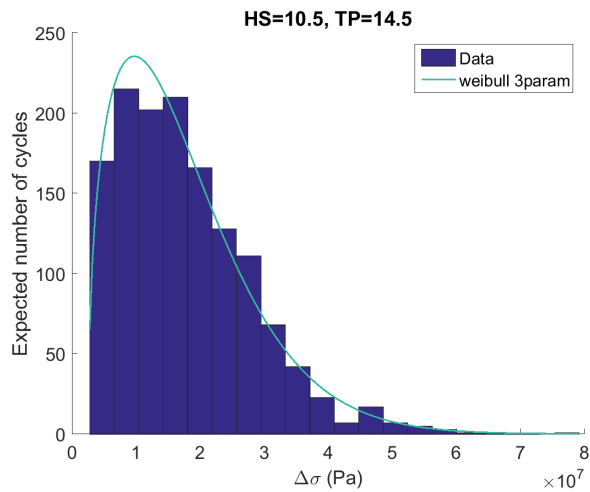
Figure B.86: *Probability distributions of stress range during 3h realizations HS:10.5 TP:13.5*

Figure B.87: *Probability distributions of stress range during 3h realizations HS:10.5 TP:14.5*
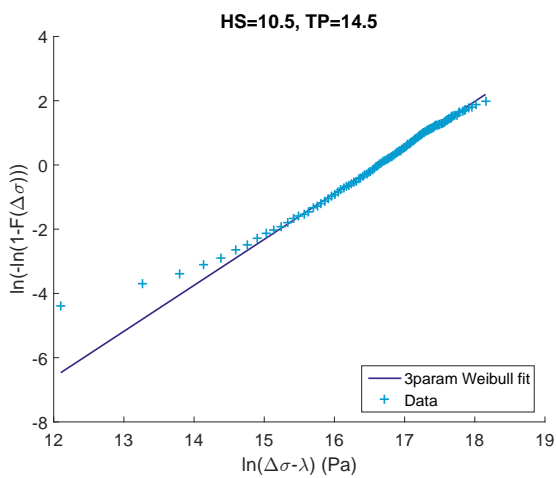
Figure B.88: *Probability distributions of stress range during 3h realizations HS:10.5 TP:15.5*
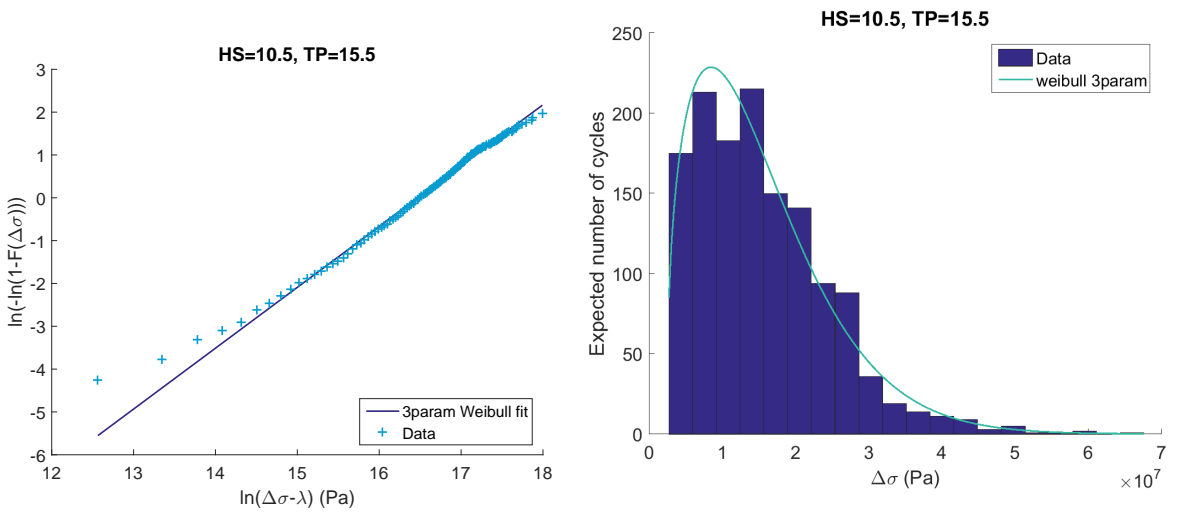

Figure B.89: *Probability distributions of stress range during 3h realizations HS:10.5 TP:16.5*

Figure B.90: *Probability distributions of stress range during 3h realizations HS:11.5 TP:13.5*

Figure B.91: *Probability distributions of stress range during 3h realizations HS:11.5 TP:14.5*

Figure B.92: *Probability distributions of stress range during 3h realizations HS:11.5 TP:15.5*
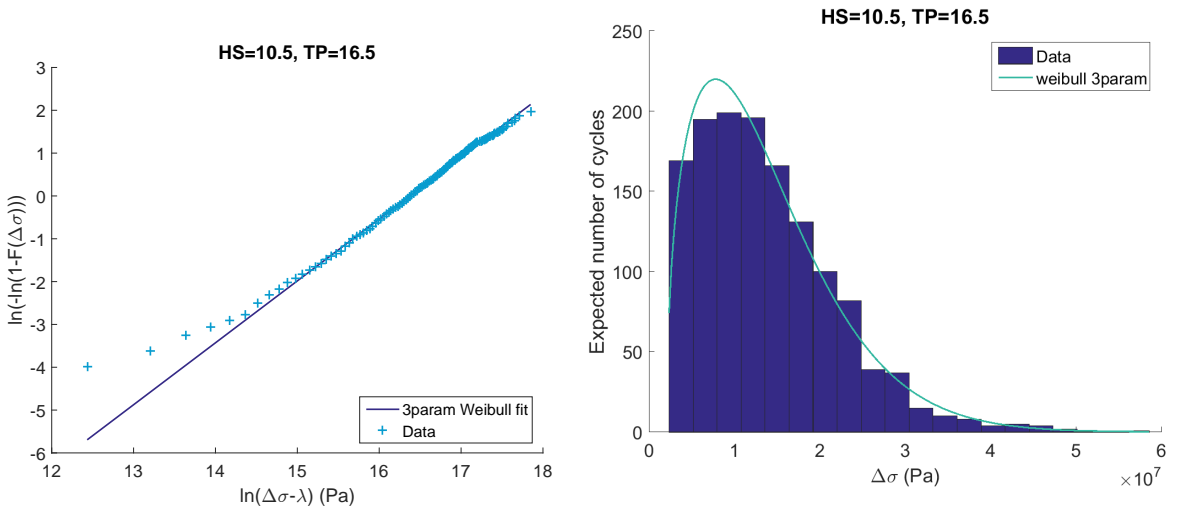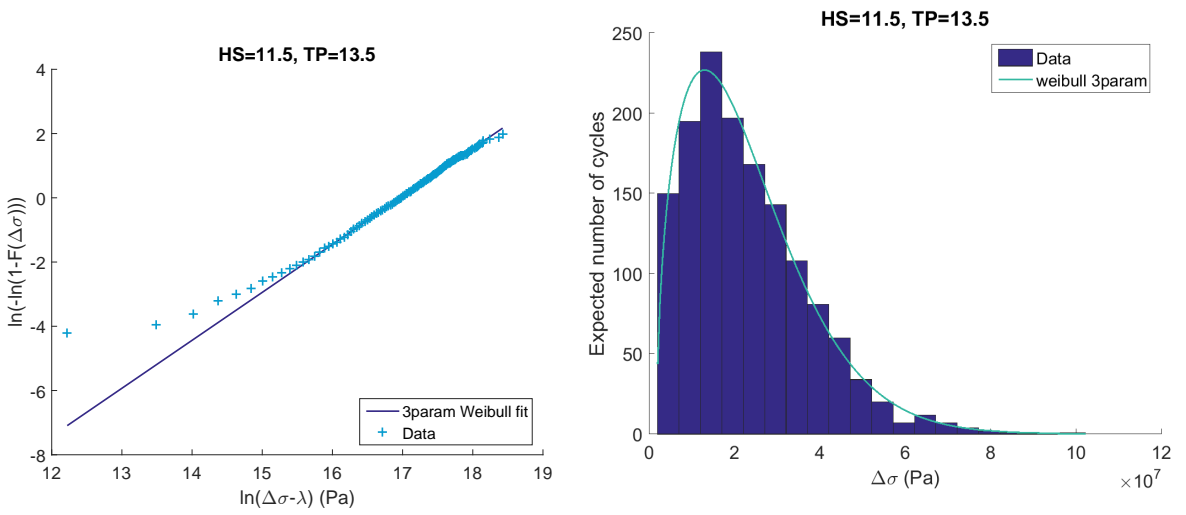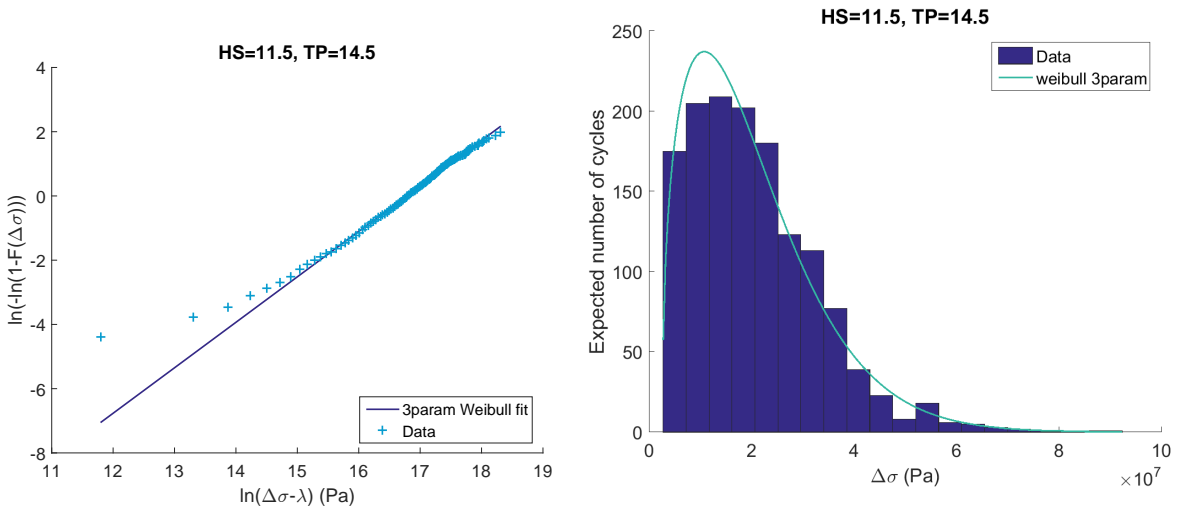

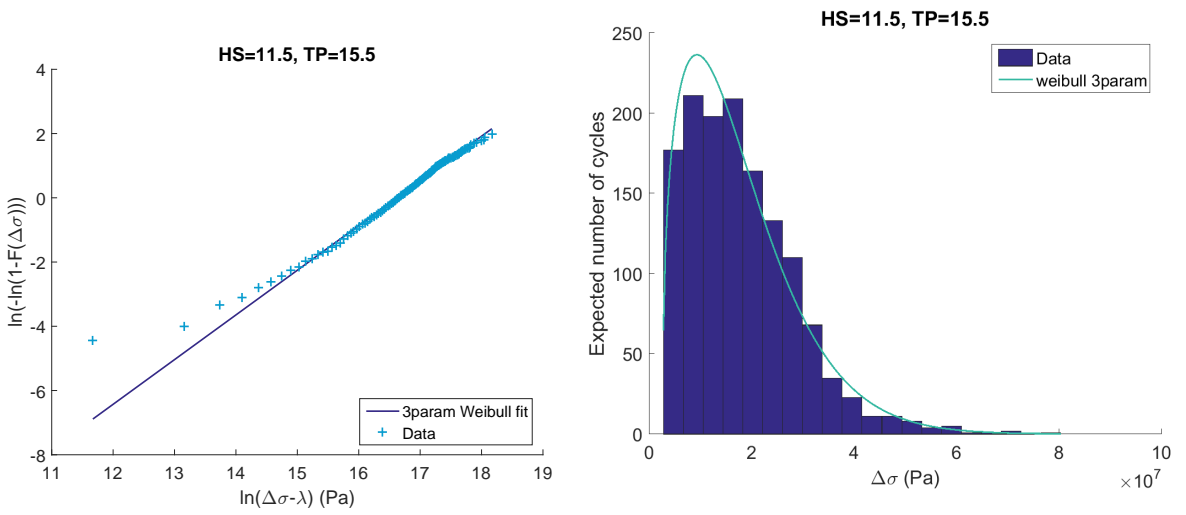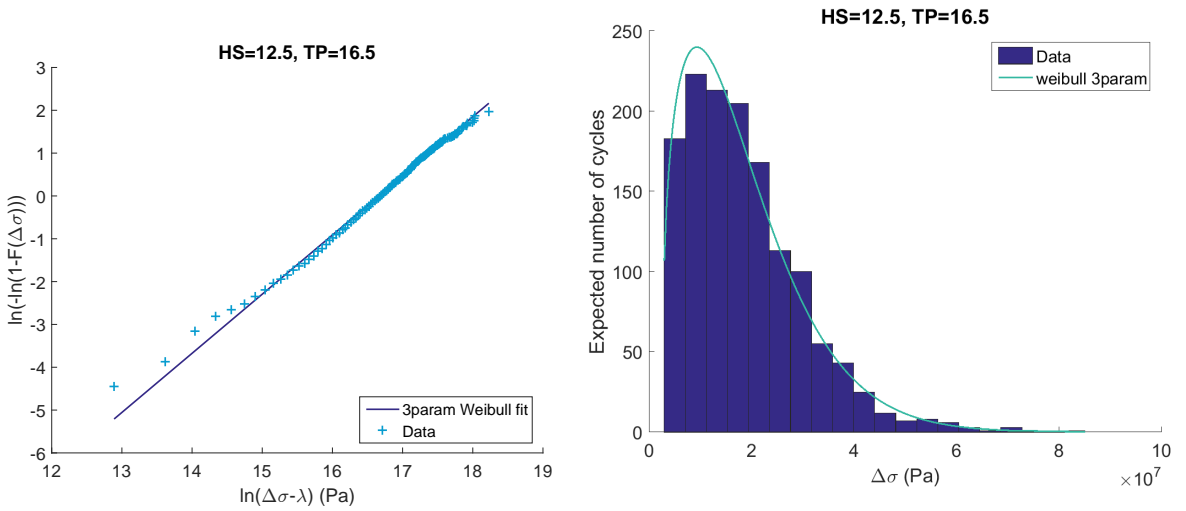**Figure B.93:** *Probability distributions of stress range during 3h realizations HS:12.5 TP:16.5*

Appendix C

Problem description

MSc theses 2017

Title: **Adequate linearization scheme for a jack-up in order to obtain sufficiently accurate fatigue assessments using a linear stochastic fatigue analyses**

Student: Marius Tveit Karlsson

Background

The topic to be investigated in this thesis is fatigue assessment of a typical jack-up platform. Properties of a jack-up structure making a fatigue assessment cost effective are:

- Non – linear hydrodynamic loading due to the drag-term of Morison equation.
- Largest natural periods are typically well inside the energetic frequency band of the wave spectrum – even for storm seas – which may result in considerable dynamic amplifications of stress width for a broad range of sea states.

The overall aim of this thesis is to establish some guidelines on how to linearize the hydrodynamic loads such that a stochastic fatigue analysis will give results of sufficient accuracy.

The topic for the thesis is suggested by MsC Antonio Goncalves, DNV-GL. His background for the thesis is given below:

"In stochastic fatigue analysis the relation between forces in each members and wave height is calculated with the assumption that exist a linear relationship between the wave height and the resulting force. However, typically jacket and jack-up with lattice leg design are drag dominated; where the drag forces are proportional to the square of the wave particle velocity. For such structures, the wave height to wave force relation is therefore not linear.

In offshore industry, the linearization with respect to wave height is generally used. It is based on the selection of a characteristic or linearization wave height for each wave frequency of the scatter diagram. Constant wave steepness is frequently used for select the linearize wave height. However, there are no proper guidelines or recommendations for selection the correct wave steepness for a specific location, and constant wave steepness usually results in over predicted drag at small wave frequencies and under predicted drag at large wave frequencies.

Due to fatigue results at typically jack-ups are strongly dependent on assumptions made in the wave linearization; an appropriate linearization wave height method is highly required.

Our proposal is to create an analytical method that estimates a linearization wave height that globally produces the same fatigue damage as the waves defined in the scatter diagram, for a given frequency, by using an equivalent jack-up leg model. The equivalent linearization wave height estimated with the analytical method will be then applied in the stochastic fatigue FE analysis."

Suggested work plan

Below a possible division into sub-tasks is given.

1. Present a brief overview of methods for assessing fatigue damage due to waves for jacket and jack-ups. Discuss pro and contra for the methods in view of linear versus non-linear loading and static versus dynamic behaviour.

2. Present in detail the stochastic fatigue analysis in frequency domain. Discuss possible approaches for linearizing the non-linear hydrodynamic load. A topic that should be considered is consequence of current for the linearization? Can we neglect current for fatigue assessment?

3. In order to evaluate the accuracy of fatigue assessment for various linearization methods, we an approach that we will consider state-of-the-art fatigue damage. For a stationary short term sea state this would be a proper time domain solution of the structural problem together with a rain-flow counting of accumulated fatigue damage for the sea state. Discuss and describe in detail how this can be extended to a full long term fatigue assessment.

4. Do a long term fatigue assessment for the jack-up under consideration using approaches outlined in 3.. It shall be discussed how many sectors the weather is divided into. A sector width of 30° or 45° seems reasonable. A proper modelling of wave conditions for the various sectors maybe found in literature or it may have to be established by the candidate using hindcast data (NORA10) for a proper location. (One must consider the work load of including all sectors. If found convenient one can limit the assessment to the worst sector. If time permits one can include more sectors.)

5. Do a long term stochastic fatigue analysis using linearized response amplitude operators for the stress process. Compare with estimated damage in 4.. Test eventually several approaches for the linearization. Recommend a best approach for the platform under consideration. Discuss how general you thing recommendation is.

6. Conclusion and discussion for further work.

The candidate may of course select another scheme as the preferred approach for his work. The work may show to be more extensive than anticipated. Some topics may therefore be left out after discussion with the supervisor without any negative influence on the grading.

The candidate should in his report give a personal contribution to the solution of the problem formulated in this text. All assumptions and conclusions must be supported by mathematical models and/or references to physical effects in a logical manner. The candidate should apply all available sources to find relevant literature and information on the actual problem.

The report should be well organised and give a clear presentation of the work and all conclusions. It is important that the text is well written and that tables and figures are used to support the verbal presentation. The report should be complete, but still as short as possible. The final report must contain this text, an acknowledgement, summary, main body, conclusions, suggestions for further work, symbol list, references and appendices. All figures, tables and equations must be identified by numbers. References should be given by author

and year in the text, and presented alphabetically in the reference list. The report must be submitted in two copies unless otherwise has been agreed with the supervisor. From the report it should be possible to identify the work carried out by the candidate and what has been found in the available literature. It is important to give references to the original source for theories and experimental results.

The supervisor may require that the candidate should give a written plan that describes the progress of the work after having received this text. The plan may contain a table of content for the report and also assumed use of computer resources. As an indication such a plan should be available by end of March.

The report must be signed by the candidate, include this text, appear as a paperback, and - if needed - have a separate enclosure (binder, diskette or CD-ROM) with additional material.

Supervisor: Sverre Haver, NTNU.
Co-supervisors   Jørgen Amdahl, NTNU